FINAL SCIENTIFIC/TECHNICAL REPORT

Playas Grid Reliability and Distributed Energy Research

Prepared for the
U.S. Department of Energy
Office of Electricity Delivery and Energy Reliability

Award Number DE-FC26-06NT42854

Recipient: New Mexico Institute of Mining and Technology

Principal Investigator:

Van Romero

Co-Principal Investigators:

Don Weinkauf
Mushtaq Khan
Wes Helgeson
Kevin Weedeward
Corey LeClerc
Paul Fuierer

Report Date: July 18, 2013

Acknowledgement

This material is based upon work supported by the United States Department of Energy under award number DE-FC26-06NT42854.

Disclaimer

TABLE OF CONTENTS

Executive Summary

The future looks bright for solar and renewable energies in the United States. Recent studies claim that by 2050, solar power could supply a third of all electricity demand in the country's western states. Technology advances, soft policy changes, and increased energy consciousness will all have to happen to achieve this goal.

But the larger question is, what would it take to do more throughout the United States? The studies tie future solar and renewable growth in the United States to programs that aim to lower the soft costs of solar adoption, streamline utility interconnections, and increase technology advances through research and development. At the state and local levels, the most important steps are:

- Net metering: Net metering policies lets customers offset their electric bills with onsite solar and receive reliable and fair compensation for the excess electricity they provide to the grid. Not surprisingly, what utilities consider fair is not necessarily a rate that's favorable to solar customers.
- Renewable portfolio standards (RPS): RPS policies require utilities to provide a certain amount of their power from renewable sources; some set specific targets for solar and other renewables. California's aggressive RPS[1] of 33% renewable energy by 2020 is not bankrupting the state, or its residents.
- Strong statewide interconnection policies: Solar projects can experience significant delays and hassles just to get connected to the grid. Streamlined feasibility and impact analysis are needed. Good interconnection policies are crucial to the success of solar or renewable energy development.
- Financing options: Financing is often the biggest obstacle to solar adoption. Those obstacles can be surmounted with policies that support creative financing options like third-party ownership (TPO) and property assessed clean energy (PACE). Attesting to the significance of TPO is the fact that in Arizona, it accounted for 86% of all residential photovoltaic (PV) installations in Q1 2013[2].

Policies beyond those at the state level are also important for solar. The federal government must play a role including continuation of the federal Investment tax credit,[3] responsible development of solar resources on public lands, and support for research and development (R&D) to reduce the cost of solar and help incorporate large amounts of solar into the grid.

The local level can't be ignored. Local governments should support: solar rights laws, feed-in tariffs (FITs), and solar-friendly zoning rules. A great example of how effective local policies can be is a city like Gainesville, Florida[4], whose FIT policy has put it on the map as a solar leader. This is particularly noteworthy because the Sunshine State does not appear anywhere on the list of top solar states, despite its abundant solar resource. Lancaster, California[5], began by streamlining the solar permitting process and now requires solar on every new home. Cities like these point to the power of local policies, and the ability of local governments to get things done. A conspicuously absent policy is Community Choice energy[6], also called community choice aggregation (CCA). This model allows local governments to pool residential, business, and municipal electricity loads and to purchase or generate on their behalf. It provides rate stability and savings and allows more consumer choice and local control. The model need not be focused on clean energy, but it has been in California, where Marin Clean Energy[7], the first CCA in California, was enabled by a state law -- highlighting the interplay of state and local action.

Basic net metering[8] has been getting a lot of attention. Utilities are attacking it[9] in a number of states, claiming it's unfair to ratepayers who don't go solar. On the other hand, proponents of net metering say utilities' fighting stance is driven by worries about their bottom line, not concern for their customers. Studies in California[10], Vermont[11], New York[12], and Texas[13] have found that the benefits of net metering (like savings on investments in infrastructure and on meeting state renewables requirements) outweigh the costs (like the lowered revenue to cover utility infrastructure costs). Many are eagerly awaiting a California Public Utilities Commission study[14] due later this year, in the hopes that it will provide a relatively unbiased look at the issue.

Meanwhile, some states continue to pursue virtual net metering policies. Under Colorado's Solar Gardens Act[15], for example, utility customers can subscribe to power generated somewhere other than their own homes. The program allowed by that bill sold out in 30 minutes, evidence of the pent-up demand for this kind of arrangement. And California solar advocates are hoping for passage of a "shared renewables" bill [16] in that state, which would provide for similar solar installations. Laws like these are significant in bringing solar power to the estimated 75%[17] (likely a conservative number) of us who can't put solar on our own roof.

As great a resource as the sun is, when it comes to actually implementing solar or other renewables, technology advances, policy changes, bureaucratic practices, and increased energy consciousness will all have to happen to achieve a 30% by 2050 national goal. This project incorporated research activities focused on addressing each of these challenges. First, the project researchers evaluated several leading edge solar technologies by actually implementing these technologies at Playas, New Mexico, a remote town built in the 1970s by Phelps Dodge Mining Company for the company's employees. This town was purchased by the New Mexico Institute of Mining and Technology in 2005 and converted to a training and research center. Playas is an all-electric town served by a substation about seven miles away. The town is the last user on a 240 kV utility transmission line owned by the Columbus Electric Cooperative (CEC) making it easy to isolate for experiment purposes.

The New Mexico Institute of Mining and Technology (NMT) and the Department of Homeland Security (DHS) perform various training and research activities at this site. Given its unique nature, Playas was chosen to test Micro-Grids and other examples of renewable distributed energy resources (DER). Several proposed distributed energy sources (DERs) were not implemented as planned including the Micro-Grid. However, Micro-Grid design and computer modeling were completed and these results are included in this report.

As part of this research, four PV (solar) generating systems were installed with remote Internet based communication and control capabilities. These systems have been integrated into and can interact with the local grid So that (for example) excess power produced by the solar arrays can be exported to the utility grid. Energy efficient LED lighting was installed in several buildings to further reduce consumption of utility-supplied power. By combining reduced lighting costs; lowering HVAC loads; and installing smart PV generating equipment with energy storage (battery banks) these systems can greatly reduce electrical usage drawn from an older rural electrical cooperative (Co-Op) while providing clean dependable power.

Several additional tasks under this project involved conducting research to develop methods of producing electricity from organic materials (i.e. biofuels, biomass. etc.), the most successful being the biodiesel reactor. Improvements with Proton Exchange Membranes (PEM) for fuels cells were demonstrated and advances in Dye Sensitized Solar Cells (DSSC) were also shown.

The specific goals of the project include:

- Instrumentation of the power distribution system with distributed energy resources, demand-side control and intelligent homes within the town of Playas, NM,
- Creation of models (power flow and dynamic) of the Playas power distribution system,
- Validation of the models through comparison of predicted behavior to data collected from instrumentation, and
- Utilization of the models and test grid to characterize the impact of new devices and approaches (e.g., distributed generation and load management) on the local distribution system as well as the grid at large.

In addition to the above stated objectives, the research also focused on three critical challenges facing renewable distributed energy platforms: 1) hydrogen from biomass, 2) improved catalyst support systems for electrolysis membranes and fuel cell systems, and 3) improved manufacturing methodologies of low cost photovoltaics.

The following sections describe activities performed during this project. The various tasks were focused on establishing Playas as a "…theoretical and experimental test bed…" through which components of a modern/smart grid could be characterized. On a broader scale, project efforts were aimed at development of tools and gathering of experience/expertise that would accelerate progress toward implementation of a modern grid.

Task 1.0: Micro-Grid Reliability, Instrumentation and Testing

Instrumentation of the power distribution system with distributed energy resources, demand-side control and intelligent homes within Playas, NM was completed. The following paragraphs describe the various activities of Task 1 that were completed during the project and associated results and accomplishments.

Classroom Bowling Alley Community Center

Figure 1. System Installations

Smart Meters

Electrical sub-meters were installed at three of the larger commercial type buildings as shown by Figure 1. These provide data recording, power quality information and time of use monitoring. Monitoring includes real time baseline recording including power quality and the electrical power consumed at each of the sub-metered buildings. General Electric EPM 4000 Sub-meters were chosen. The meters have 24 single phase or 6 3-phase registers to monitor energy for residential, commercial, or industrial applications.

These meters have two communication modes: power line carrier (PLC), which utilizes existing AC power lines as the communication medium, and Mod Buss (RS232, RS485). NMT researchers used a RS485 to Ethernet converter and GE's EnerVista Viewpoint "proprietary" monitoring software. Regrettably, this proved to be a disadvantage for the research performed. However, the project later implemented a device that can be programmed by "writing script" that reads the individual data registers inside the meter and logs these values.

Residential Energy Monitors

Energy meters inform residents in real time of exactly how much electricity the household is consuming. A wireless sensor was installed inside the main breaker box of each home used for the study. This sensor is connected to and measuring both the line and load sides of the voltage and is line powered by the same. The sensor also clamps around both wires measuring the current entering the home.

Power Line Carrier is used to transmit power consumption information through the house wiring to a small gateway plugged inside the house. The gateway is linked through a local Ethernet connection for remote monitoring, and transmits information (via wireless technology) to a portable receiver that can be carried throughout the house. This portable receiver

displays energy usage information on a large LCD screen such as depicted by Figure 2. Various electricity rates can be programmed for extreme accuracy, including single (flat) rates, tiered rates, and time-based rates. By monitoring energy costs the resident can decide when to cut back on energy usage.

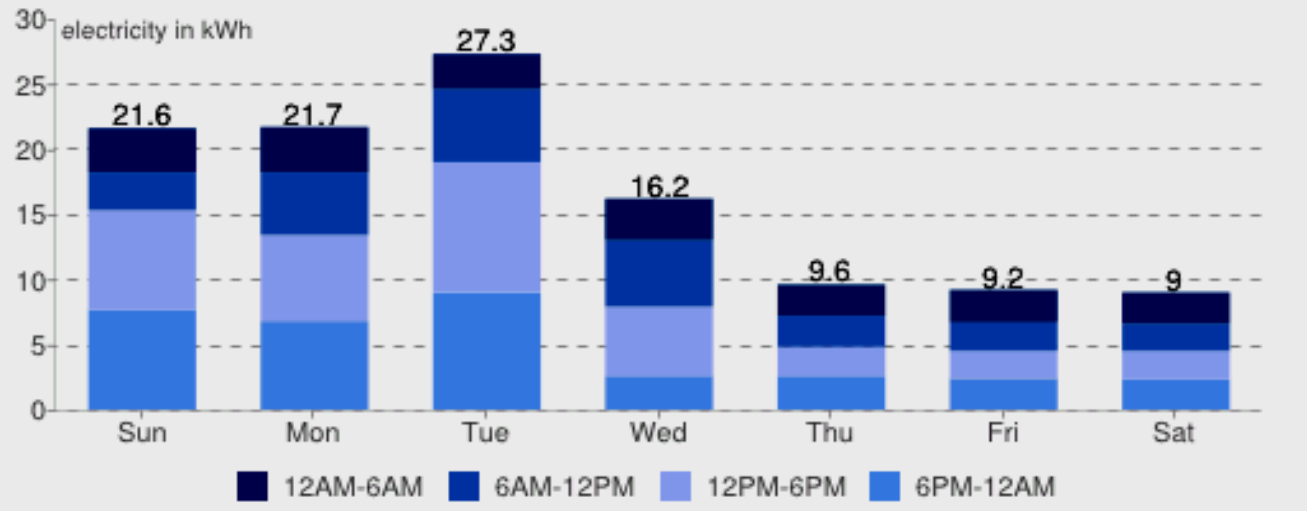

Figure 2. Sample Readout from a TED 5000 home energy monitor

Effectiveness of Energy Meters

Energy usage is not very noticeable to most users. Some residents only have a vague idea of how much energy they are using and what sort of difference could be made by changing daily habits. The two residential 2.2 kW PV systems installed at Playas have demonstrated that awareness is a key to saving energy. Excitement was present when the residents actually saw their utility power meter spin backwards. The metering of real-time information (cost) allows the residents to switch appliances on and off and record the difference. Thus the energy monitor is useful as a self-teaching tool to help reduce energy consumption.

Power Outages at Playas

Typically, phase loss associated with power outages can cause 3-phase refrigeration compressors (and similar equipment) to burn out, and damage sensitive electronic equipment. Playas uses this type of equipment in many locations and has experienced many problems as a result of utility grid outages. The three PV systems that serve the community center and two residential units have battery banks that provide an Uninterruptable Power Supply (UPS) and can easily ride through these outages without missing a cycle on the 60 Hz waveform. The charts of Figure 3 on the following page show sample data runs for several outages that occurred at the community center.

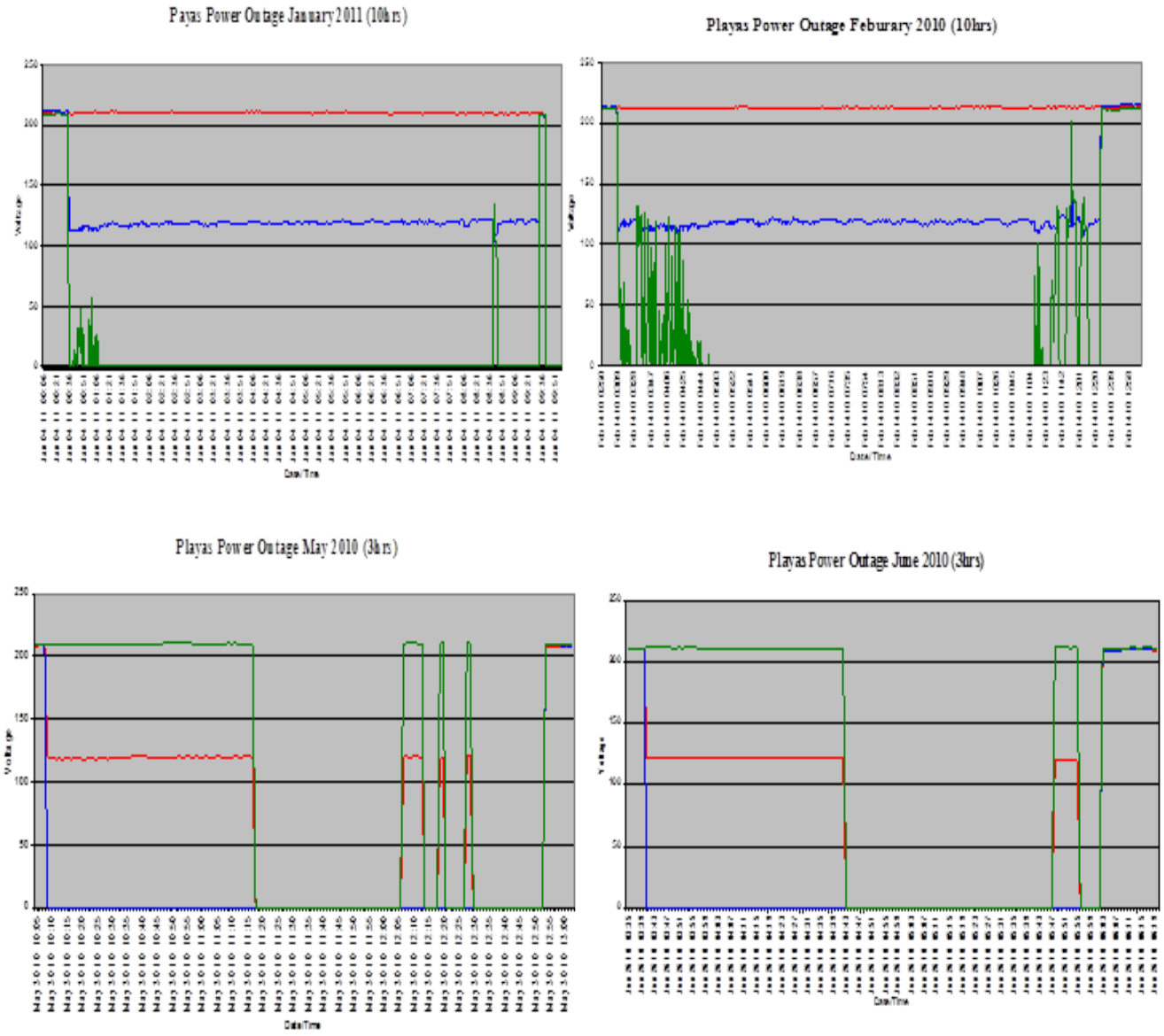

Figure 3. Playas Community Center Power Outages

Playas Substation

When NMT Engineers first visited the Playas substation it was immediately obvious that no recent upgrades had been performed especially with devices capable of measuring and recording electrical usage. Existing, older reclosers and voltage regulators required frequent maintenance compared to newer devices. After several discussions between NMT and the Columbus Electric Cooperative (CEC), the following upgrades of the substation and distribution feeder were implemented as part of the Task 1 effort. In addition to enhancing reliability, the upgrades also allow the utility to remotely monitor and control the substation and feeders from its headquarters in Deming, NM. All system upgrades located off the Playas town site were paid by CEC. As part of this project, costs associated with the upgrades described in the following section were paid with project funds.

Measuring Current Draw from Playas

Pyramid 10 MW Substation

Figure 4. Playas Electric Substation

Recommended Substation Upgrades

- Replacement of the three existing 400 amps, 25 kV oil filled recloses with the latest available technology, i.e., vacuum and/or SF6 technology, with state of the art digital relaying with communications, and metering quality instrument transformers (CTs, PTs). The reclosers can be remotely controlled by the CEC. As part of the control function, the recloser can be opened, closed and its relay can be set to "hot line hold" status, which places the recloser into non-reclose mode. This is normally performed by the utility prior to a crew working on the line.
- Replacement of the existing three 288 kVA single phase voltage regulators with state of the art digital control and communications hardware. As a result of the retrofits, the voltage regulators can be controlled remotely.
- Installation of a GE D400 substation data manager, along with four GE PQMII meters allow CEC to remotely monitor the output of the substation main transformer plus the three feeder circuits.
- GE software will be used to view, trend, control, etc. information from meters located at the substation. The software will reside on a dedicated server located at CEC's main headquarters. The software will also be used to view metering information from the various instrumented buildings within Playas.
- For redundancy and added reliability, communications to/from the meters, relays, controllers and control center will incorporate at least two of the following three communications methods: Cyber Secure Microwave, Satellite Link or Fiber network.

Residential 2.2 kW PV systems

The purpose of these systems was to test new solar technologies and components and the control and communications devices connected to them. During a total power outage these battery backed PV systems provide necessary critical power for devices such as refrigerator/freezer, microwave oven, computers, televisions and several compact fluorescent lighting (CFL) circuits. Researchers have the ability to actively balance the generation and consumption of loads within a residential electrical system. The goal of this experiment is to coordinate the operation of onsite power generation (in this case, Solar/PV) with energy storage and controllable loads in such a way as to minimize the amount of energy normally supplied by the utility at times of peak demand on the distribution feeder. The following photographs depict the residential PV systems (designated as Laguna 10 and Laguna 12) installed at Playas during this project.

Laguna 12

Laguna 10

Figure 5. Two Residential 2.2 kW PV Systems

The grid interactive PV system is designed to balance available onsite PV generation capacity with demand, either by selling excess power back to the grid or storing it in a battery system. The systems can be software configured to sell back during periods of peak demand on the utility's grid, and/or use grid power at night to make up energy deficiencies as required. The two residential 2.2 kW PV systems at Playas are fully operational. Power from these systems is first used to supply the critical loads in the house, and then sell any excess power back to the utility. The critical loads in the house are supplied directly from a DC/AC inverter/charger/battery system installed at the home.

Using the latest control technologies inverter settings can be changed through the Internet. This feature uses commercially available software but is secured using passwords. This feature may be used to change the inverter settings based upon signals from the home's energy management system (EMS). In an effort to compare and contrast current solar technologies, PV components from two different manufactures were chosen. Both of the selected systems performed with greater than 94% efficiency. The Outback system uses built in temperature controlled fans, whereas the Xantrex system uses heat sinks and natural convection for cooling. The systems were designed to completely "fill" or charge the battery bank after one day of full sun and minimal loads (discharge). For an extended outage the resident would likely become their own energy manager watching power consumption and saving power for essential activity such as communications, food preservation, and meal preparation. Figure 6 represents a schematic of the residential PV systems used for this project, while Figure 7 depicts an example of typical operating performance.

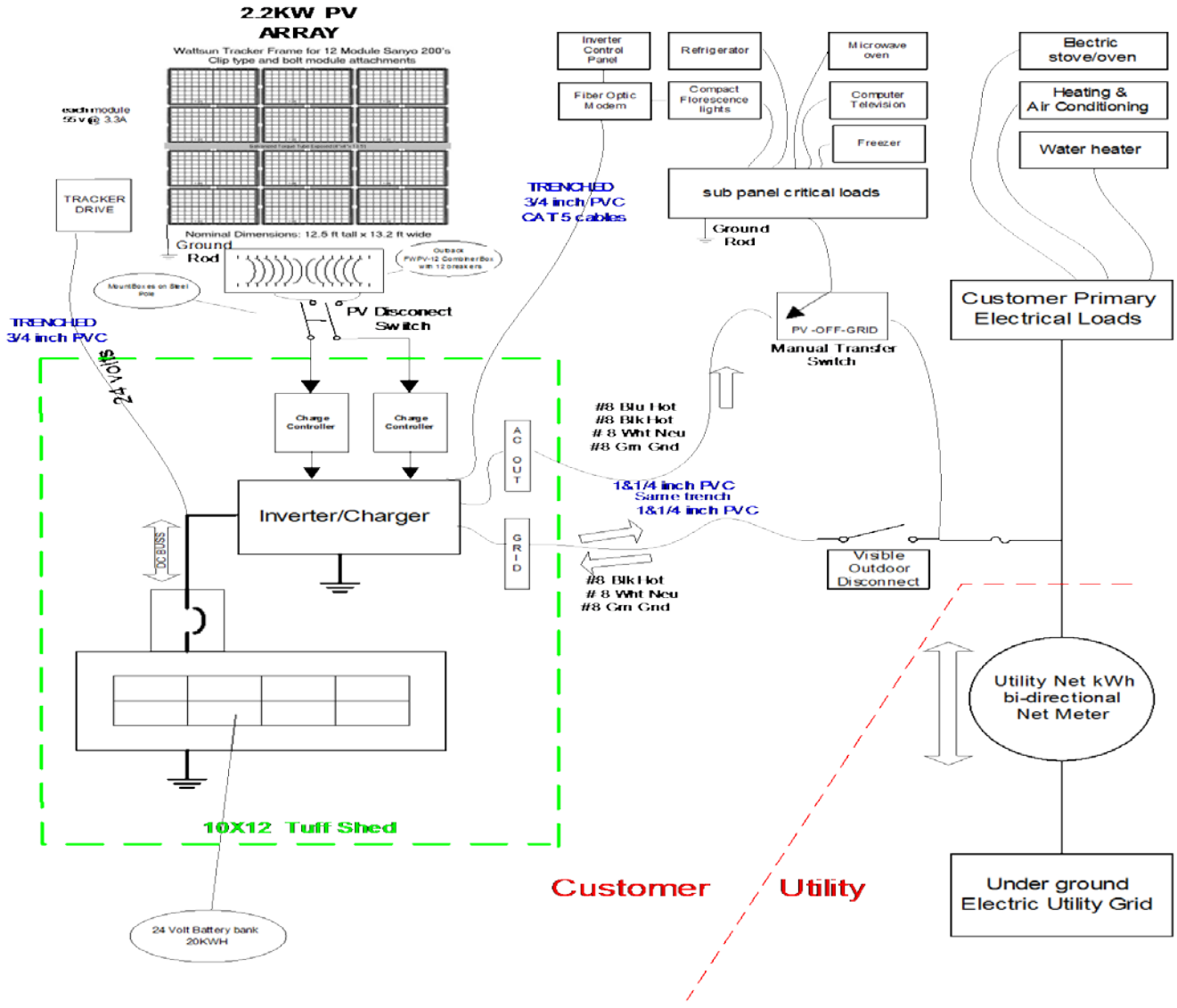

Figure 6. Schematic: Residential System Backed PV Systems 4 kW Inverters, 2.2 Kw PV & 20 kWh Battery Storage

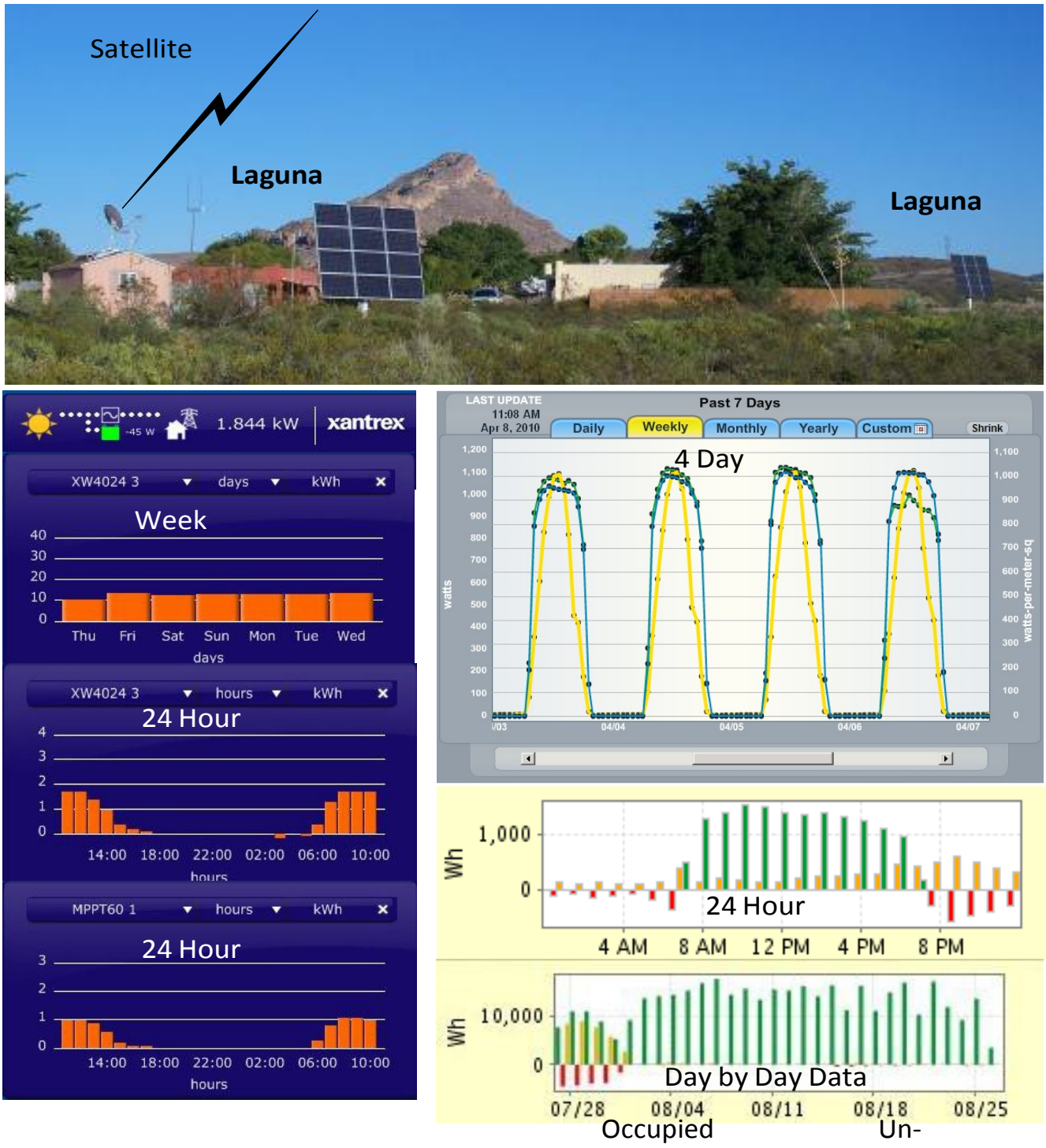

Figure 7. Residential 2.2 kW PV System Performance

Bi-Facial PV Modules

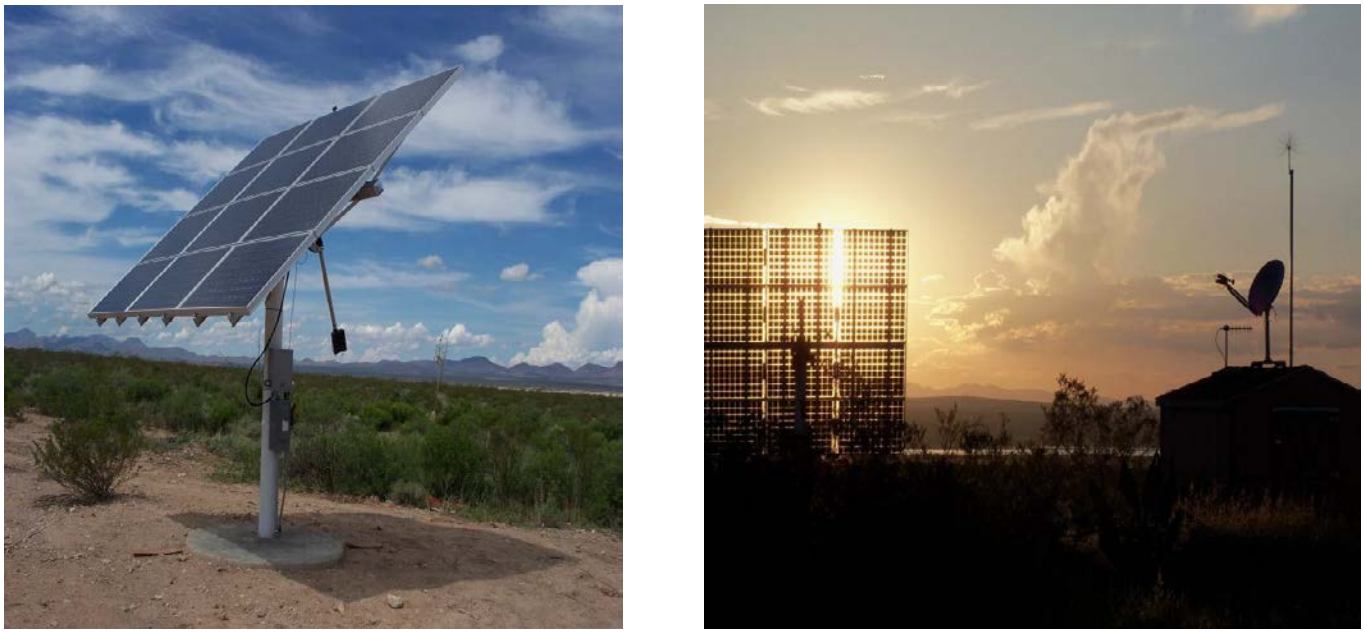

Figure 8. Sanyo Bi-Facial PV Modules

Bi-facial and thin film technologies from Sanyo were chosen for the PV modules shown by Figure 8. Bifacial Modules absorb light from both sides as illustrated in Figure 9. This dual absorption technology enables backscattered sunlight to be absorbed from reflected light arriving at the back of the panel. On this system, up to 26% greater power over the name plate rating was measured (2715 W) during the experiment. Shown here at sunset, the modules can seem to be somewhat transparent. At the time of this photograph, the system was generating 1 kW.

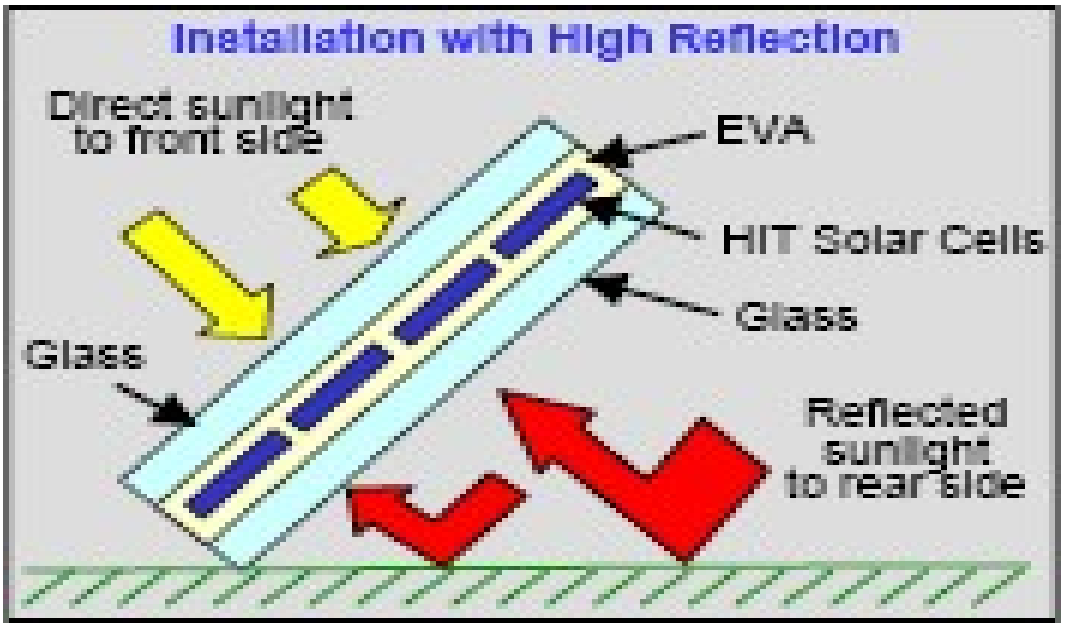

Figure 9. Sanyo Bi-Facial Modules Function

Figure 10. Laguna 10 Control Systems

A lightning prevention and protection system was designed and installed on both residences. The system, shown in Figure 10, uses a spine ball field emitter to neutralize charged clouds in the vicinity thereby reducing the possibility of a strike. The system is also capable of withstanding a direct lighting strike, and provides a layer of protection (security) for the electronic devices inside. Lightning grade transient absorbing Metal Oxide Var-resistors (MOV) arrestors were installed on both the AC and DC busses of these systems.

Controller, inverters, and battery installation for the residences are depicted by Figure 11 (Laguna 10) and Figure 12 (Laguna 12) on the following pages.

Figure 11. Laguna 10 Inverter and Batteries

Figure 12. Laguna 12 Inverter and Batteries

In designing the residential PV systems, NMT researchers purposefully minimized changes to the existing wiring of the residences used for the subject research. Also, upon examination, it was noted that the as built drawings did not reflect the actual wiring that was in place. For these reasons new wiring was added so that no electrical modifications to the existing wiring were necessary. The photos below show the new "plug mold" wiring and CFL lights. This arrangement worked out very well during utility outages. The residence could still have light; prepare food; keep food cold/frozen; watch TV; use the Satcom Internet transceiver, local Microwave WAN, computers and related equipment. Pictures of the typical wiring for several appliances are shown in Figure 13 on the following page.

Refrigerator and Microwave Power and Light

Television, Modem Power and Light

Freezer Power and Light

Figure 13. New Wiring

50 kW Grid-Connected EMCORE PV System

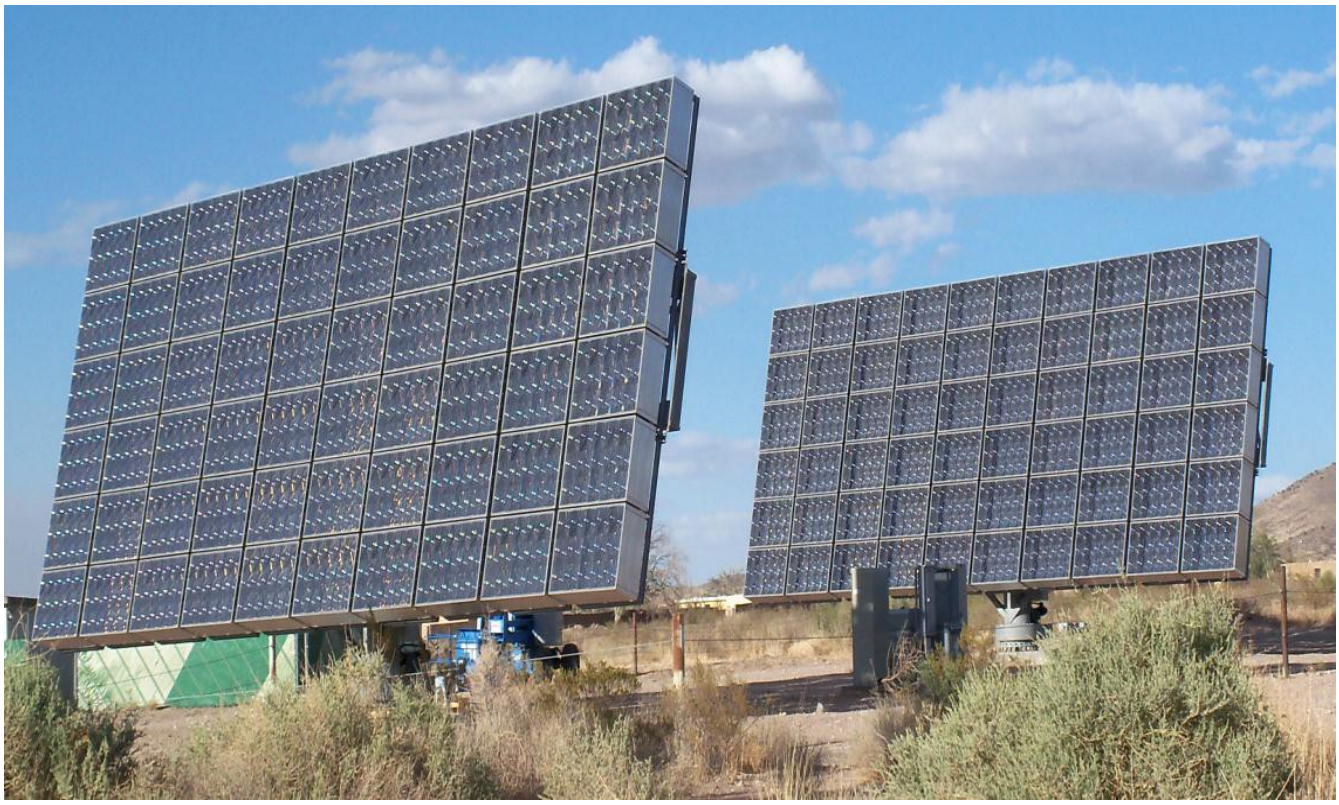

Figure 14. 50 kW Grid-Connected EMCORE PV System

EMCORE Multi-Junction solar cells consist of three separate solar cells combined in series monolithically. Each cell, or junction, is formed with materials that capture different portions of the solar spectrum. The selection of appropriate materials and junction thicknesses allow for optimization of the cell efficiency and response to the solar spectrum.

This 50 kW system was installed in 2009 and connected to the grid after approval by the local utility, Columbus Electric Cooperative. The purpose of this system was to test EMCORE's Concentrated Photovoltaic (CPV) technologies and perform advanced testing of the newest version of PV inverters available at the time. It was also intended that, during this research project, any power generated by this installation would be used to offset the local power consumption at Playas. Physical specifications for the system are shown in the following table (Figure 15). Other attributes of the CPV solar array, as well as pictures of the actual installation, are shown by Figures 16 through 20 on the following pages.

Specifications	Metric Measurement	Standard Measurement
Width	18.1 m	59.38 ft
Height	7.5 m	24.6 ft
Collecting Area	98.95 square meters	1,065.1 square feet
Weight	10,191 kg	10.029 tons
Wind Survival	145 kilometers/hour	90.10 miles/hour

Figure 15. EMCORE PV System Specifications

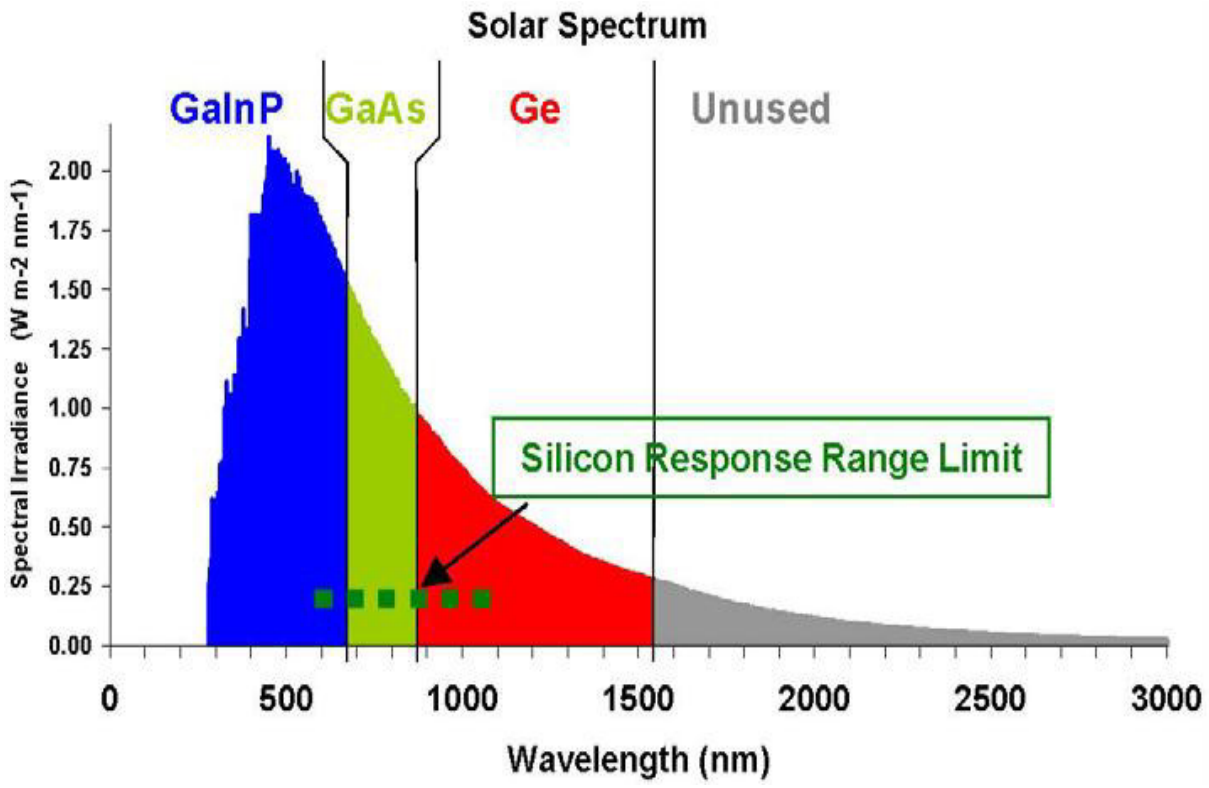

Figure 16. Solar Spectrum and Wavelength Captured by the EMCORE III-V Triple-Junction Solar Cells

The tracking control system uses variable speed motor controllers. The motors and controllers are wired with positional encoder and reference sensors with positional resolution of 0.01 degrees. The tracking control operates continually during the day rather than use a stop/start operation. This affords a tracking accuracy of better than 0.02 degrees in operation. The operating principal for tracking the sun is a hybrid. Motor control is closed loop using motor encoders for feedback. Position control is open loop using an accurate sun position algorithm. Adjustments to the position algorithm can be automated using current, voltage, or power measurement of the solar array.

Inverters

Connecting System to the Grid

Visible Grid Connect/Disconnect

Figure 17. Inverter Testing

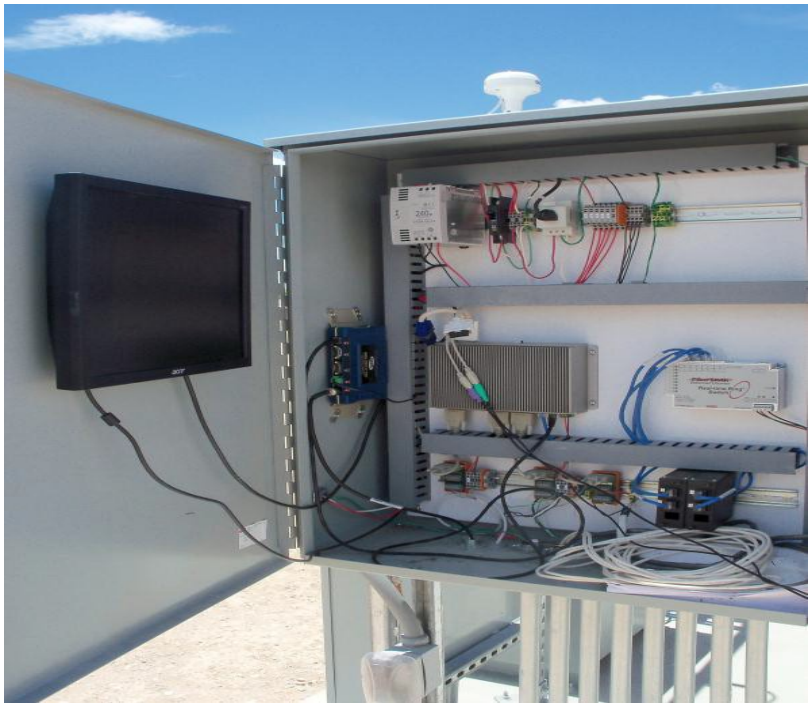

Figure 18. Supervisory Control and Data Acquisition System (SCADA)

The SCADA system includes a Graphical User Interface (GUI) that displays tracker position, energy production, meteorological data, synchronous two-axis tracker motion control with max energy tuning function, manual movement control, severe weather stow protection, continuous and historical event recording, a trouble or fault messaging system, SQL data storage with firewall security protection, WEB data publishing and user level security.

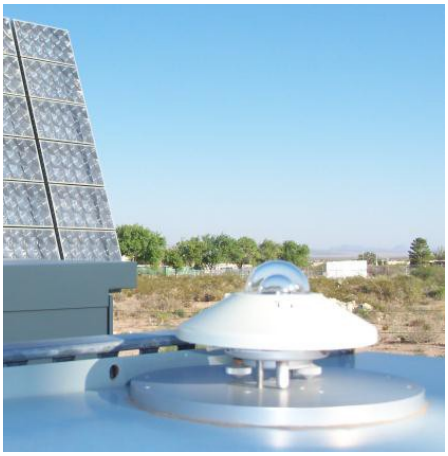

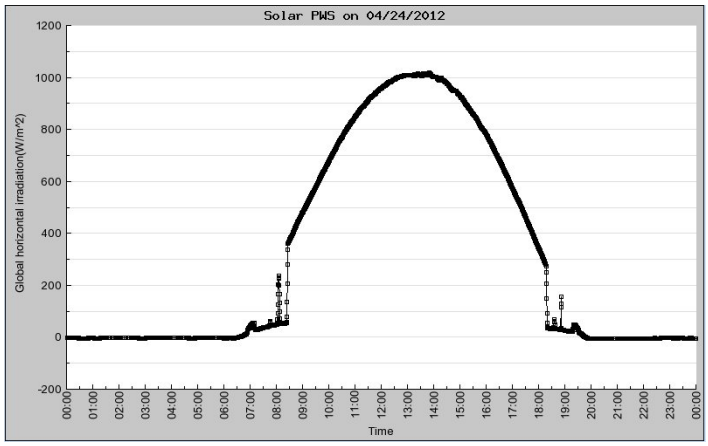

Figure 19. Kipp & Zonen CMP-11 Pyranometer

This system also includes an Irradiance (Sunlight) Sensor and records waveform in watts per square meter. Solar intensities of over 1150 w/m^2 were measured during this project.

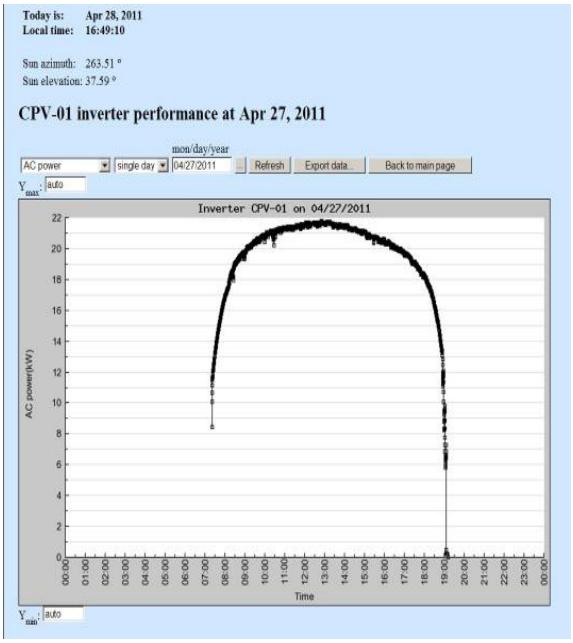

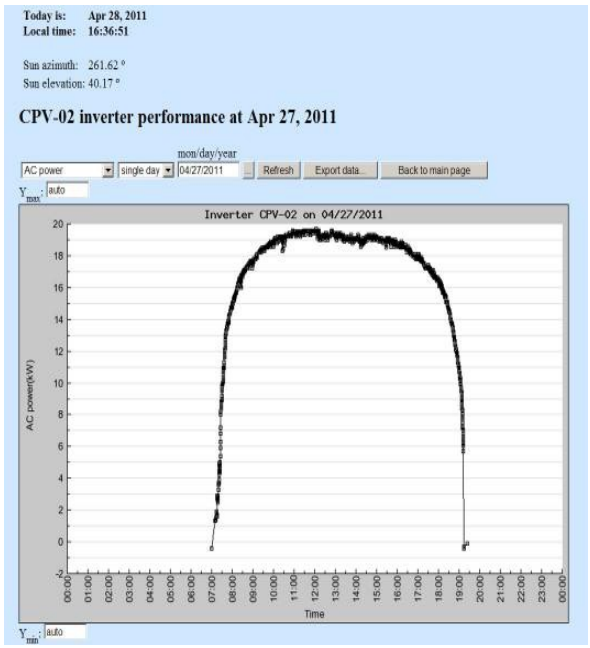

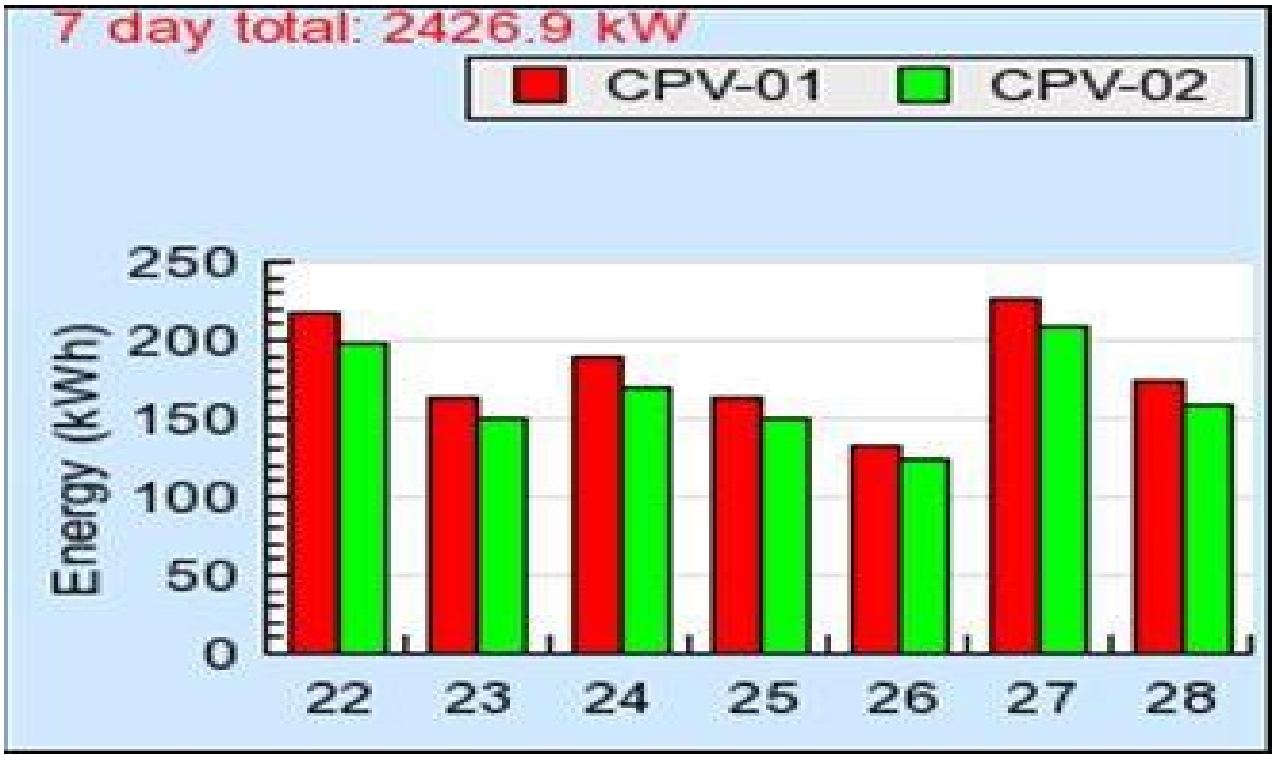

Figure 20. Inverter Performance

EMCORE claimed that their CPV cells could withstand full concentrated (500) suns without damage. Their Gen2 design, however, was not adequately sealed against dust and dirt and, over a short time; dust absorbed by the system damaged the cells' optical coating. This caused the cells to fail prematurely.

The failed cells also developed ground faults and the system was shut down while EMCORE provided a newer design of CPV cell and a newer Gen3 module. The Gen3 modules preformed at up to 86% of the 50 kW specifications. The best solar to electrical efficiency recorded during this project was 23%.

Occasionally, one or both inverters would fail to start harvesting energy in the early morning. This problem was brought to the attention of the inverter manufacturers and several site visits were performed. The self-start problems were never totally resolved and user intervention was required to manually stop the trackers. NMT engineers were concerned that the new Gen3 cells could be damaged because, during the harvesting process, energy is being extracted from the cells. This removal of electrons provides some cooling effect.

During June and July of 2011, manpower was reduced at the site and user intervention was not always possible. The PV cells in the modules were damaged due to excessive irradiation and heat as illustrated below by Figure 21, and the associated impact on energy output shown by Figure 22.

Figure 21. CPV Cell Damage from 500 Suns

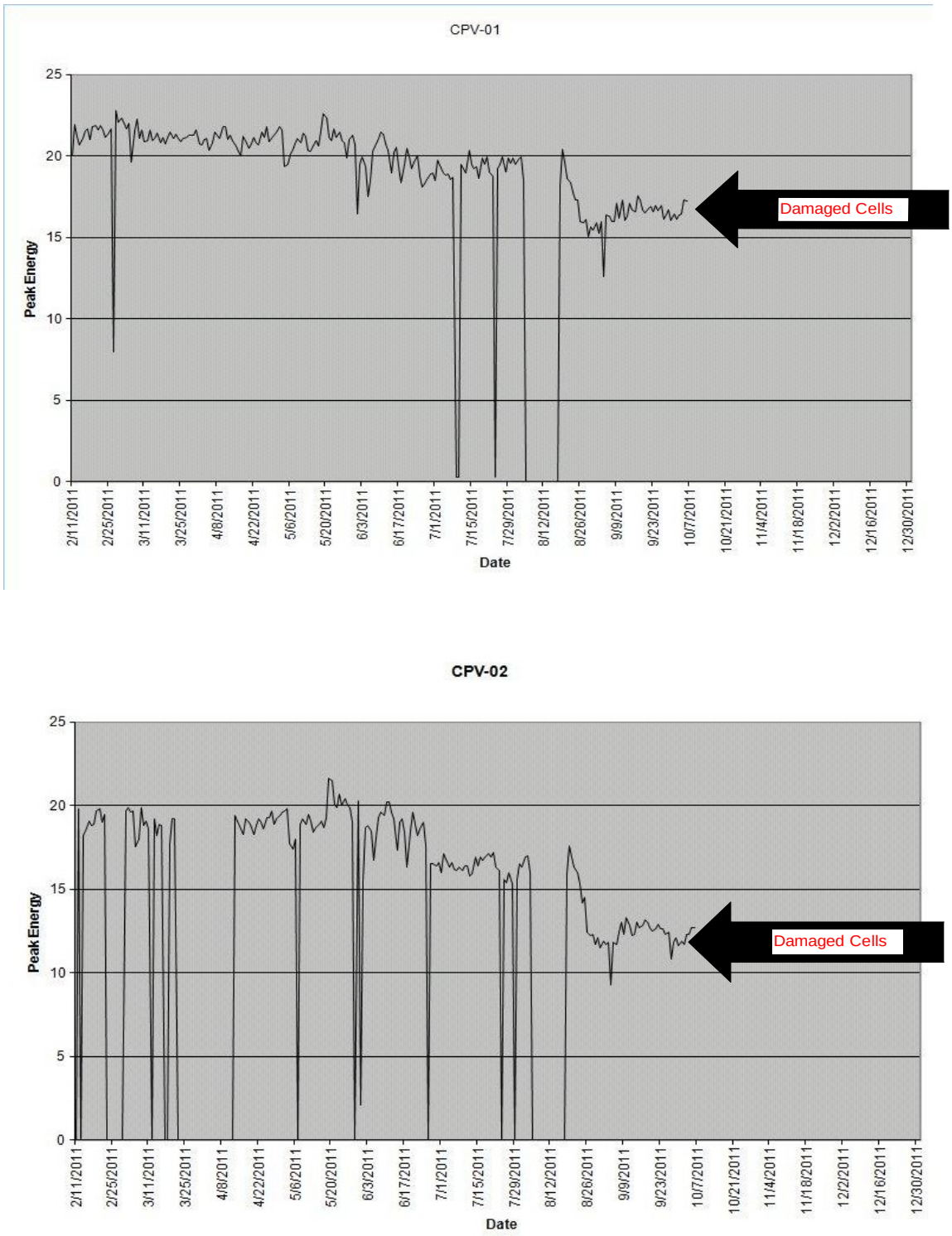

Figure 22. Decreased Energy Output Due To Damaged Cells

NMT engineers worked with the manufacturer to replace the cell units and installed a software interlock using a Kipp & Zonen CMP- 11 Pyranometer interfaced with the SCADA. This new interlock simply stops the tracker thereby preventing damage. The fault is cleared the next day by the SCADA unit and the unit is restarted.

Micro-Grid Design

The proposed Micro-Grid (depicted by the single line diagram of Figure 23) would normally be connected to the existing electric power utility through the Point of Common Coupling (PCC). Through the PCC the Micro-Grid can disconnect from and export power to the utility grid at any time. These features provide researchers the ability to perform testing, make measurements, and to add new Distributed Energy Resources and supply critical loads without any grid support if necessary. At the time, Playas management was considering converting the medical building into a data center. Many plans were evaluated that would include using the Micro-Grid as reliable power for the new data center. It was finally decided to leave the main information technology (IT) functions in the Command, Communications, and Control (CC&C) building. This building is also referred to as the Classroom Building.

Due to limited availability of wind resources at Playas, a wind turbine renewable energy system was not implemented during this project. A 48 VDC wind system could be added to the classroom critical power system at any time.

Loads Connected to the Micro-Grid

Under normal grid connected conditions, power from the grid will flow through the 2 UPS systems and on into the building loads. Thus building power is supplied by the UPS inverters at all times. The exception to this would be if the inverter by-pass switch is in the by-pass setting. During a power outage the inverter continues to provide power without missing a cycle. This is because the UPS is now running from energy stored in the batteries that have been float charged by the grid. If at the moment of the outage the Micro-Grid DERs were producing power and connected to the UPS buss they would shut down as required by UL 1741.

An electrically operated circuit breaker will open, separating the Micro-Grid from the Utility. During this time the reciprocating engines are started, speeds matched and then allowed to connect to the Micro-Grid. Upon reenergizing of the Micro-Grid the DERs will see a stable 480 VAC signal and they will come back on and provide power into the Micro-Grid. The UPS systems will now be running from the Micro-Grid.

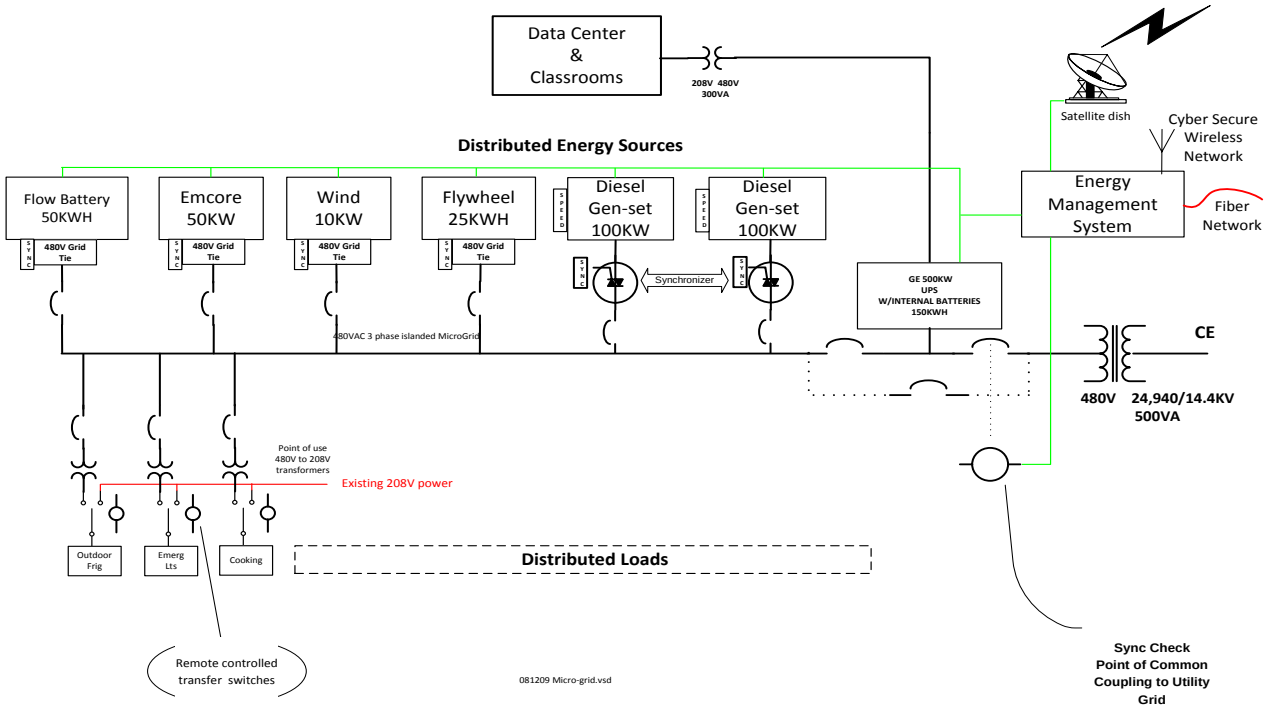

Figure 23. Micro-Grid Design

Figure 24 shows the initial layout of the Playas Micro-Grid Distributed Energy Resources (DERs) that were considered for installation at Playas including:

- 2 identical 100 kW Reciprocating engines (flex fueled) Bio Diesel, #2 Diesel, kerosene, or JP-4
- 2 identical 25 kW EMCORE PV tracking Modules with 480 V Grid Tie
- 5 to 10 kW of Wind turbines with 480 V Grid Tie
- Flow Battery Storage technologies with 480 V Grid Tie

The DERs can be any technology interfaced to the Micro-Grid through synchronized power electronics and intelligent controls. Any and all DERs will only be connected after the PCC. Each DER power inverter connected to the Micro-Grid will be able to respond to load changes in a predetermined manner without data from other sources or locations. This arrangement enables DER to be added to the Micro-Grid without hardware changes to the control and protection of units that are already part of the PCC system.

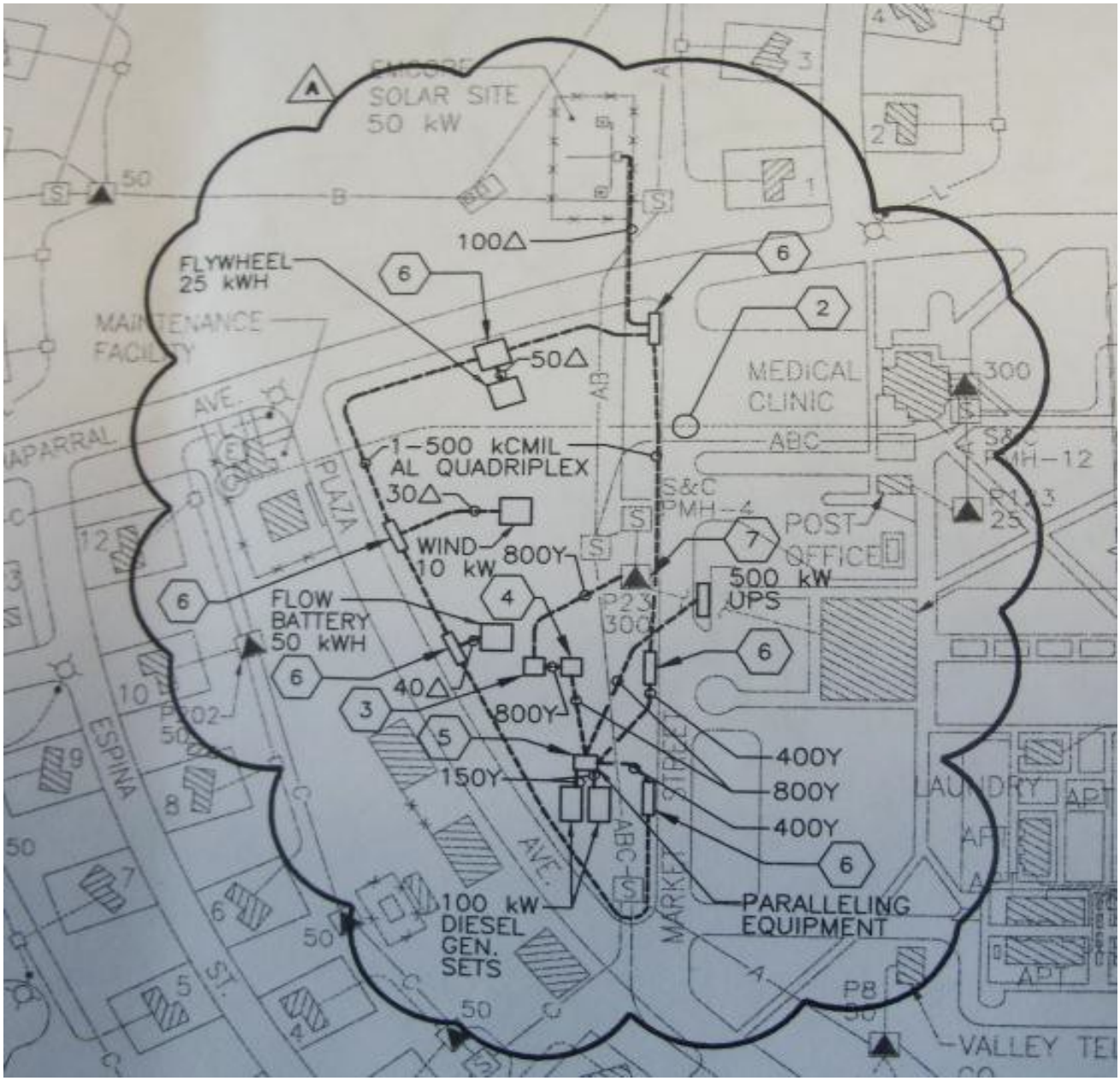

Figure 24. Initial Design of Playas Micro-Grid

3-Phase Micro-Grid Research & Development Overview

The proposed New Micro-Grid was designed to provide clean, reliable and sustainable electric power at all times (24/7/365) much like an Uninterruptible Power Supply. Similar to the Micro-Grid, all grid interactive DERs at Playas will automatically disconnect from the utility feeder if the utility power supply fails. The Micro-Grid will contain energy storage devices that will sustain its operation for a period of time. During this time intelligent decisions will be made by a pre-programmed energy management system or by manual or remote operation. Selected critical loads that are normally powered from the grid will be electronically rerouted and connected to the active Micro-Grid.

The Point of Common Coupling defines the separation between the utility grid and the Micro-Grid. At this point, the Micro-Grid must meet all prevailing interface requirements, such as defined by the New Mexico Public Regulatory Commission, the National Electrical Code, and the local electric utility. Included in the PCC was a visible disconnect (switch) that the electric utility can access. The PCC device has the ability to sense power flow in any direction, phase angles, utility and Micro-Grid voltages and has programmable trip points.

Depending on the voltage class, the speed of operation required, and fault current capability, the PCC separation device incorporates a high-speed static switch. In all cases, the protection scheme is designed for the characteristics of the specific interconnection so that the Micro-Grid separation device will trip as needed. This design is relatively simple, such as monitoring current magnitude and direction on each phase and sending a trip signal to the separation device if preset limits are exceeded.

Micro-Grids can provide premium power functions using control techniques where problems such as slight errors in frequency generation at each inverter and the need to change power-operating points to match load changes need to be addressed. Depending on the programming of the energy management system, when the Micro-Grid is connected to the grid, critical loads will receive power both from the grid and from local DERs. If the grid power is lost because of voltage drops, faults, blackouts, etc., the Micro-Grid will transfer smoothly to an islanded operation mode.

The Micro-Grid contains battery storage of approximately 200 kWh so that a brief outage (i.e., several minutes to several hours) will not affect the ability of the Playas Training and Research Center (PTRC) to continue business as usual. Reciprocating engines using flex fuel will synchronize with the Battery UPS systems to sustain the Micro-Grid if the utility power outage exceeds the kWhs stored in the batteries and renewable sources (such as at night time or with no wind).

Finally, once utility service has been restored the Micro-Grid must have the means to synchronize and reconnect with the grid. Ideally, this should take place as soon as the grid has had an opportunity to pick up all previously disconnected loads and to stabilize, which may require several seconds to several minutes. The Micro-Grid must have a control scheme that can bring all DER on the Micro-Grid into synchronization with the main bulk power provider, based on measuring the voltage on both sides of the PCC separation device. Whether this resynchronization and reconnection are done automatically or manually may vary depending on the characteristics of the Micro-Grid and the utility grid. Resynchronization philosophies and techniques are being studied to determine appropriate approaches. Most conventional distribution protection is based on short circuit current sensing.

There are many types of DERs – including fuel cells, micro-turbines, photovoltaic systems, wind turbines, and battery energy storage systems – that use inverters to interface with the grid. This class of DER may be capable of supplying not more than twice the load current to a fault, so the orders-of-magnitude larger fault current on which conventional overcurrent protection is based is not present. Some overcurrent sensing devices will not even respond to a small amount of overcurrent. Those that do respond will take many seconds to do so rather than the fraction of a second that is required. Thus, alternate means of detecting an event need to be adopted. There are alternate means available, such as the use of impedance methods, zero sequence current and/or voltage relaying, and differential current and/or voltage relaying. None of these alternate means were tested during this project.

Classroom Critical Power System

Figure 25. Command, Communication & Control (CC&C) (Classroom Building)

The Classroom Power System was completed and began producing power on June 10, 2011. Some of the installed equipment is depicted in Figures 25 and 26, the diagram of Figure 27, and the schematic of Figure 31. System components are programmable, interactive, and grid connected and can sell excess power back to the local electric utility. Features include:

- 18 kW of 3 phase uninterruptible power
- 36 kW of surge capacity
- Subpanel feeds critical IT infrastructures and lighting
- 12.5 kW of Solar PV Modules
- 70 kWh of Absorbed Glass Matt batteries
- Information Technology communications platform & energy management system
- Easy to add additional DER sources to the 48 VDC buss
- Easy to add AC generating source; bio-diesel; propane; gasoline
- Dual AC busses with a 48 VDC storage buss create small Micro-Grid at this site.

New wiring was added so that no electrical modifications to the existing building wiring were necessary.

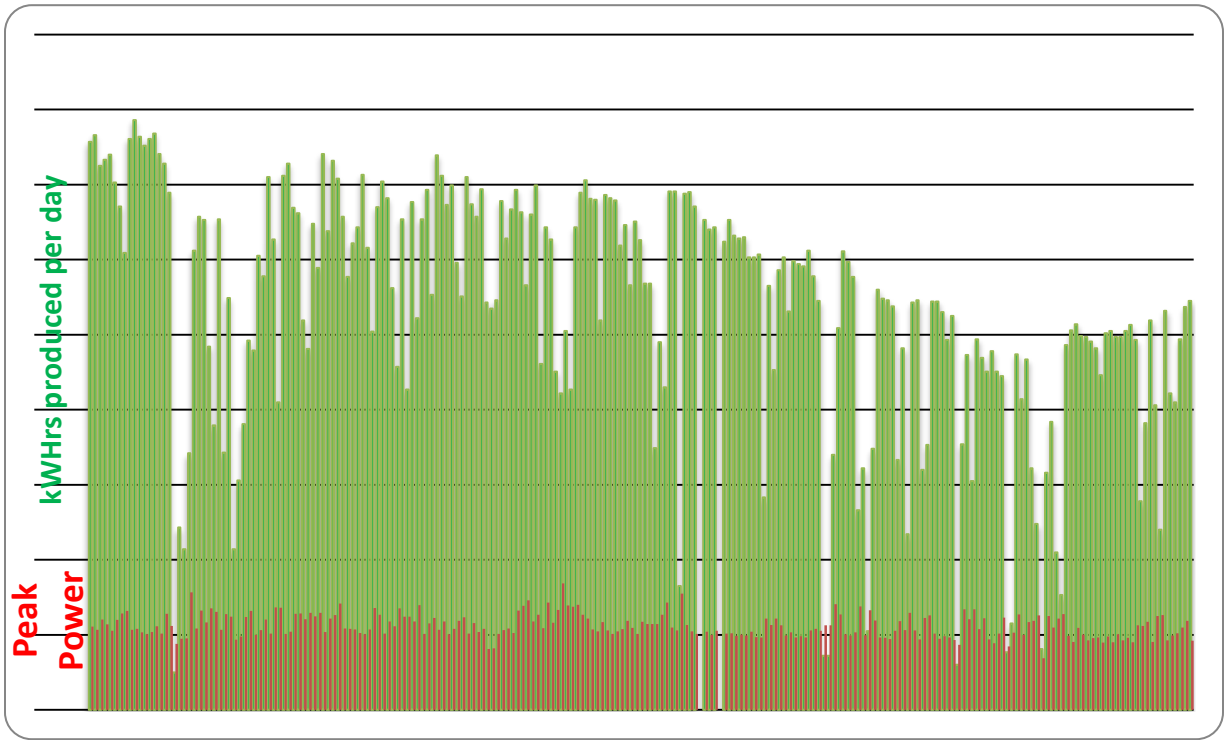

Figure 26. Peak Power (RED) and kW hours (GREEN) produced from Classroom 12.6 kW PV Array

Critical Loads for the Classroom Training center

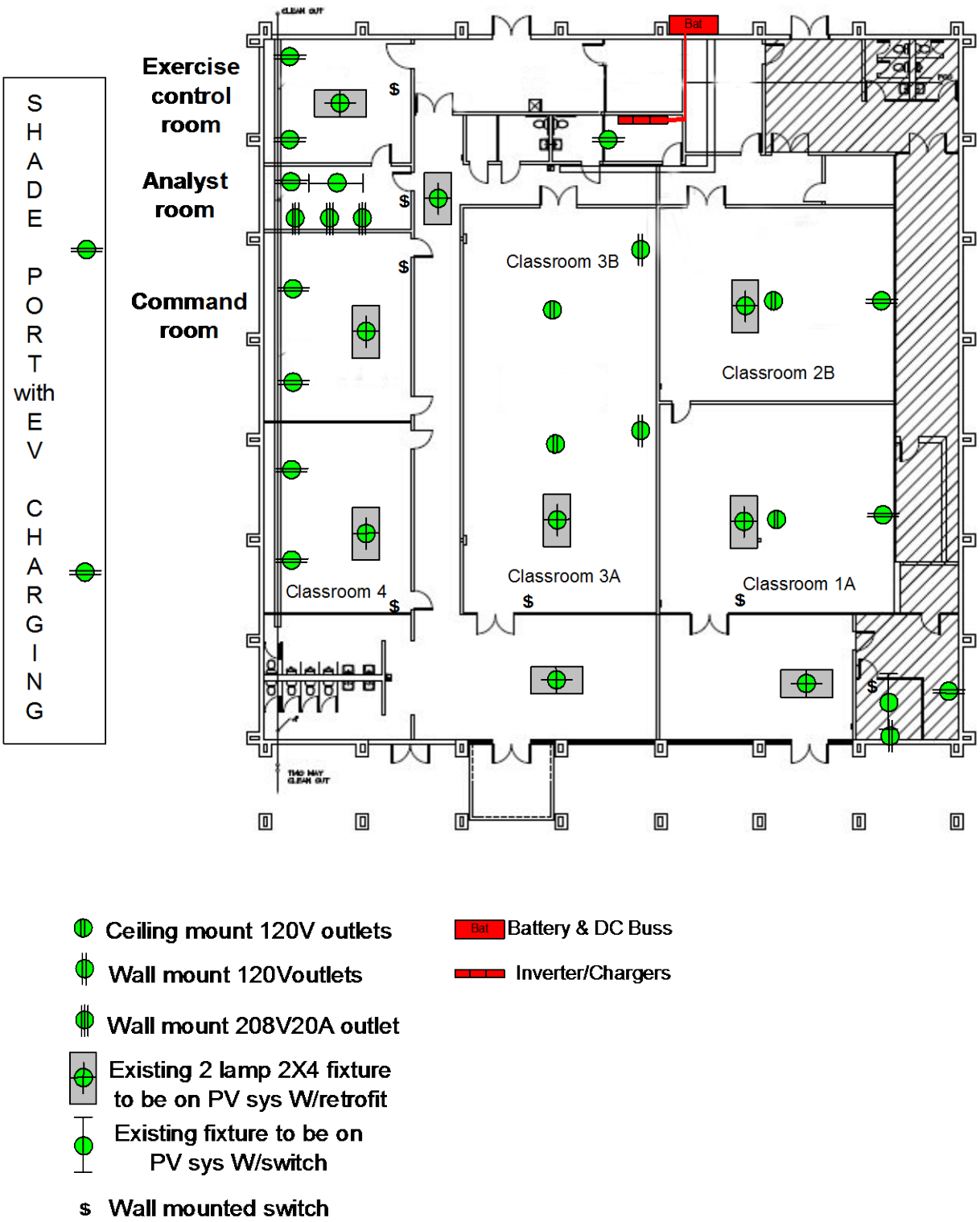

Figure 27. Critical Loads, Command, Communication & Control (CC&C) Building

Information Technology System Platform

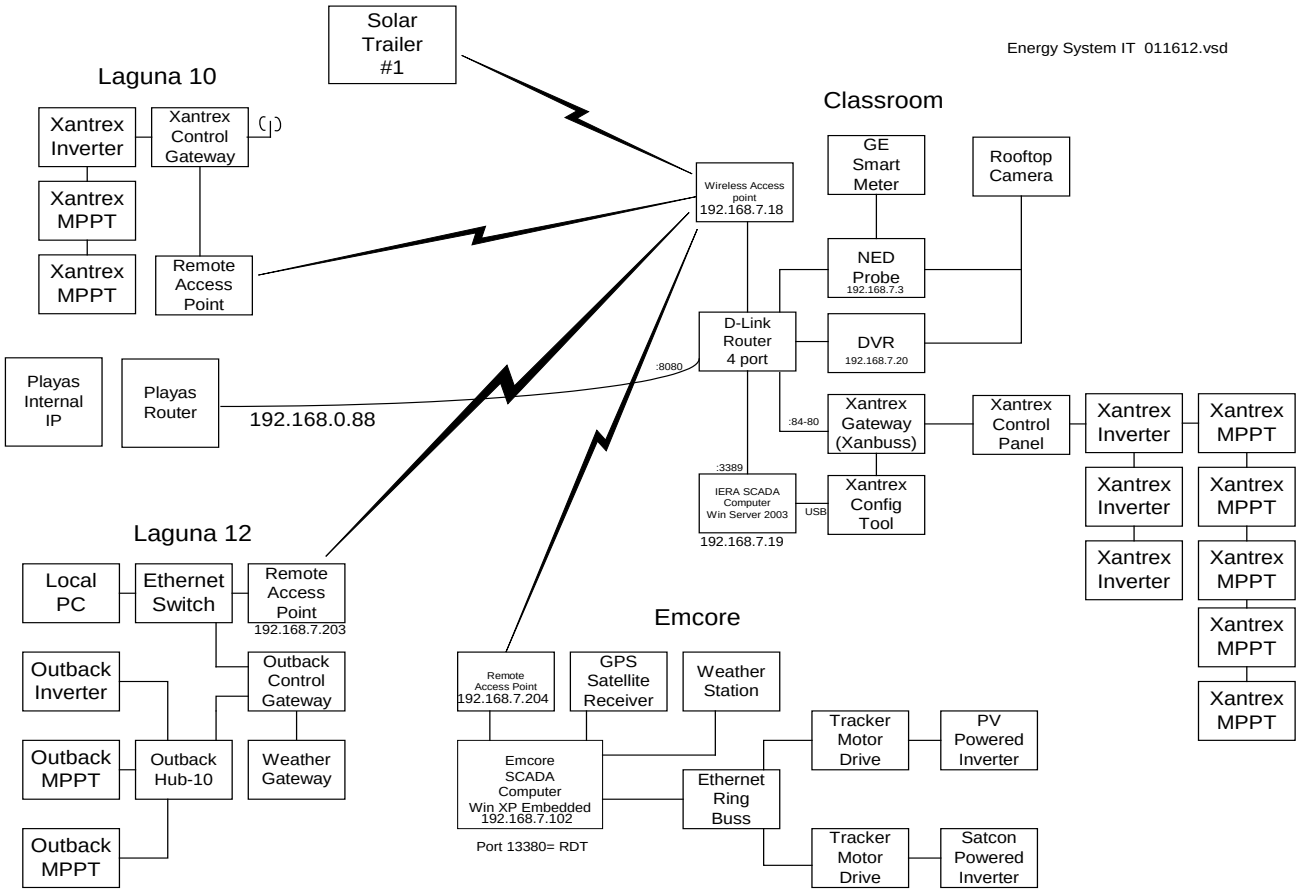

Figure 28. Information Technology Systems and Energy Management System

The Information Technology platform (shown by Figures 28 and 29) sends messages to key personnel. The project has implemented a special IT system for connecting the existing Playas fiber network and the WLAN. This computer server has dual Ethernet capabilities and manages control and communications between the Ethernet, Fiber, and Microwave information exchange. These new components, secure server, microwave, and fiber modem are powered by the classroom's battery backed PV system that stays energized when the utility power fails. Combining these technologies forms a powerful, reliable and uninterruptible IT platform. Many other functions and alerts are programmed into the IT platform including energy management. Features include:

- NEDProbe utilized for advanced control of the energy management system
- Web server USB connected to the SCADA computer in the IT platform
- NEDProbe can monitor 80 sensors and graph 16 sensors
- Video and snapshots recorded from video sky cam overlooking trackers
- Built in graphing and logging
- Full Modbuss support (RS-485)
- Expandable Intelligent Detection Sensors and Dry Contact Modules

Users can create programs that make intelligent decisions controlled by the SCADA computer.

Figure 29. IT Platform Running During Total Grid Failure

It is vital to understand current power consumption and gain a better understanding of where energy use is high or low and identify areas where consumption can be reduced. For Telecoms and Data Centers it is important to keep on top of power consumption. This is now possible through smart or sub-metering where power is measured coming into specific rooms or buildings. This IT platform combined with power monitoring sensors intelligently monitors power consumption and sends out notification and alerts to give managers complete control over our site's facilities. Data recorded by the IT platform using a "NEDProbe" and GE smart meter as the sensor is shown by Figure 30.

Grid Frequency
Recorded by IT platform

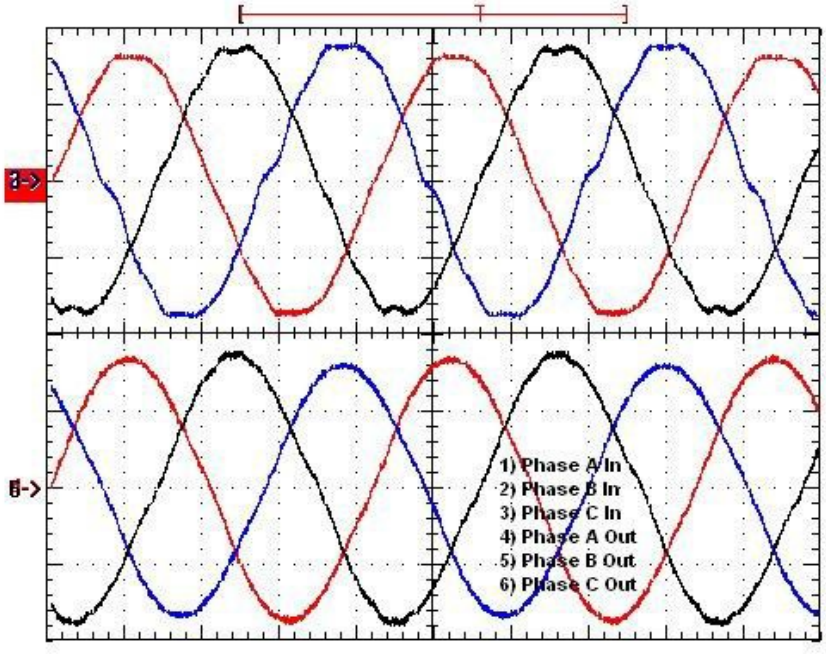

Incoming
208VAC 3 phase grid voltage

Output of DC\AC inverters
Power is supplied throughout
the building

Figure 30. Data Recorded By IT Platform Using “Nedprobe” and GE Smart Meter

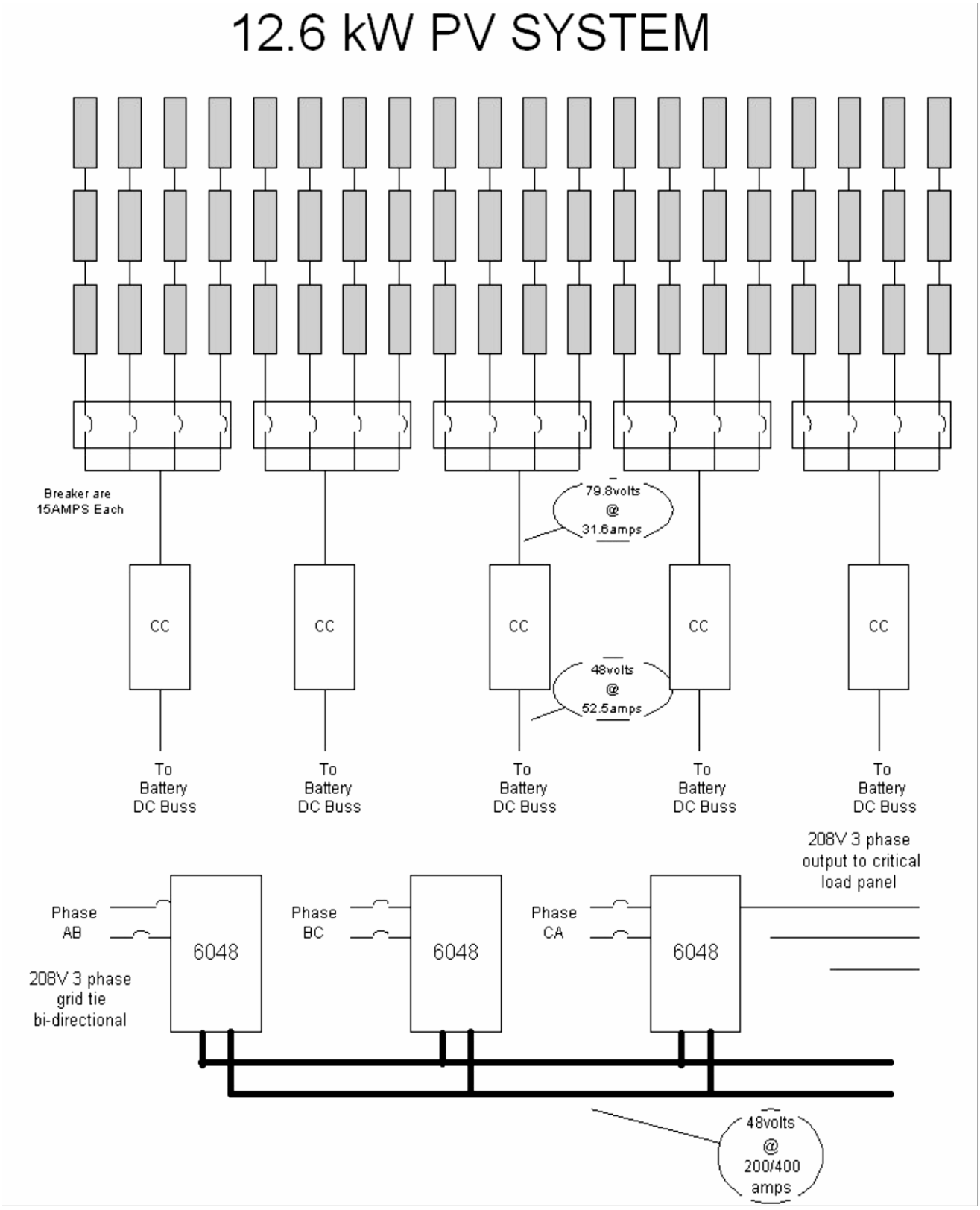

Figure 31. Command, Communication & Control (CC&C) System Schematic

Task 2.0: Micro-Grid Reliability Modeling (Co-PI: Kevin Weedeward)

The grid modeling portion of this project focused on several aspects related to incorporation of distributed generation, and modeling and analysis of power consumption at the building and town-level. In particular, accomplishments were made in the following areas:

1. Modeling the power delivery system at various levels (transmission line that feeds Playas, NM, three-phase distribution system within Playas, and the power consumption of the Command, Communication and Control (CC&C) building within Playas);
2. Parameter estimation for inventory model of loads when high-frequency power quality data is available at substations or buildings;
3. Forecasting loads making use of calendar, temperature and voltage dependencies;
4. Coordinated control of distributed generation; and
5. Analysis of a renewable energy system to determine viability to supply the grid-connected CC&C building.

Each accomplishment is summarized below along with data gaps and future work.

Modeling Playas Power System

Accomplishments

A transmission-level, single-phase model was developed of the area in which Playas is located. A geographic and one-line diagram of the electric power transmission system in that area is shown in Figure 32. A corresponding load-flow (sinusoidal steady-state) model of the transmission system was built and the resulting solution is shown in Figure 33. This load-flow solution gives nominal operating conditions for the transmission system that feeds Playas, and would serve as the basis for studies where the broader impact of distributed generation was of interest.

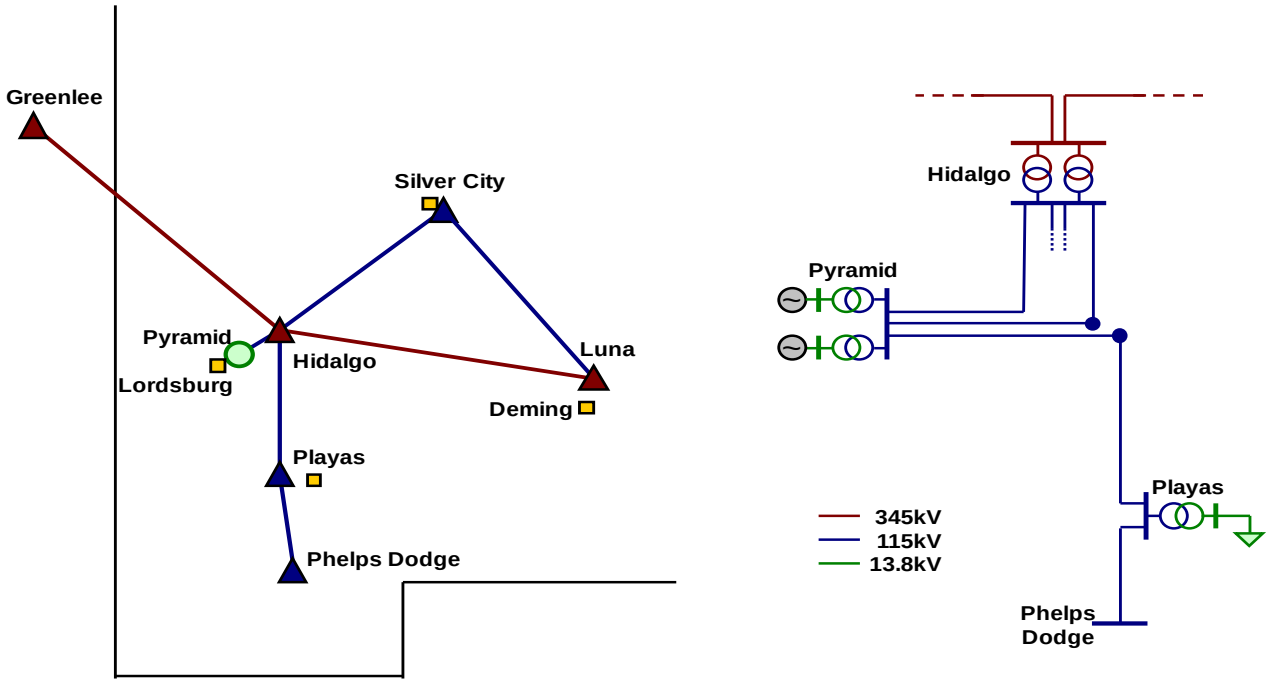

Figure 32. Geographic (Left) and One-Line (Right) Diagrams of Transmission-Level Power System Feeding Playas

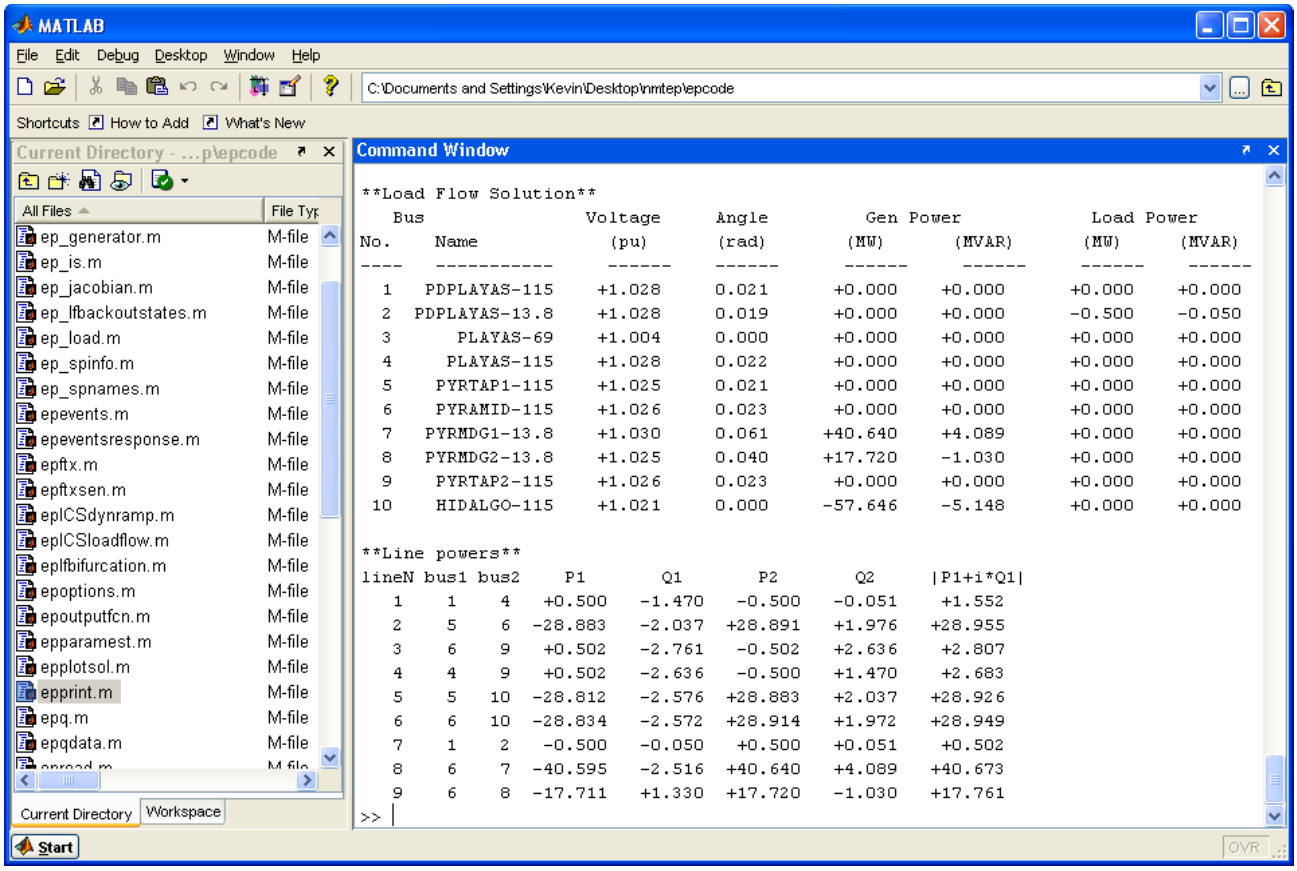

Figure 33. Load-Flow Solution of Model of Transmission System that Feeds Playas

Initial data was compiled and a three-phase diagram constructed to facilitate modeling the power distribution system of Playas. The three-phase diagram is shown geographically by Figure 34 with the corresponding schematic depicted by Figure 35. Together, these representations serve as the topology of the distribution system for which line, transformer and load data would need to be compiled.

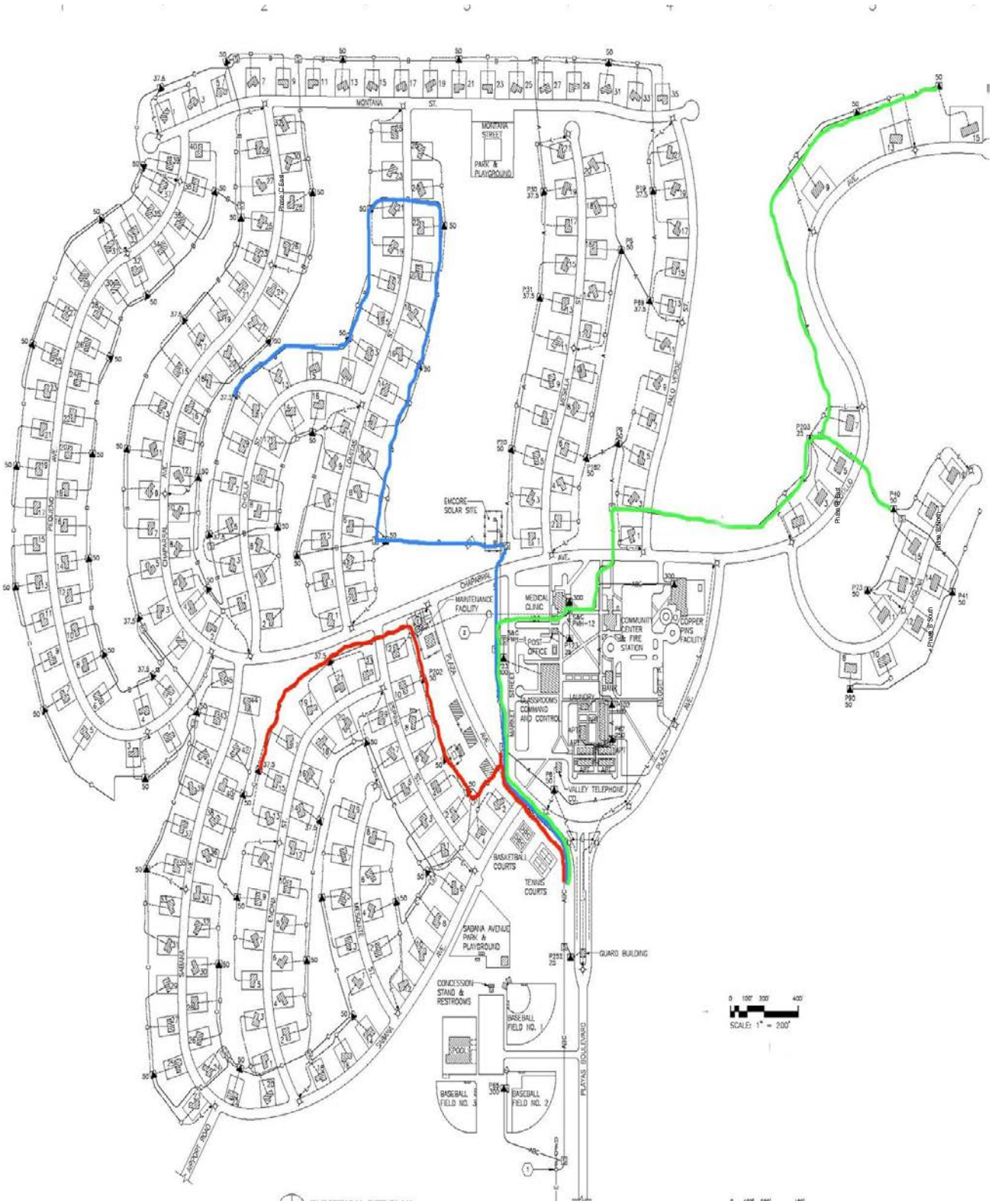

Figure 34. Map of Three-Phase Distribution System in Playas

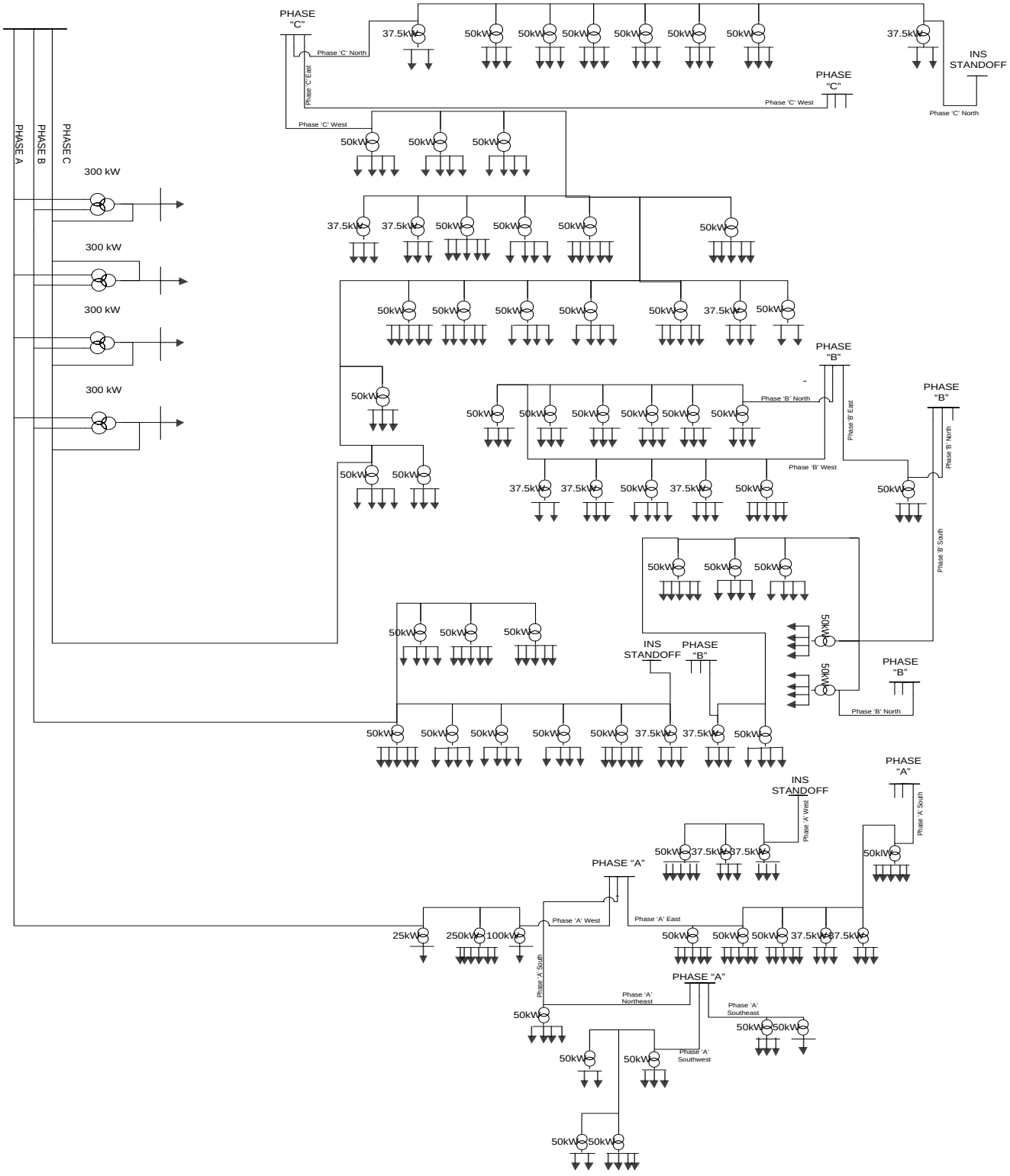

Figure 35. Parameter Estimation for Load Inventory Models in Electric Power Systems

An approach was developed to characterize power system loads through estimation of contributions from individual load types. A conceptual diagram (Figure 36) of the notion is shown where multiple load components contribute to the total power consumption by the fractional parameters λ_i that sum to one. In contrast to methods that fit one aggregate model to observed load behavior, this approach estimated the inventory of separate components that compose the total power consumption. Common algebraic and dynamic models were used to represent the loads, and parameter estimation was used to determine the amount each individual load component contributes to the cumulative consumption. Trajectory sensitivities formed the basis of the parameter estimation algorithm and gave insight into which parameters were well-conditioned for estimation.

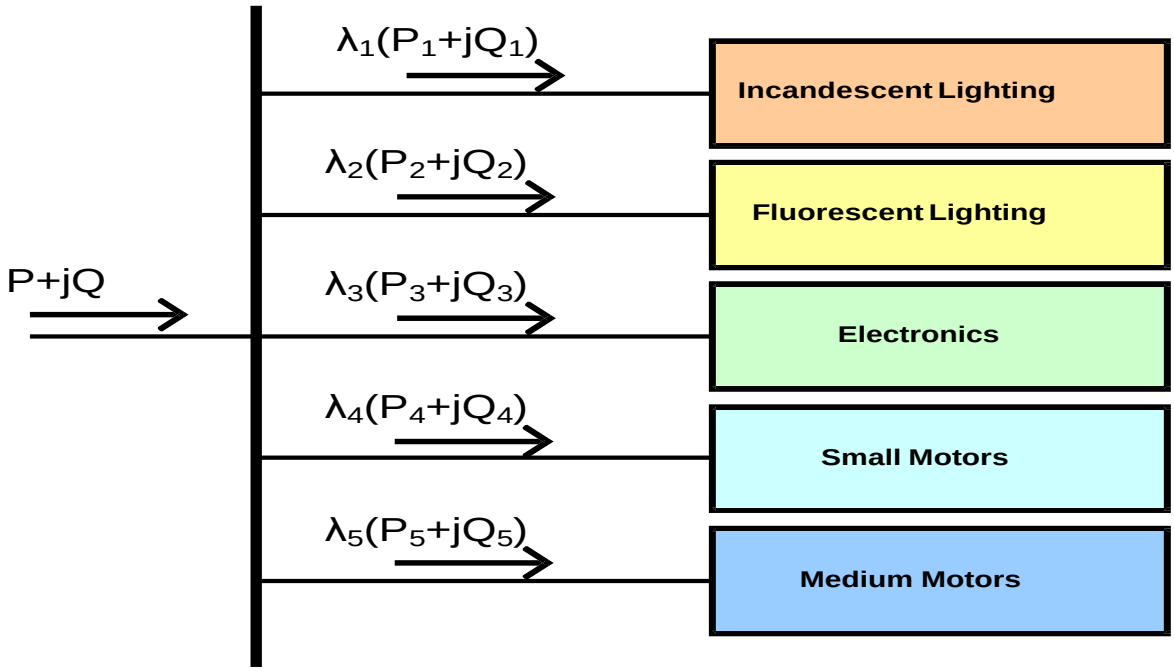

Figure 36: Conceptual Diagram of Load Inventory Model

As power system models and simulations used for planning and stability studies become more advanced, higher fidelity models of all power system components are needed. Loads are particularly difficult to describe due to their diverse composition and variation in time. The load inventory approach was implemented through simulation on power consumption data generated synthetically (via simulation) for a single phase. The results showed which load contributions were well-conditioned for estimation and those parameters that can be accurately estimated in the presence of measurement error. The results showed that the initial conditions of the load components' states are difficult to identify, however the load contribution coefficients are readily identifiable.

Figures 37 and 38 show the estimates of the composition parameters as they converge over iterations to their actual values.

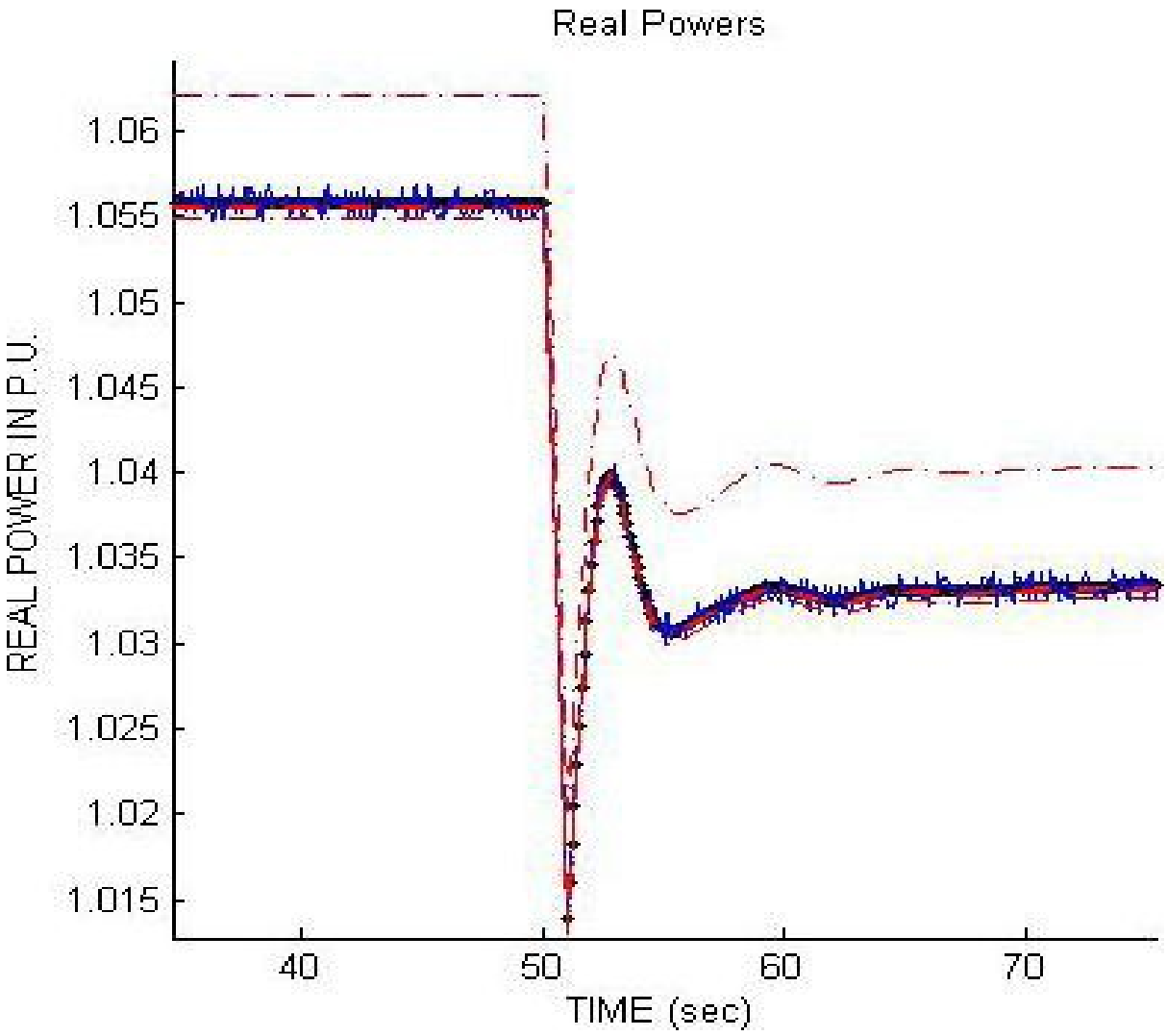

Figure 37. Simulated active power (blue), measurements (black diamonds) and trajectories (red) that correspond to iterative updates to load composition parameters

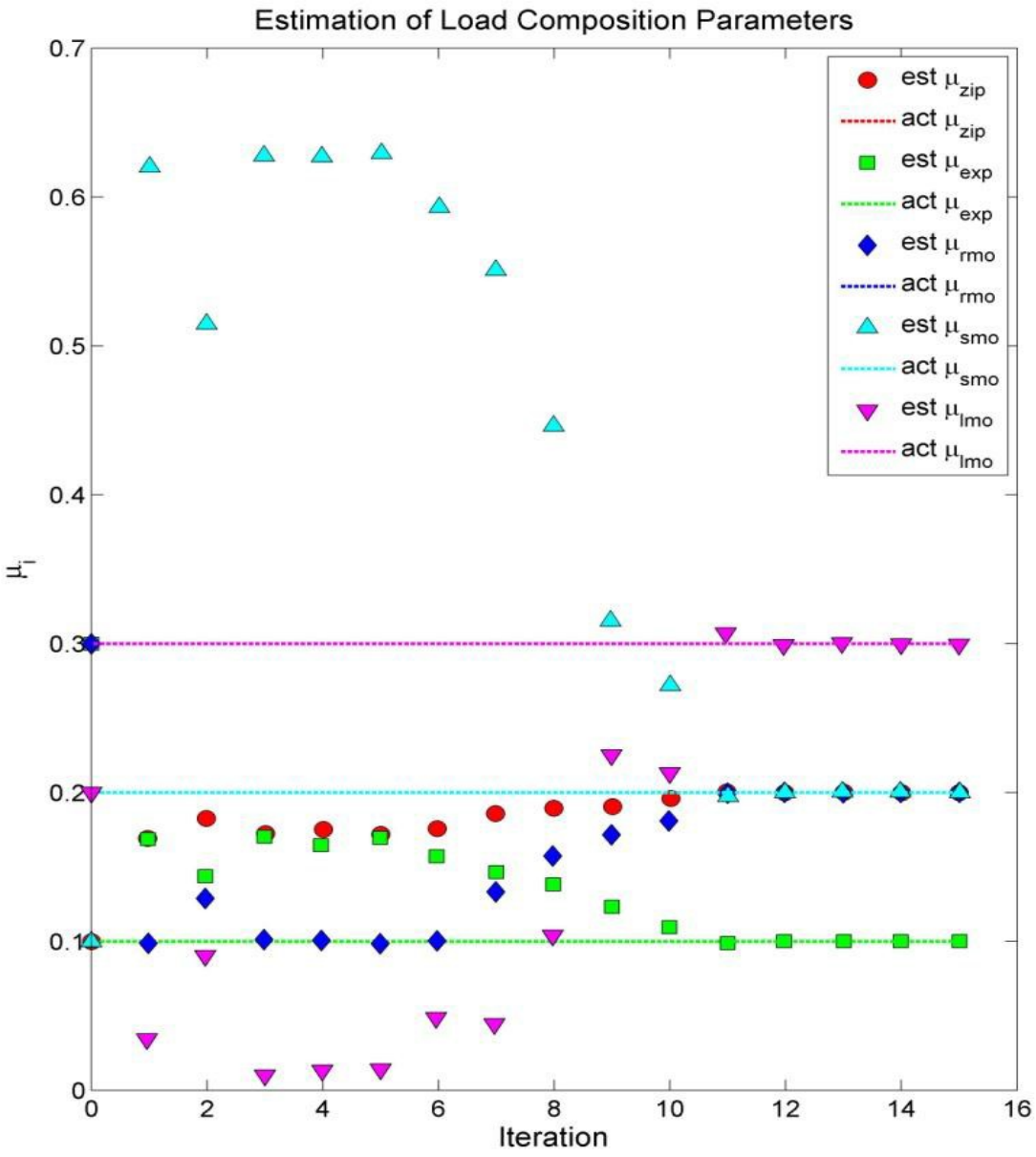

Figure 38. Load Composition Parameters Updated Per Iteration

Model with Voltage Dependencies for Electric Load Forecasting of Small Towns

A model was developed for short and medium-term load forecasting of the power demand for small towns. The heuristic model was developed and the coefficients of the model estimated using multiple linear regression. Based on analysis, polynomial-like terms were utilized to compose the model, which captures the relationship between the total load, and temperature and calendar variables such as hour of the day and month of the year. In addition to weather and calendar variables, the voltage dependencies were also included in the model to facilitate load-flow studies used in system planning and contingency analysis.

As a case study, historical data consisting of load demand, voltage and temperatures for a group of small towns in New Mexico was used to develop a model and forecast the short and medium-term load. The proposed model was used to

predict active power consumption for an upcoming month and favorable results were obtained for one week ahead to one month ahead. The predicted power consumption and actual power consumption for one week is shown in Figure 39. The mean absolute percentage error (MAPE) was less than 10% for the forecasted periods which indicates a favorable performance of the proposed model. The model was also tested on the CC&C building in Playas, but poor correlation between the building's power consumption, and temperature and calendar variables did not facilitate reasonable forecasts.

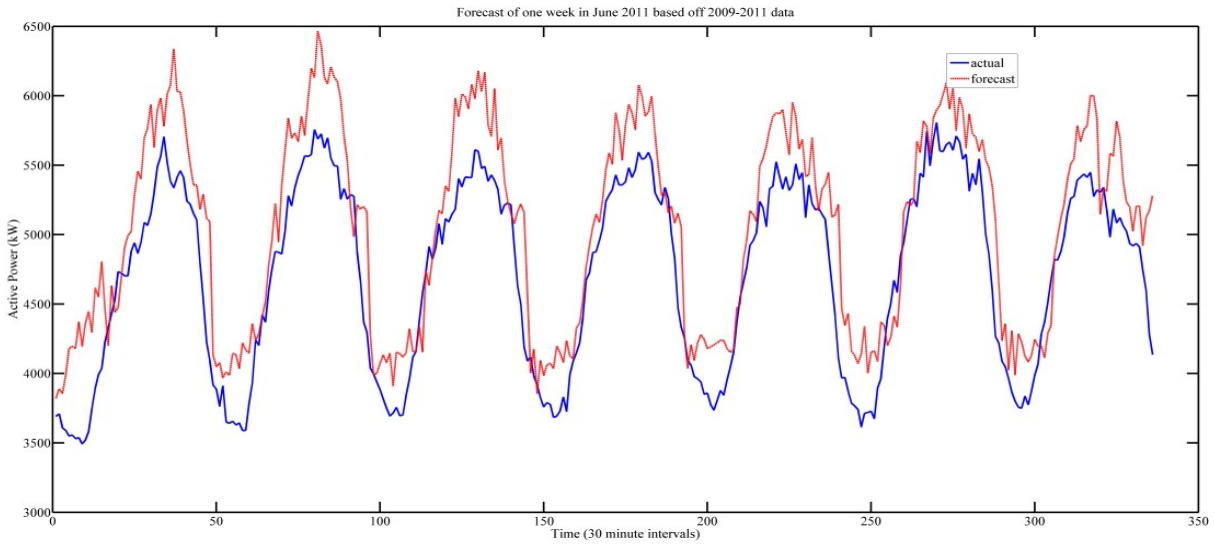

Figure 39. Forecast and Actual Load Consumption of Small Towns in NM

Coordinated Control of Distributed Generation

Although analysis and design of a three-phase, alternating-current power system typically assumes that the system will be balanced, many times that is not the case. An approach was developed to coordinate Distributed Energy Resources to balance characteristics among an unbalanced distribution system and correct power factor. Models for both the DER and the three-phase distribution network were developed and then combined to form a set of Differential Algebraic Equations (DAE) that represented the behavior of a distribution system. Two full state-feedback controllers with reference inputs were designed for coordinated control of DER. Both controllers were designed based upon linearization of the DAE model and permit closed-loop poles to be placed as desired. The first uses an additional matrix selected so that the outputs match the reference values in steady-state while the second uses an internal model design with integral to drive the outputs to the reference values. The internal model controller is more robust when it comes to model uncertainties such as network parameters or outside disturbances such as changes in loads.

A 5-bus test system (Figure 40) and a 10-bus test system (Figure 41) with inverter-connected DER are simulated and analyzed, and results are presented in Figures 42, 43, and 44. The control objective for the 5-bus test system is to balance active line power as seen from the transmission system, across all three phases. Control objectives for the 10-bus system include balancing active line power as seen from the distribution system. This figure also shows that even with a 25 percent load increase and p to 25 percent uncertainty in network parameters, the controller still performs as expected.

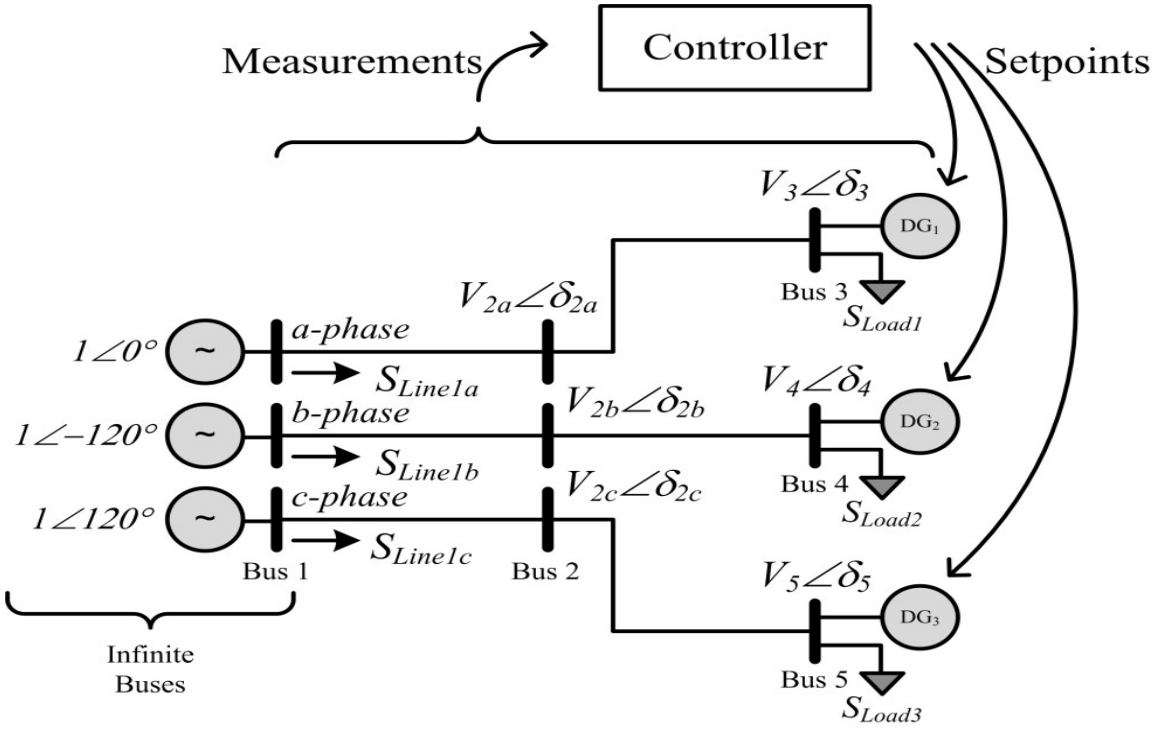

Figure 40. 5-Bus, Three-Phase Distribution System

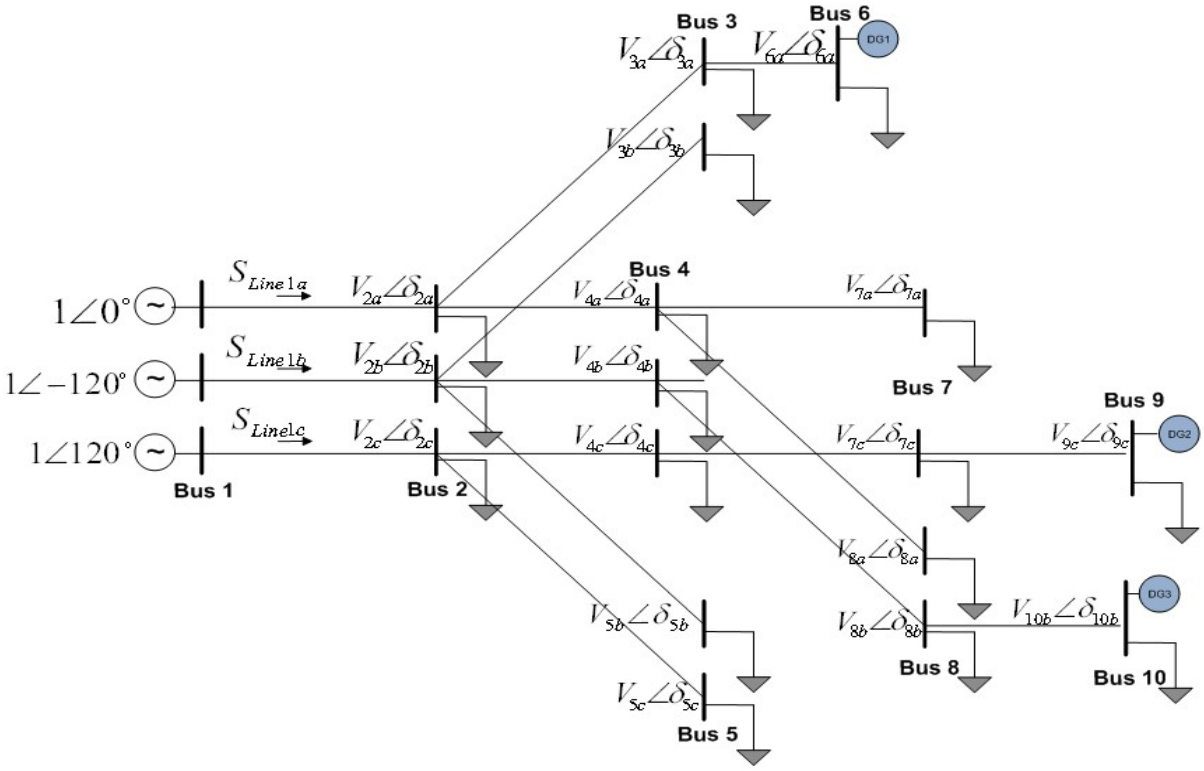

Figure 41. 10-Bus, Three-Phase Distribution System

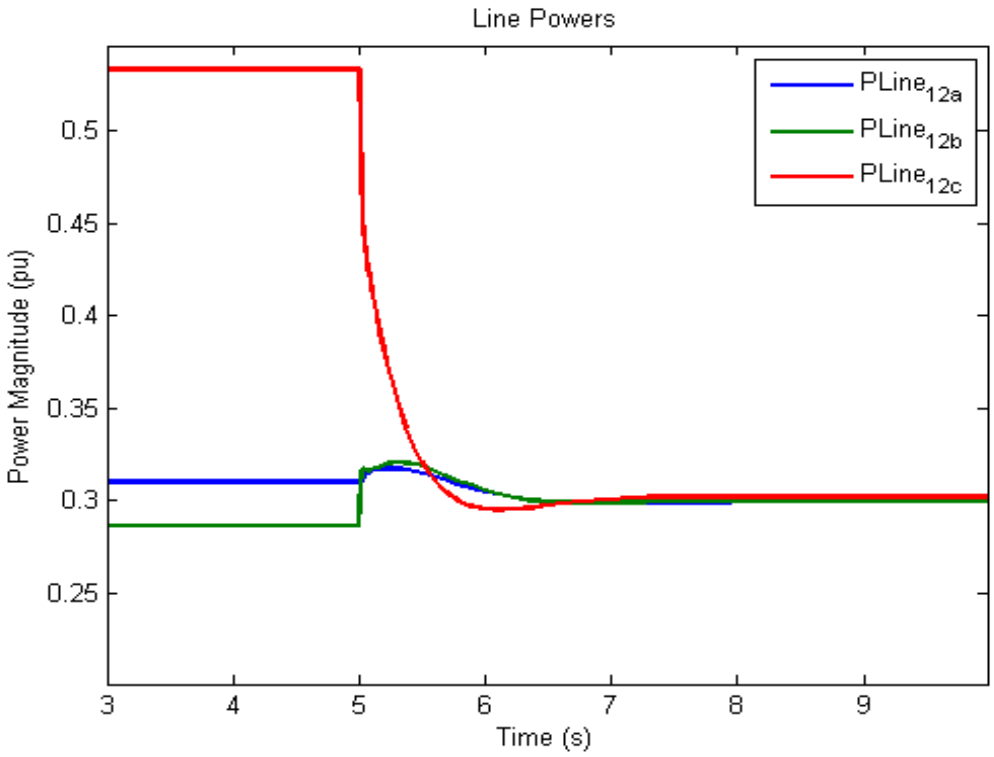

Figure 42. Active Line Power Delivered from the Infinite Bus For 5-Bus Distribution System Using State-Feedback with Reference Input Controller

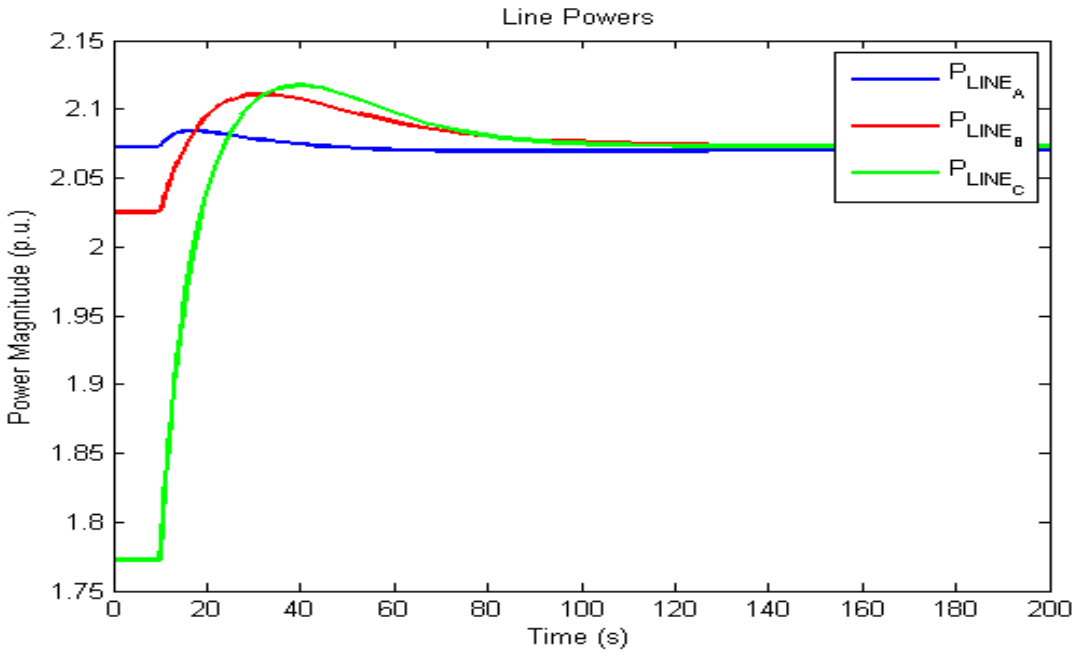

Figure 43. Active Line Power Delivered from the Infinite Bus for 10-Bus Distribution System Using Internal Model Controller

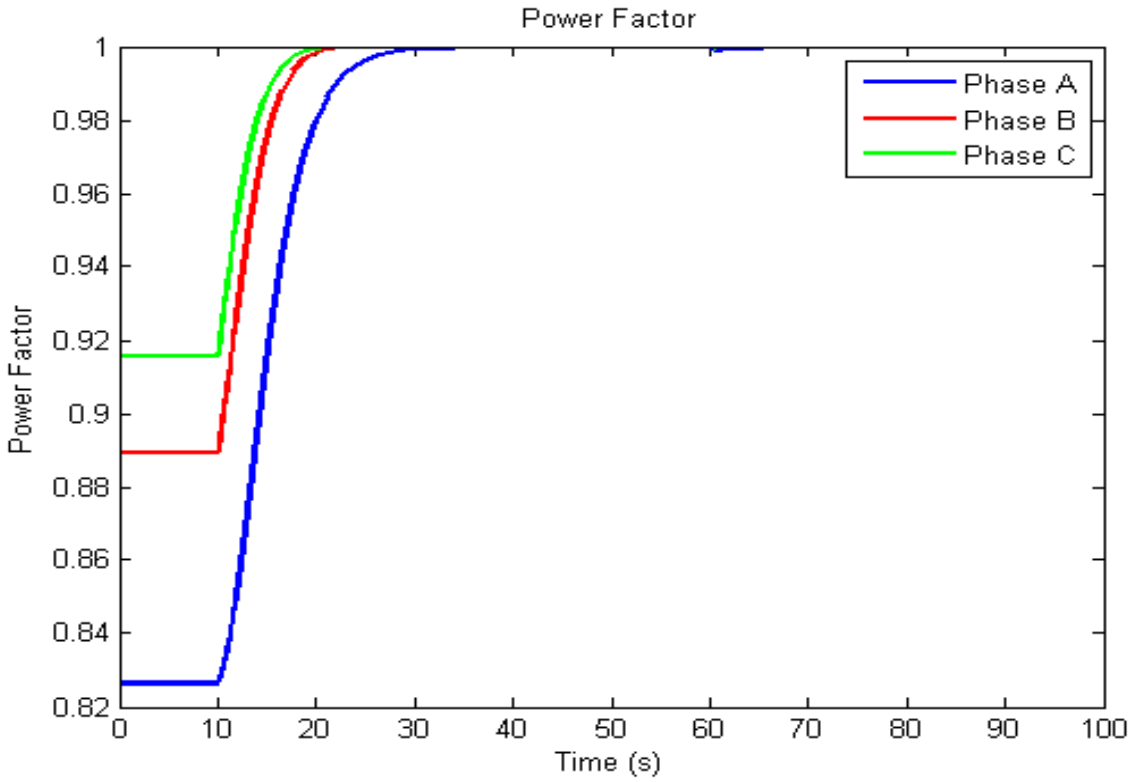

Figure 44. Power Factor Line Power Delivered from Infinite Bus for 10-Bus Distribution System with Internal Model Controller

Decision Support Analysis for a Renewable Energy System to Supply a Grid-connected Commercial Building

This task studied the integration of a solar concentrator photovoltaic array (CPV) system with a commercial building. Solar resource conversion, load characterization, power quality, and grid integration were the primary aspects addressed by the study. Local solar radiation and renewable energy source (RES) conversion data were used to determine a profile for annual energy production of the CPV, which uses a non-traditional method of solar energy conversion.

Figure 45 shows the measured power output of the CPV for a day, and the predicted output using solar radiation measurements for that same day. The load was characterized by creating an annual profile for the CC&C building's power demand in Playas using a combination of historical monthly billing data and a week of detailed real and reactive power consumption data as shown by the graphs in Figures 46 and 47.

Various simulation approaches were considered to evaluate the integration of system components with the supply grid. Because of the high-frequency resolution necessary for the study, which evaluated a number of parameters that traditional methods have not addressed, a custom analysis was performed, both in time segments and total project lifetime figures. This quantified, at one- minute resolution, the energy produced by the RES, consumed by the building, and metered to and from the supply grid. Example results for one week are shown in Figure 48.

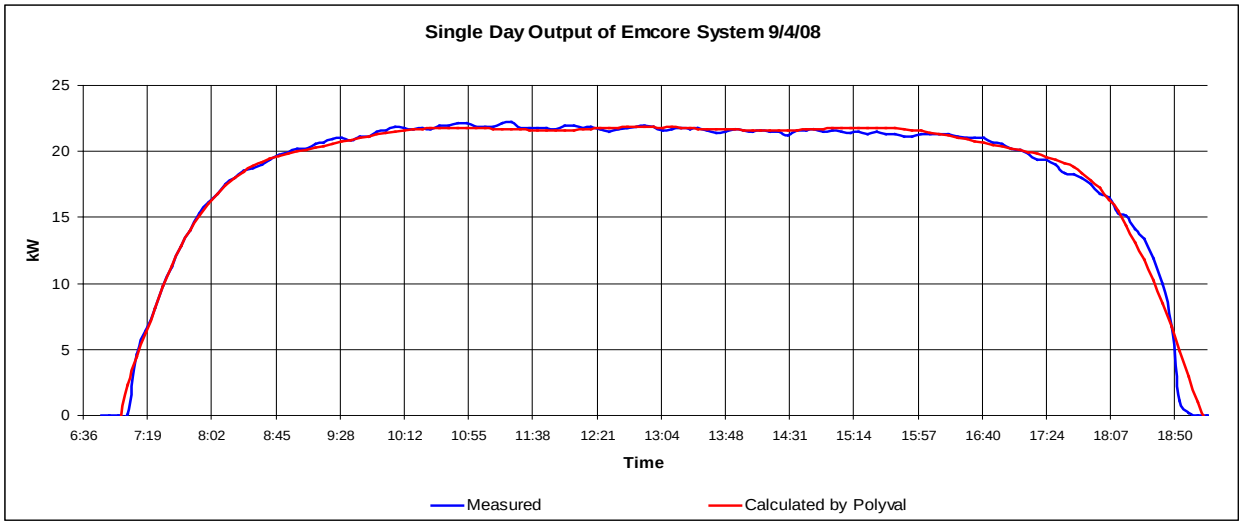

Figure 45. Single Day CPV Power Output: Experimental and Theoretical Values

The study concluded that the CPV system will make a valuable contribution to the energy supply, it can pay for itself in energy savings over a number of years, and it provides a substantial environmental benefit by reducing pollutant emissions. Financial considerations are dependent upon a number of variables, including the panel quantity, buy/sell prices of grid energy, project lifetime, financing options, and renewable energy credit programs.

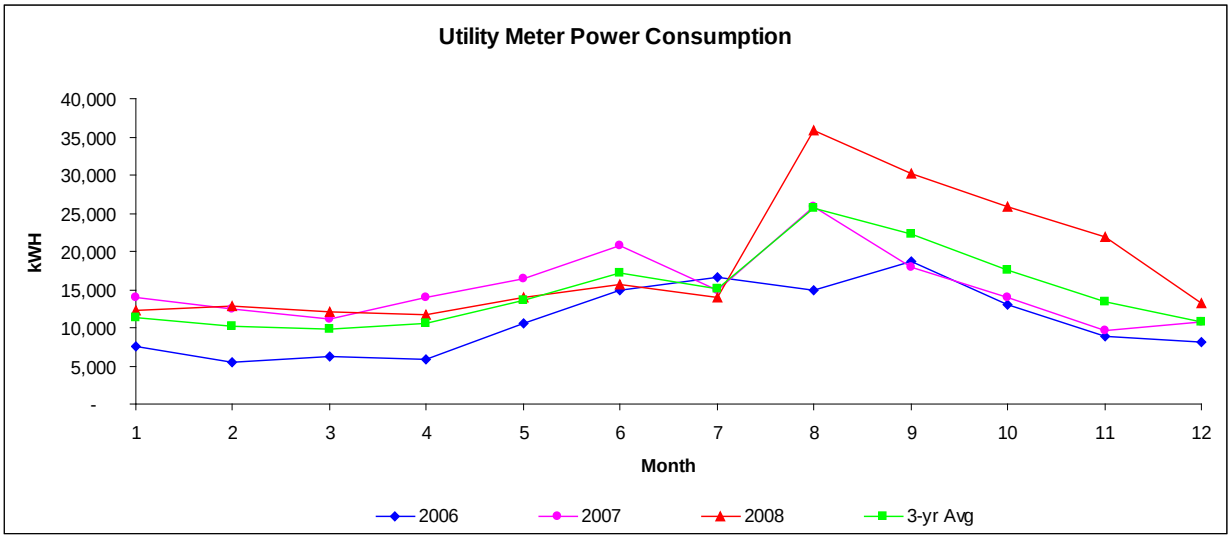

Figure 46. Monthly Energy Consumption of CC&C Building Based on Utility Meter Readings

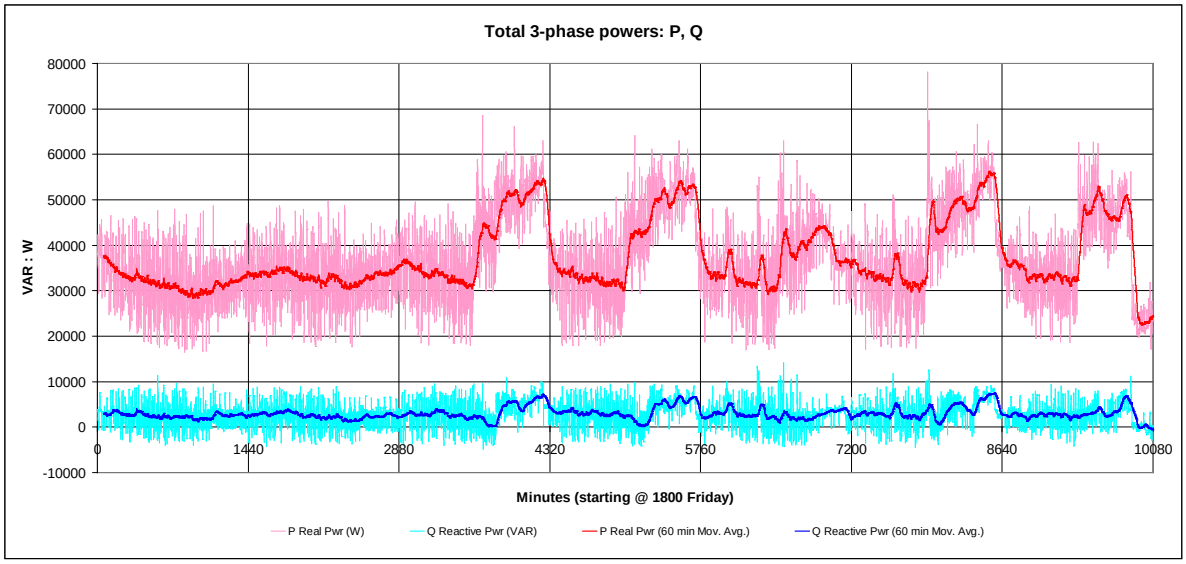

Figure 47. Weekly Profile of Active and Reactive Power Consumption of CC&C Building

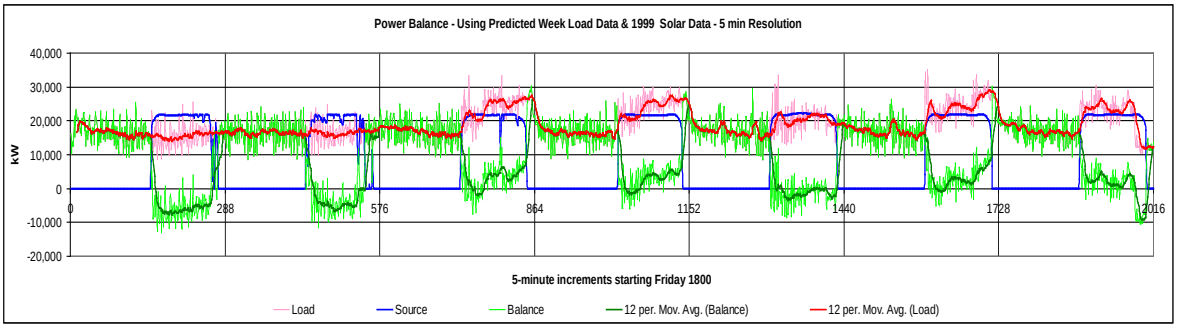

Figure 48. Power Balance for Profiled Data Sets Over One Week

Energy Reduction of the Largest Power Consuming Buildings

The Institute for Engineering Research and Applications (IERA) at NMT has received estimates from the energy assessment that was performed. The goal of this assessment was to identify large power consuming devices and how power could be saved by either upgrading the devices or using intelligent controls to save energy. The estimates shown below are for HVAC and lighting only.

Classroom 12,770 square feet
HVAC: Savings up to 25% by installing economizer controls
Lighting: Savings up to 20% by retrofitting electronic ballasts and occupancy sensors.

Copper Pins Bowling alley 10,020 square feet
HVAC: Savings up to 25% by replacing seventies vintage rooftop units with economizer controls
Lighting: Savings up to 40% by replacing all existing light fixtures with new electronic ballasts, lamps and occupancy sensors.

Community Center 7,070 square feet
HVAC: Savings up to 25% by replacing seventies vintage rooftop units with economizer controls
Lighting: Savings up to 86% by replacing all quartz halogen light fixtures with 15W LED lamps and replacing fluorescent tubes with LED “retro fit” tubes.

NMT/IERA intends to use technologies that will save the most energy for the least expenditures that have also been evaluated for optimum pay back value. Photographs showing some of the retrofits are included in Figures, 49, 50, and 51 along with graphs depicting corresponding power consumption comparisons.

Figure 49. Community Center

The energy savings using Tungsten Halogen Light Emitting Diode bulbs was 94% when compared to the original tungsten filament bulbs.

44 each 250 Watt
Tungsten Halogen
Usage (44X250) = 11,000W

44 each 14.5 Watt
Light Emitting Diode
Usage (44X14.5) = 638W

Figure 50. Replacement LED Bulbs

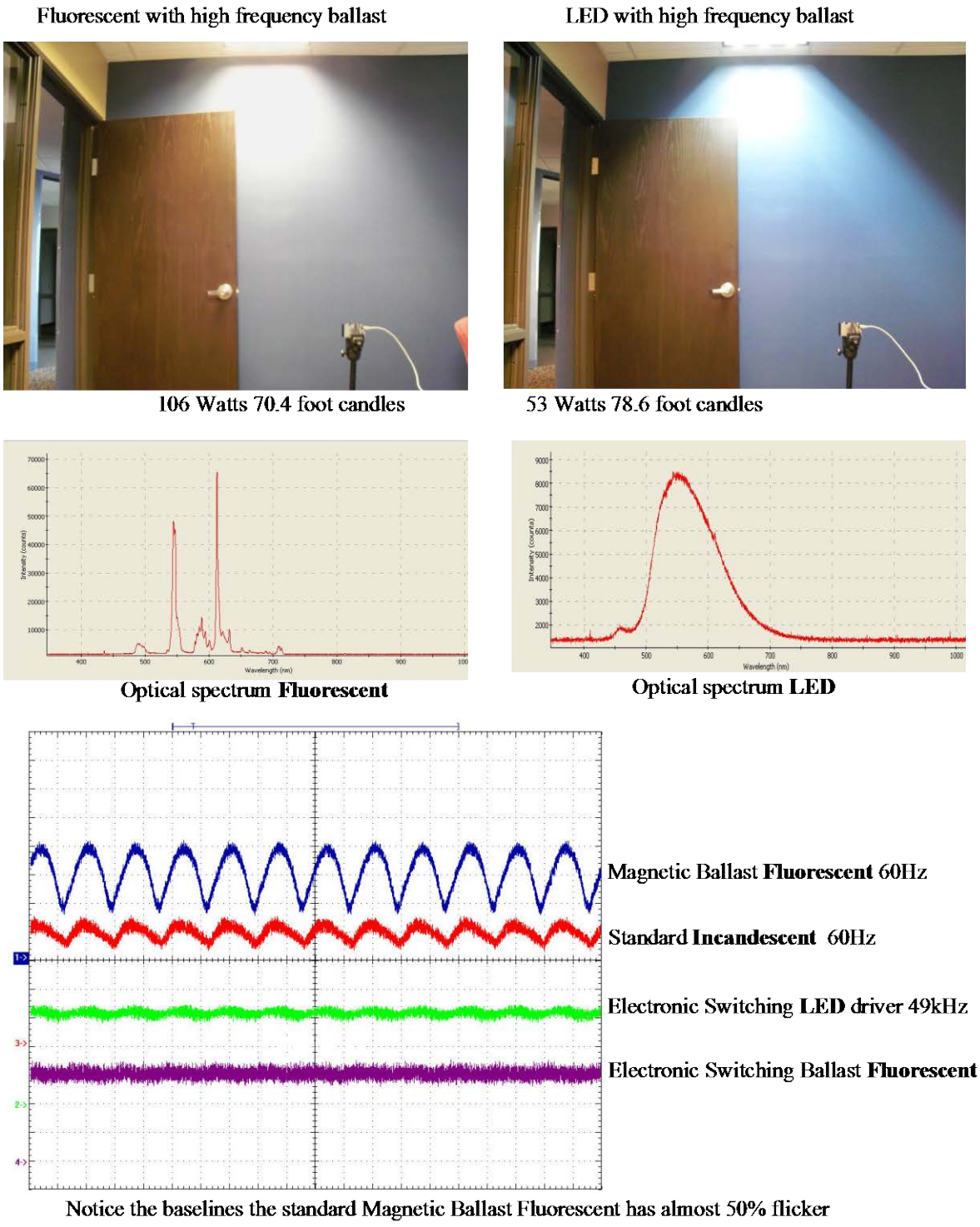

Figure 51. Replacement Fluorescent Bulbs

Replacing fluorescent tubes with LED "retro fit" tubes saved 50%. On site employees have reported more energy, less headaches and decreased fatigue when work spaces have been re-fitted with the LED lights.

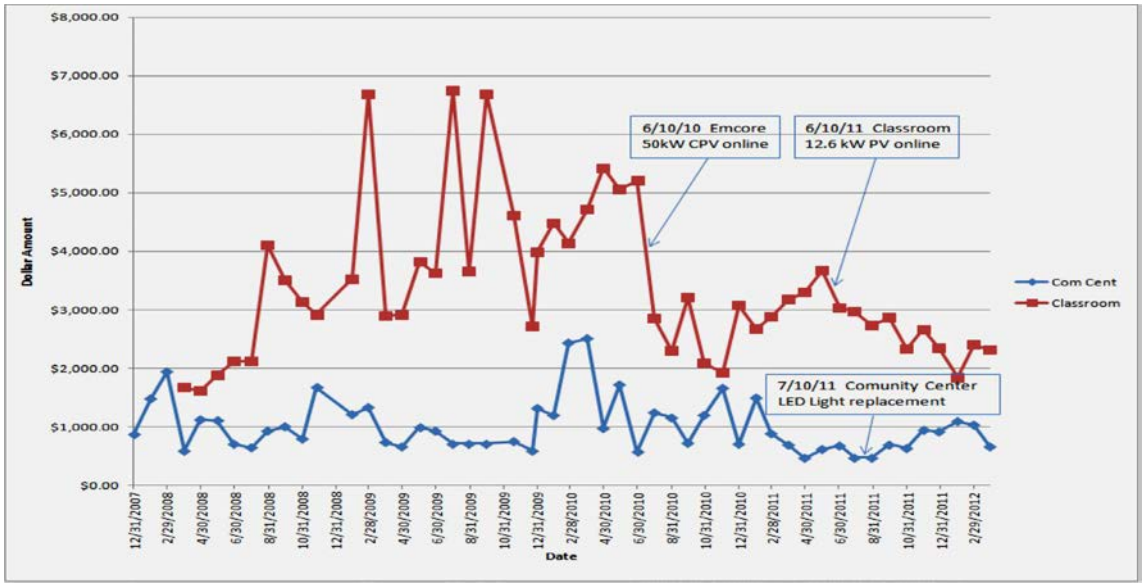

Figure 52. PV Systems and Efficient Lighting Improvements Effect Power Consumption

This monitoring demonstrates that when the two largest power consuming buildings were modified with newer technologies, electricity consumption from the local utility was reduced. The classroom (red) has two PV solar electric generating systems attached to it: the EMCORE 50 kW and 12.6 kW PV. The community center (blue) had a complete retrofit with LED lamps thereby reducing consumption even further. These systems can be used by future research programs as a national test bed.

Task 3.0: Challenges in Developing Renewable Distributed Energy Resources

Distributed energy networks that incorporate renewable energy resources and fuels, would mark the ultimate advance in energy security, self-reliance and sustainability. The Modern Grid must incorporate renewable sources of energy to achieve envisioned environmental benefits, affordability, and reliability goals. NMT has advanced technical research programs in the production of hydrogen, synthesis of PEM electrolysis and fuel cell catalyst supports, and processing of low-cost flexible photovoltaic systems.

Task 3.1: Biomass to Hydrogen Reforming (Co- PI: Corey LeClerc).

Hydrogen, produced from renewable biomass instead of non-renewable fossil fuel sources is an alternative source of environmentally clean renewable energy. The major disadvantage with bio-fuel reforming is the lack of an inexpensive catalyst that is able to break down bio-based fuels, like methanol, ethanol, and glycerol, as well as producing desired products with high selectivity. Additionally, the catalyst must be resistant to deactivation through sintering, coke formation, and other mechanisms.

Reactions studied for Aqueous-Phase Reforming (AFR) of ethylene glycol over various supported metals indicated that platinum (Pt) and palladium (Pd) catalysts are selective for production of H_2 and Pt shows higher catalytic activity, but at a very high cost. Researchers investigated the aqueous phase reforming of alcohols for hydrogen production. Aqueous phase reforming as a high pressure, moderate temperature process is advantageous for low concentration aqueous solutions of alcohols such that distillation is not required. Furthermore, the moderate temperature favors water gas shift equilibrium to produce hydrogen and remove carbon monoxide. Our primary focus investigated non-noble metal catalysts. In our case, nickel was used.

The first major objective evaluated three different alumina supports for the nickel catalyst. The researchers investigated commercial alumina, sol-gel (SG) synthesized alumina, and solution combustion synthesized (SCS) alumina. The catalytic effect of alumina supported nano-scale nickel catalysts made by a sol-gel (SG) and a solution combustion synthesis (SCS) route for Aqueous-Phase Reforming (AFR) of ethanol to hydrogen has been evaluated. Compared to SG and commercial catalyst the SCS sample showed higher EtOH conversion, H_2 production, and H_2 selectivity and lower CO production and CO selectivity.

The basic interests for using sol-gel and SCS route are to obtain porous and nano/submicron particle catalyst powders of high surface area which will help to increase hydrogen production for per gram of the catalysts and hopefully increase the activities of the catalysts. We prepared three batches of other catalysts; Ni/CeO_2, Ni/SiO_2, Ni/ZrO_2 by SCS and SG methods. Our aim is to understand the microstructure of the supports, metal- support interaction, and how preparation conditions are affecting the properties of these individual catalysts. We are currently carrying out the APR of ethanol at 200-300°C and 20-40 bar of pressure.

As a benchmark, we used 1% platinum coated on gamma-alumina as a catalyst. Our results show that 63% of the ethanol is converted in the reactor. Of the carbon that is converted, 95% forms gaseous products. The carbon selectivity in the products is 50% CO2, 25% methane, 20% ethane, and tiny amounts of others such as carbon monoxide. Compared to literature values this is a very small amount of carbon monoxide.

For hydrogen selectivity, 50% forms molecular hydrogen, 45% forms alkalines, and the rest forms liquid products. This catalyst is currently our benchmark for the APR system. Our focus on non-noble metal based catalysts was important since these metals are much cheaper than platinum. Our supports have higher surface areas than g-alumina, which will lead to a higher activity. We have begun production of combustion synthesized ceramic supports such as ceria, zirconia, and alumina. Thus far only the ceria is crystalline with an average crystallite size around 15nm. There tend to be larger pores which will be advantageous when we examine large fuels.

In order to understand these catalytic activity results we ran a series of microstructural and temperature programmed characterizations. The experiments found that, compared to the commercial and SG powders, the particle size of SCS Al_2O_3 support is much smaller (XRD) and surface area is much higher (BET). Compared to the commercial sample $Ni\text{-}Al_2O_3$ interaction is much stronger for SCS and SG powders (TPR) and that, after being used in reactor the SCS catalyst showed less carbon deposition than that of the SG and commercial powders (TPO). Bright field TEM showed nanostructure and wide dispersion of Ni metals on SCS Al_2O_3 sample (Figure 53). The particle size analyzed from TEM images match well with the sizes calculated from the corresponding XRD profile. The SCS sample clearly has higher surface area and smaller particle size which leads to higher catalytic activity.

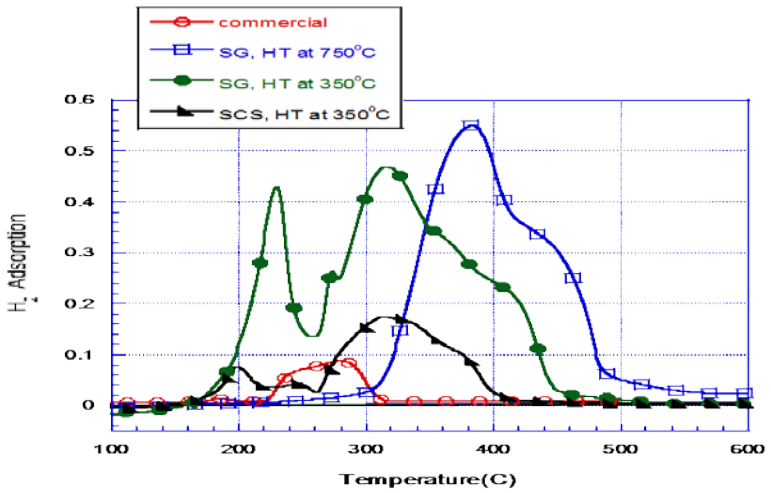

Fig 5: TPR spectra for different 10wt% Ni/CeO_2 catalysts

Figure 53. TPR Spectra for Different Catalysts

The NiO peaks sharpened little as a sign of sintering of these particles. For the SCS CeO_2 powder particle size (14 nm) showed stronger support-metal interaction as a consequence of the preparation method. These results infer that the SCS and SG prepared catalysts provide better catalytic activity than the commercial powders.

Our results were published in two papers in the International Journal of Hydrogen Energy[18]. We found that use of the SCS alumina resulted in significant per gram activity of the catalyst. The differences in activity between the three supports were a result of two different phenomena. First, the dispersion of nickel on the SCS alumina catalyst was highest. More nickel on the surface per gram led to higher activity. Second, coke build up on the surface led to a further decrease in activity. The more highly dispersed nickel had a lower tendency for coke formation.

The second major investigation looked at the effects of plasma modification of the support prior to metal deposition. This work was also published in the International Journal of Hydrogen Energy[18]. We found that the non-thermal nitrogen plasma modification of the SCS alumina led to an even higher nickel dispersion thus increasing the activity. This has been a major new direction for our lab. We hypothesize that the plasma disrupts the ability of hydroxide formation at the ceramic surface in aqueous solutions. This disruption, in theory, can make it easier or more difficult to adsorb metal salts onto the surface and achieve higher dispersion.

The third major investigation looked at conversion of bio-butanol to hydrogen. This work was published in the Journal of Power Sources[19] with more results in preparation. Overall, similar results were found compared to ethanol except coking was a greater problem. We then transitioned from alumina to ceria due to the well-known redox properties of ceria which prevent significant build-up of coke.

The final piece of this task further considers the role of ceria for ethanol reforming. This work is in preparation and there are a few pieces of information that need to be finalized. One important result found for ethanol and butanol independent of the support is the presence of a volcano type plot in activity versus pressure. In the gas phase, as the pressure increases the activity increases as well leading to a higher hydrogen yield. This increases peaks at the bubble point. In transitioning from gas to liquid phase reforming, the activity tends to decrease as the pressure further increases.

We will continue to use DTA/TGA, XRD and TPR for the regular characterization of the catalysts. A SEM and/or TEM equipped with energy-dispersive x-ray spectroscopy (EDX) will be used for typical microstructure imaging and elemental analysis. The specific surface area, pore volume, and pore size distribution will be extracted from the N_2 adsorption/desorption spectrum. The H_2 chemisorptions will be carried out to understand the dispersion of metals on the supports. Temperature-programmed desorption (TPD) analysis will be used to understand the acidic nature of the support. The FTIR studies of the pyridine adsorbed oxide powders will provide better understanding of the acidity/basicity of the supports. Feedback from these characterizations will be continually used to tune the synthesis conditions of catalysts.

A custom-built continuous flow stainless steel reactor (2.5cm inner diameter and 7.5 cm length) set inside a box furnace with a fixed bed catalyst powder will be used to study the catalytic activity of the powders. The products from the reactor will pass through a homemade condenser. The gas and liquid collected from the condenser will undergo gas chromatography analysis. The research program will investigate a matrix of time, temperature and carrier gas pressure inside the reactor to figure out the selectivity and activity of the catalysts.

We plan to develop new materials for studying H_2 production from biomass. BIMEVOX, a group of solid oxide electrolytes with much higher O^{2-} conductivity, have extensive potential to be used in next generation industrial applications such as fuel cells or catalysts. Our focus will be on increasing the surface area, micro-porosity, and decreasing particle size to enhance the catalytic performance of the BIMEVOX powders in fixed bed reactors.

Task 3.2: Nanoclay based Membranes and Electrodes for Fuel Cells

Fuel cells face a number of limitations including cost, durability, and thermal/water management. Direct-Methanol Fuel Cell (DMFC) systems face additional problems with methanol crossover. Limited work incorporating nano-sized layered silicate clays into membrane structures has shown promise by reducing methanol crossover in DMFC cells and improving membrane water retention in PEM cells thereby allowing higher operating temperatures. However, little work has been done with layered silicates and fuel cell electrodes.

NMT researchers focused on the study of nano-sized layered silicate-based fuel cell membranes and electrodes. This research investigated incorporation and characterization of stable proton-exchanged layered silicates into the electrode structure, as well as complementary membrane materials. It also studied the deposition of platinum directly to the clay minerals to examine if it improved the platinum-proton junction thereby improving platinum utilization and allowing reduced platinum use.

Researchers constructed an epoxy molded, O-ring sealed conductivity cell for easy fabrication, duplication, assembly and cleaning. The design allows use of 1 mm Pt electrodes for liquid and gel conductivity measurements as well as ¼" stainless steel electrodes for film/membrane conductivities. A temperature control fixture shown in Figure 54 was designed and fabricated. It accommodated two conductivity cells and connected to a recirculating, refrigerated bath.

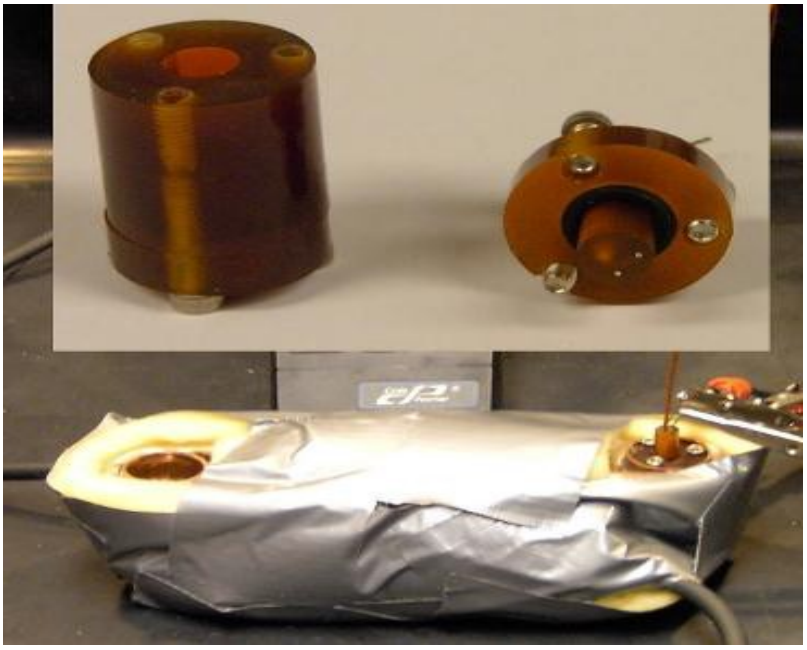

Figure 54. Temperature Control Fixture

Conductivity measurements were obtained on native sodium clay as well as lithium-exchanged clay as shown in Figures 55 and 56 on the following page. Proton exchange of clay was investigated, incorporating smectite clays in membranes with a focus on fuel cells with no reported concerns over proton-form stability. In-house proton exchange experiments yielded clays with much poorer gelling performance and conductivities than anticipated. The reduced performance is attributed to proton attack of inner octahedral layer as described in literature examined during the research. Our investigation expanded in anticipation of proton stability issues to include protection of octahedral layer by functionalizing clay edges with hydrophobic groups. Cross-linkable groups will be a later focus to allow fixation of the clay gel network structure for the creation of stable membrane and electrode structures.

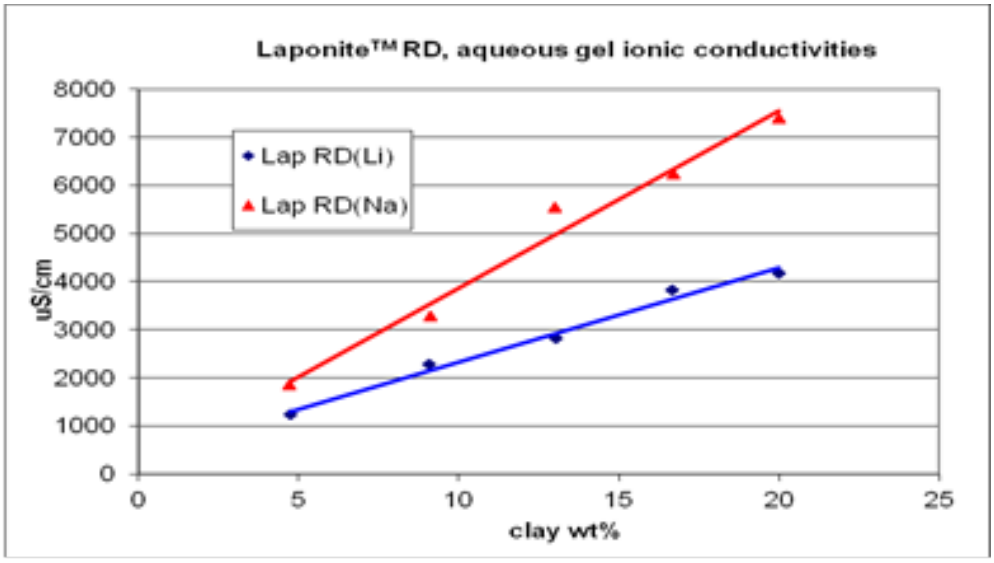

Figure 55. Effect of Clay Concentration on Aqueous Laponite[tm] Gel Conductivities

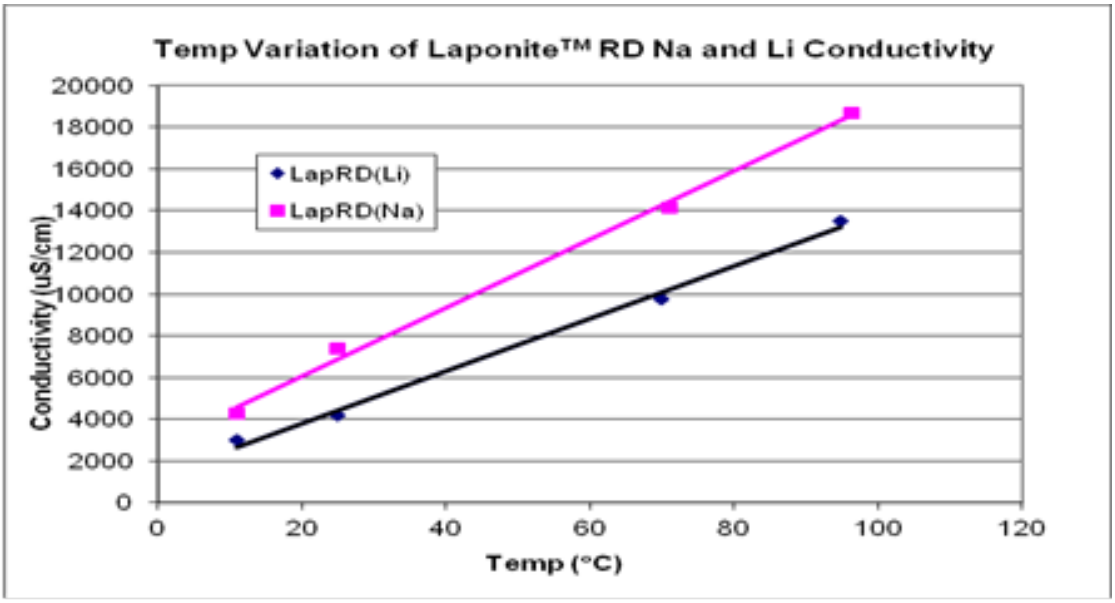

Figure 56. Effect of Temperature on Aqueous Laponite[tm] Gel Conductivity

As an initial precursor to functionalization and cross-linking of the clay platelets, interpenetrating TetraMethyl OrthoSilicate (TMOS) cross-linked networks to lock in place and stabilize the clay structures are being investigated. Using techniques borrowed from biological researchers, the TMOS is transported to the aqueous clay gel through the vapor phase and cross-links throughout the gel, thereby preventing the aggregation and collapse of the clay platelet network. This should allow exchange to non-gelling cations such as protons while maintaining high ionic conductivity as well as preventing collapse of the clay network structure in variable humidity environments. The technique appears to be successful with the clay gels in initial trials, but characterization is required.

Beidelite, an aluminum and silicon based smectite, was chosen as a possible acid-stable clay. A synthesis route in the literature originating in the 1930's has been identified. The synthesis route involves high temperatures and pressures as well as a noble metal based reaction vessel. Synthesis routes for the more common clays (e.g., hectorites) use milder conditions and will be investigated as well. Hectorite synthesis and characterization is a model clay/starting point for development of an in-house system for synthesizing a wide variety of clays, including beidelite and hectorite.

Research has begun on anion-exchangeable clays (layered double hydroxide, or LDH) for application to direct ethanol fuel cell systems. They are traditionally non-swelling (unless exotic solvents are employed), and therefore, high surface areas and high ionic conductivities are not as readily achievable as with the smectites as the individual clay platelets remain aggregated. A method to exchange these clays to acetate or propionate form allowing them to swell in water was identified during the research. In house attempts to exchange and swell a commercial LDH (hydrotalcite) has not yet been successful

Task 3.3: Novel Thick Film Microstructures for Dye Sensitized Photovoltaic Cell s (Co-PI: Paul Fuierer)

The main objective of the research was to develop novel TiO_2 (anatase) thick films with hierarchical microstructures to serve as the wide band-gap anode material in a dye sensitized solar cell (DSSC). The ultimate goal is to build such solar cells with greater efficiency and lower cost. Figure 57 illustrates two ideal architectures NMT worked to create. The main embodiments are acicular rutile in "stand-up texture", and/or microspheres in order to assist in electron transport and photon scattering, decorated with nano- anatase to retain high surface area for maximum dye interaction and photon absorption.

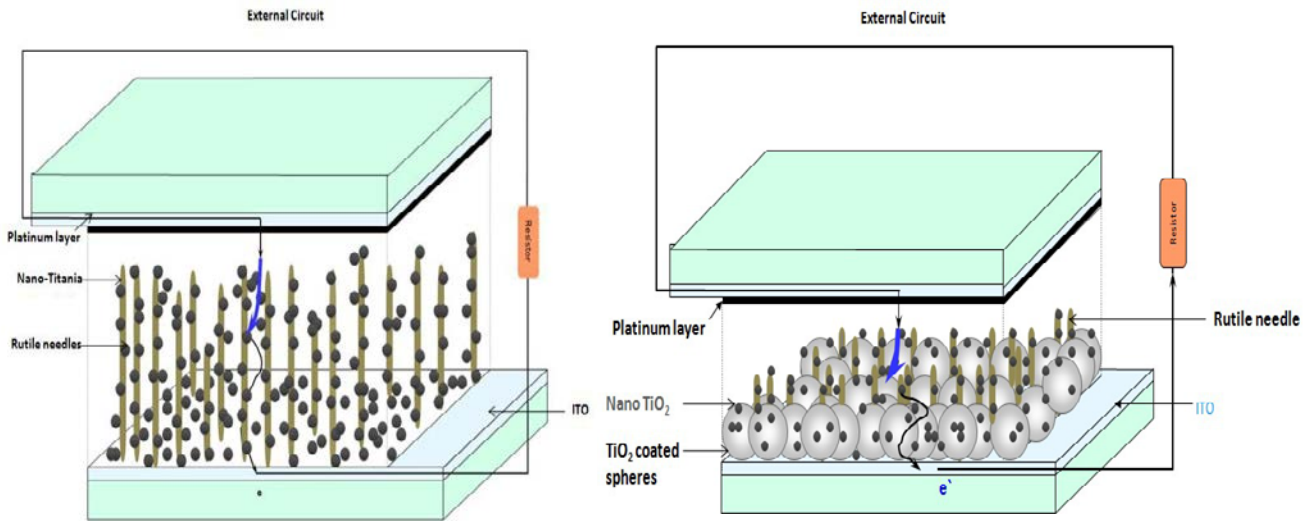

Figure 57. Schematic DSSC Containing Proposed Ideal Thick Film Semiconductor (Tio_2) Architectures

One problem associated with the dye sensitized nanocrystalline solar cell (DSSC) is the long electron percolation path between weakly linked nano-anatase particles in the widebandgap semiconductor (TiO_2) anode layer. This creates a high internal resistance, and low current output. Our goal is to develop novel heterogeneous TiO_2 composite layers containing microscopic electrical conduits which effectively reduce the electron path length, and the overall resistance of the cell, while maintaining large effective surface area for maximum interaction with the photon-absorbing dye. The electrical conduits can take the shape of erect rutile needles, or alternatively hollow glass spheres with dense TiO_2 thin film coating. Sol-gel techniques are then used to "chemically sinter" the nanoscopic anatase to the microscopic rutile. A central theme of the research is to develop materials processing schemes that have promise for large area commercial scale-up and cost competitiveness.

Numerous (over 25) different formulations were prepared, and thick films deposited. Previous reports have shown representative electron micrographs of the fabricated films with multi-scale structure. Hundreds of solar cells were constructed and tested using a Sciencetech SS1K Solar Simulator and PV test system. The researchers correlated the photovoltaic output of their experimental cells to fundamental characteristics of the TiO_2. These correlations are illustrated in Figure 58. No correlation with roughness at the micron scale is apparent.

However, there appears to be a trend in increased power with increasing film thickness. There is a real benefit to the incorporation of larger microscopic particles, as these enable the building of thicker films without cracking. Contrary to conventional wisdom, Figure 58(c) suggests an optimal specific surface area of between 40 and 50 m^2/g. A National Science Foundation Research Experience for Undergraduates (REU) program[20] summer student conducted isothermal N_2 absorption-desorption experiments on various TiO_2 particle mixtures. These data are being analyzed to obtain actual surface area values to compare with calculated results.

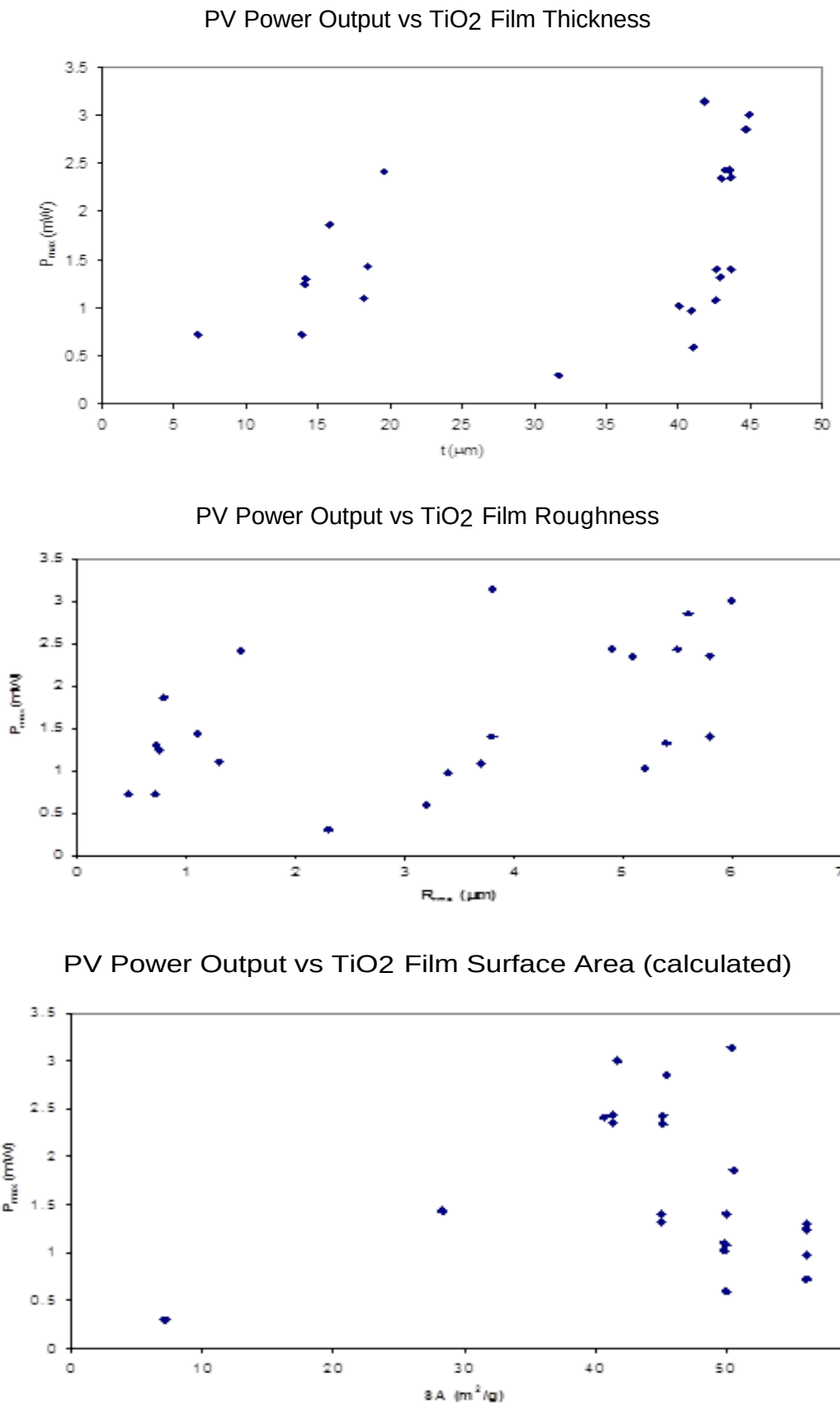

Figure 58. Maximum photovoltaic output of experimental DSSCs as a function of TiO_2 anode layer characteristics. (a) Film thickness (b) Film roughness (c) Calculated specific surface area

Research to this point has focused on improving dye-sensitized solar cell (DSSC) output through incorporation of microscopic particles acting as conduits for photo-generated electrons. While this has been a novel concept, one cannot neglect the properties of the nano-TiO_2 at the heart of the DSSC device. We have begun refocusing on optimizing the nano-TiO_2 component so that when used in conjunction with novel hierarchical microstructures, our fabricated cells can perhaps exceed the efficiencies of state of the art DSSCs.

The research team began by focusing on optimizing the nano-TiO_2 component of the DSSC. Use of a hydrothermal "bomb" (digester) has allowed synthesis, from chemical precursors, of nano-crystalline TiO_2 with high specific surface area (116 m^2/g) and the requisite meso-porosity (average radius of 23 Å) Synthesis parameters were further optimized and plasticizer and dispersants added to enable casting into thick films. The table below summarizes several batches prepared with outcomes. A key parameter seems to be very low starting pH for peptization prior to hydrothermal treatment. Progress was made in producing the crack free films (see optical micrographs of Figure 59 required for the building of quality PV cells.

	System	Autoclave Treatment	Specific Feature	Dispersant/ Plasticizer	Film Result
1.	10ml $Ti(OC_3H_7)_4$ + 60ml 0.1M HNO_3	Steam Sterilizer 125°C/16 h	[TiO2] increased to ~.200g/mL via stirring process	1. Triton X-100 2. solid PEG	Cracks & bubbles
2.	10ml $Ti(OC_3H_7)_4$ + 60ml 0.1M HNO_3	steam sterilizer 125°C/16 h	[TiO2] increased to ~200g/L using fractional distillation	1. Triton X-100 2. solid PEG	Cracks & bubbles
3.	7.6ml $Ti(OC_3H_7)_4$ + 45.6 ml 0.1M HNO_3	Hydr bomb 200°C/ 16h	[TiO2] increased to ~.200g/mL via stirring process	1. Triton X-100 2. solid PEG	Cracks
4.	7.6ml $Ti(OC_3H_7)_4$ + 45.6 ml 0.1M HNO_3	Steam sterilizer 125°C/16h	[TiO2] increased to ~.200g/mL via stirring process	1. Triton X-100 2. liquid PEG	Cracks & bubbles
5.	1ml $Ti(OC_3H_7)_4$ + 15ml 0.5M HNO_3	Hydr bomb 200°C/16h	[TiO2] increased to ~.200g/mL via stirring process	1. Triton X-100 2. liquid PEG	No cracks

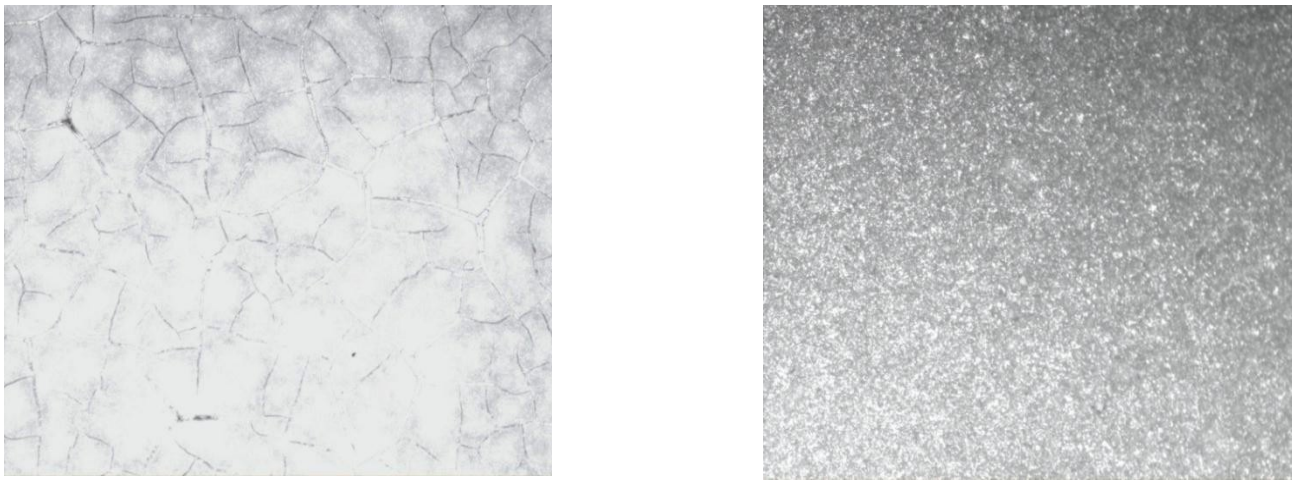

Figure 59. Left: film produced in trial #3 **Right: film produced in trial #5**

The research also focused on the incorporation of glass microspheres (GMS) into the nanocrystalline TiO_2 slurry, and the production of quality coatings for building DSSCs. The optimized hydrothermal synthesis process identified in the previous report (process #5) was utilized with the GMS added at the front end. The SEM shown in Figure 60 reveals the desirable interconnectivity between microspheres with nano-titania necks in between. A certain amount of sphere breakage is always observed and is probably unavoidable. Breakage was determined to occur not during the hydrothermal treatment, but rather during casting operations. Precautions during fabrication have been identified and adopted to minimize breakage.

One objective was to develop processing schemes to build up coating thickness. A new instrument (HIROX) and technique (high resolution, 3-D digital light microscopy) has been adopted to assess the thickness, roughness and other coating qualities, as shown in Figures 61. The differences between these two films were in the GMS loading, and also the casting procedure. The film in Figure 61 appears to be smooth at the center, with higher roughness at the edge. We believe this to be due to a "dragging" of GMS during the casting of individual 50 m layers, as well as some breakage of GMS. Figure 61b shows larger peak to valley variation (higher roughness) which persists throughout the coating from center to edge. No cracking was visible in either of these coatings. Incorporation into DSSC and PV testing is currently ongoing to determine performance differences.

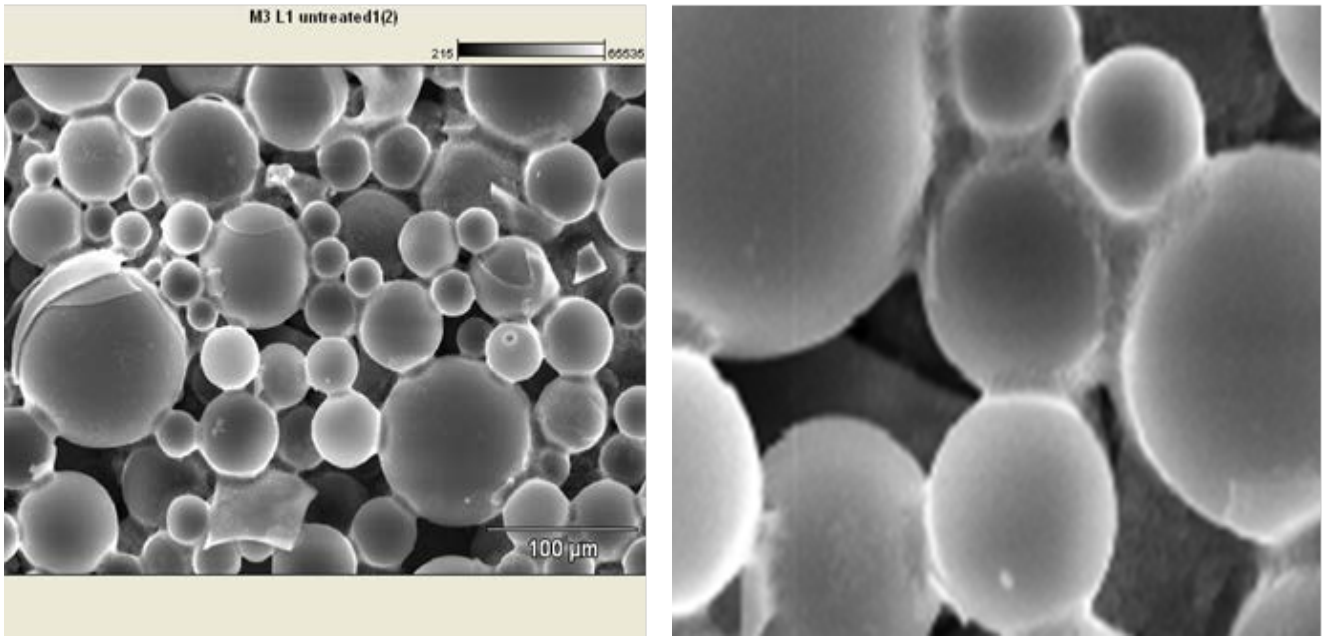

Figure 60. Glass micro-spheres covered and interconnected with nano-crystalline TiO_2 (anatase). A sol-gel /GMS mixture was treated in a hydrothermal bomb, dispersants and plasticizer added, and cast onto substrate. Subsequent heat treatment causes little change in appearance.

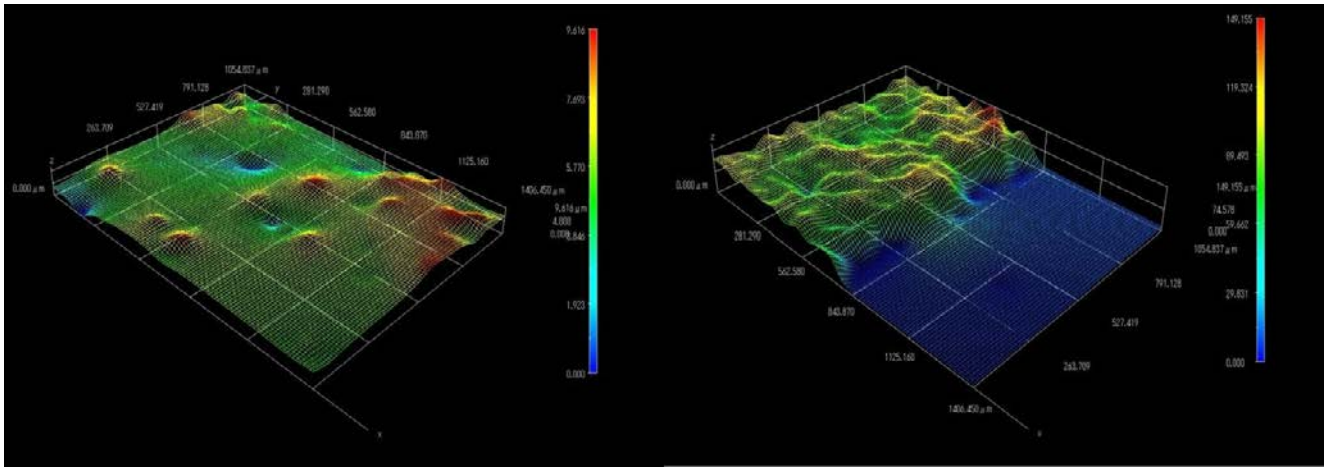

Figure 61. HIROX 3D Digital Microscope image of a nano-TiO_2 coating with a "theoretical" loading of GMS and fabricated using 3 successive castings for an average thickness of 170 ± m a) near the center of the coating b) at the edge of the coating. Both images at 245X.

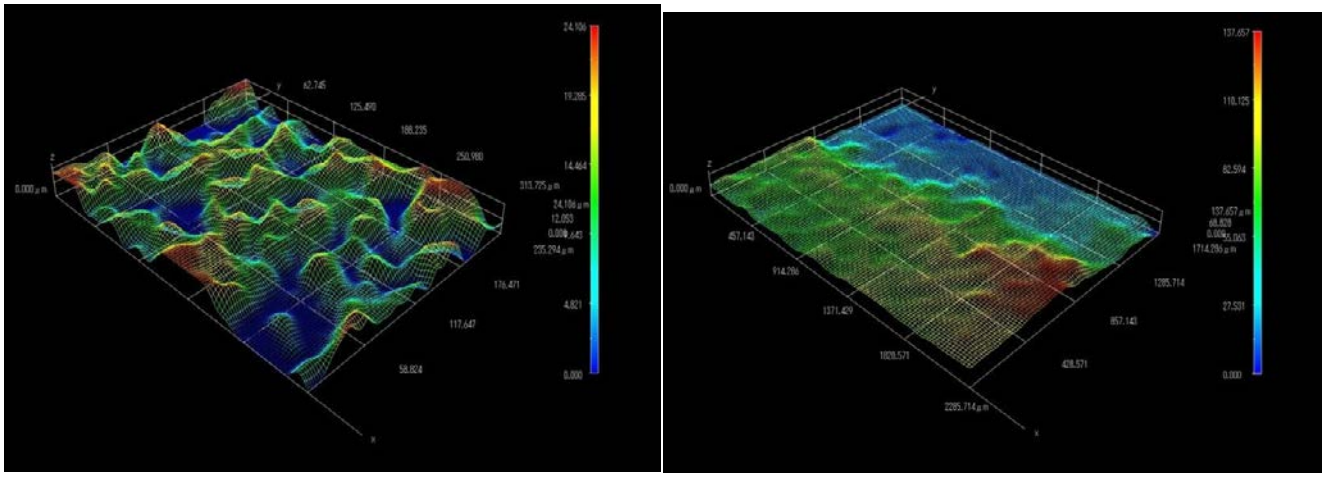

Figure 61b. HIROX 3D Digital Microscope image of a nano-TiO_2 coating with half the "theoretical" loading of GMS and fabricated using a single thick casting for an average thickness of 145 ±30 m. a) near the center of the coating (245X) b) at the edge of the coating (35X).

Figure 61b illustrates the point that high surface area of the nano-anatase is not the only factor in determining power output and efficiency. This, we think, is a significant finding, and other research groups have since reached the same conclusion with some more elaborately processed designer materials like nanotubes. The most important perceived advantage of our approach is that it offers a relatively simple and cost effective way to make high quality anode layers for large area PV with commercial viability.

Although the ideal architectures shown above were not achieved (namely the vertical orientation of rutile particles), progress and performance improvement of DSSC power output was made. The more complex TiO_2 anodes are seen to yield higher photovoltaic power output than the standard nanocrystalline anatase anode, all else being equal. This research has found that:

1. Finely divided, nanocrystalline anatase can be produced by heating at low temperature in a solid salt matrix (e.g. NaCl- DSP), a novel technique we call solid salt synthesis (SSS). The salt matrix can be used to suppress grain growth of anatase and its transformation to rutile.

2. Acicular rutile can be synthesized with controlled dimensions and aspect ratio, ranging from nano-fibers to bundled needles, using a novel molten salt synthesis (MSS). Rutile scaffolds, consisting of particles ranging from nano-whiskers to micron-size needles, can be grown on substrates using a novel seeded, MSS technique.

3. Glass microspheres can be coated with a thin layer of anatase in a continuous spray drying process, beginning with a mixture of spheres and titania sol-gel solution

4. Process methodologies explored, including screen printing, and air gun spraying, were unsuccessful in producing the ideal architecture namely the vertical orientation of rutile particles. However, multiscale, hybrid microstructures without significant alignment were produced using a simple casting procedure.

5. Experimental DSSCs incorporating TiO_2 hybrid microstructures showed performance improvement. Multiscale, hybrid anodes yield higher photovoltaic power output than the standard nanocrystalline anatase anode.

The research conclusion is that hybrid, multi-scale thick film anodes offer performance advantages for DSSCs stemming from enhanced light scattering and trapping within the cell, and better particle-electrode connectivity and thus electron transfer. High surface area of the nano-anatase is not the only factor in determining power output and efficiency. The TiO_2 anodes need not be processed from designer materials like nanotubes. The advantage of our approach is that it offers commercial viability for large area PV. Work should continue to explore methods of achieving the ideal "stand up texture" of acicular particles for additional performance improvement.

Task 3.4: N-Aryl Arenecarboximides as Panchromatic Dyes for DSSC Applications

See: http://www.hindawi.com/journals/ijp/2010/264643/[21]

Task 3.5: Biomass/BioFuel Production using Algae

NMT research on algae-derived biodiesel was initiated in 2009 and the program has continued full speed. Research focused on optimizing parameters required for the Chorella vulgaris strain suitable for a Socorro, New Mexico setting. Once this is done, a photobioreactor will be placed in a laboratory at the Materials Engineering Department and operational parameters will be optimized for that setting. The photobioreactor has been designed to allow bleach as an alternative sterilization method. Our preliminary tests indicate that Plexiglas is not affected when submerged into 6% sodium hypochlorite for two hours and is thus suitable for this undertaking.

Because of problems with fossil fuels, biomass derived fuels are being considered as an alternate. For example, due to their ability to grow rapidly and the ability of synthesis and accumulation of huge amounts of neutral lipid bodies that are stored in cytosolic lipid bodies, microalgae are one of the best sources of biomass for alternative fuel production.

Chorella vulgaris, a green algae, is an excellent source of neutral lipids suitable for biodiesel production. As a green algae, the bulk of its fatty acids are saturated and unsaturated C18s similar to vegetable oils. Chlorella tolerates high levels of CO_2, sulfur oxides, nitrogen oxides and VOCs, allowing it to thrive on the flue gas of coal fired power plants, waste incineration plants or other similar industries. This genus can grow in an air-CO_2 mixture containing up to 18% CO_2.

Chlorella has the distinctive ability of growing in autotrophic, heterotrophic or mixotrophic conditions. As an autotroph, it can use light to absorb inorganic carbon (CO_2) as its carbon source. As a heterotroph, it can grow in the dark given an organic carbon such as glucose or acetate. As a mixotroph, it can absorb inorganic and organic carbon simultaneously. This gives this algae- great potential for very high growth rates, under properly designed conditions.

The researchers determined that a modified bold 3N Medium Recipe or F/2 Medium used in fresh water would be most appropriate. This recipe is described in Figures 62 and 63. In this project, fresh water medium was chosen over saltwater medium to avoid the high concentration of salts interfering with the analytical methods, or causing precipitation and clogging problems. The medium was sterilized in an Autoclave and the vitamins were sterilized through microfiltration. The 3N Medium Recipe was prepared in two vessels. The cells were counted every day to obtain cell density and growth rates which are shown by the graph labeled as Figures 64 and 65. The figures indicate that where there was not regular cell density and growth rate. This is likely due to aeration or because light may not have been sufficient.

#	Component	Amount	Stock Solution Concentration	Final Concentration
1	$NaNO_3$	30 mL/L	10 g/400 mL dH_20	8.82 mM*
2	$CaCl_2.2H_2O$	10 mL/L	1 g/400 mL dH_20	0.17 mM
3	$MgSO_4.7H_2O$	10 mL/L	3 g/400 mL dH_20	0.3 mM
4	K_2HPO_4	10 mL/L	3 g/400 mL dH_20	0.43 mM
5	KH_2PO_4	10 mL.L	7 g/400 mL dH_20	1.29 mM
6	NaCl	10 mL/L	1 g/400 mL dH_20	0.43 mM
7	P-IV Metal Solution	6 mL/L		
8	Soilwater GR+Medium	40 mL/L		
9	Vitamin B12	1 mL/L		
10	Biotin Vitamin Solution	1 mL/L		
11	Thiamine Vitamin Solution	1 mL/L		

Figure 62. Bold 3N Medium Recipe

Macronutrients	
Stock Vol. for 1L Medium	Compound
30 mL/L	$NaNO_3$
10 mL/L	$CaCl_{22}O$
10 mL/L	$MgSO_{42}O$
10 mL/L	K_2HPO_4
10 mL/L	KH_2PO_4
10 mL/L	NaCl

Figure 63. Macronutrients for Modified Bold 3N Medium Recipe

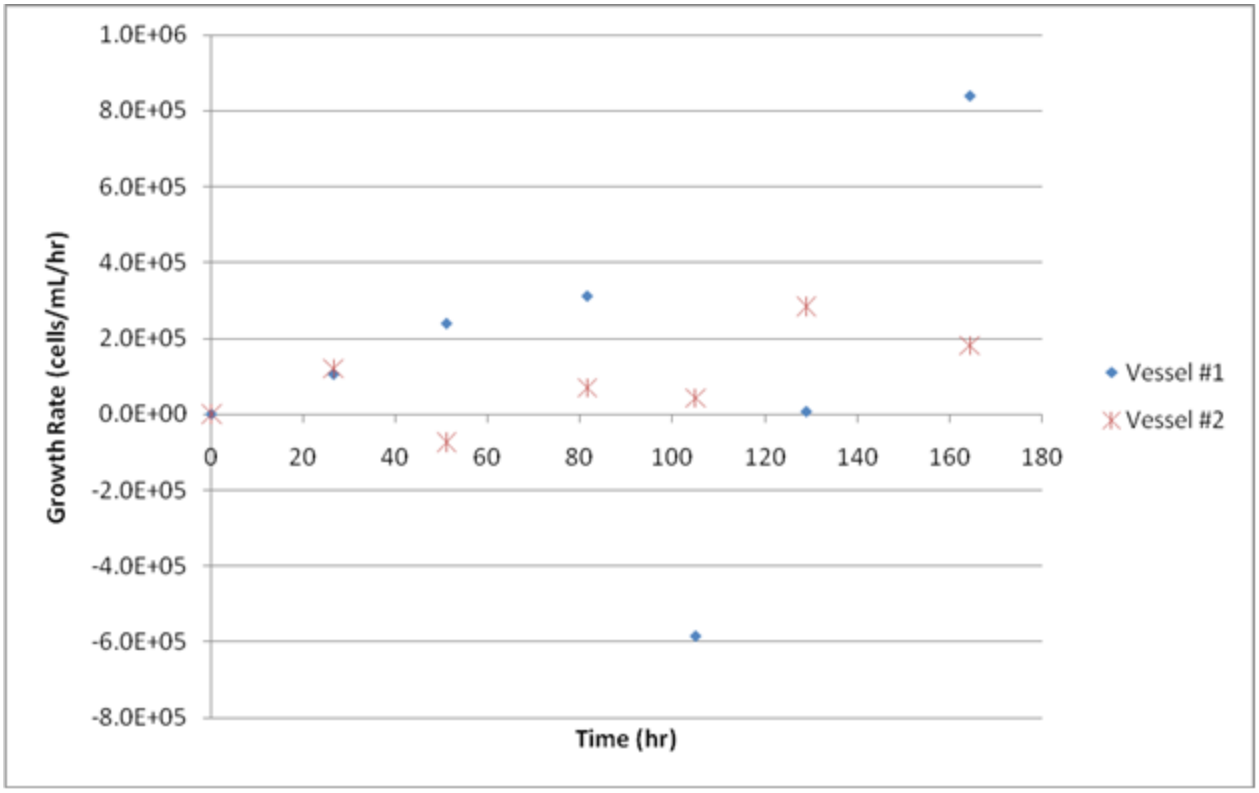

Figure 64. Growth Rate Versus Time

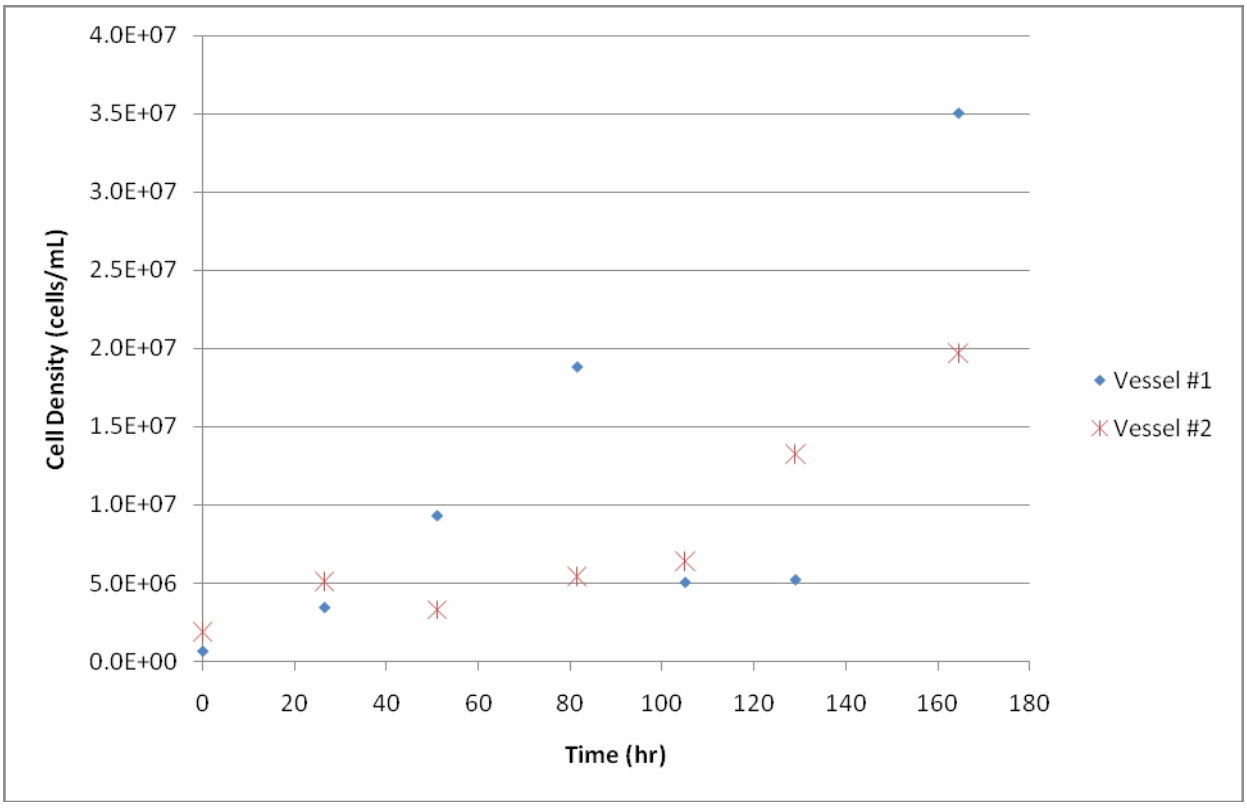

Figure 65. Cell Density Versus Time

Photobioreactor (PBR) Design

The basic design questions that must be considered for the design of a photobioreactor (PBR) are:

1) How to provide light
2) Which materials to use for construction
3) How to circulate the algae
4) How to provide CO_2, and remove O_2
5) How to control pH and temperature.

The most efficient way of artificially illuminating a PBR is with blue and red LEDs emitting at the maximum absorbance of chlorophyll *a* and *b* (around 440 and 650 nm). However, the lighting system for this PBR was chosen to mimic sunlight, in case we decide to test the effect of dyes that emit at the wavelengths most utilized by chlorophyll. T5 fluorescent bulbs were chosen because of their better lumen/watt output, as compared to more common T8 and T12 bulbs. Several wide spectrum fluorescent bulbs will be tested to determine which one best resembles the spectral distribution of sunlight.

UV stabilized acrylic (Plexiglas) was used to build the PBR. Since Plexiglas is not autoclavable, bleach was tested as an alternate sterilization method. The Plexiglas looked unchanged through visual inspection after the tests; no color change or cracks were observed.

A spectrophotometer was used to check if there was any change in transmissivity, by comparing the half dipped in disinfectant to the untreated half. This was calculated for ~1700 intensity data points corresponding to wavelengths from 372 to 811nm. Results showed that the light transmissivity of Plexiglas is not affected, even after being submerged in 6% Sodium Hypochlorite for two hours.

The dimensions for the PBR are shown in Figure 66. The volume is 2L.

	Outer Dimensions (in)	Inner Dimensions (in)
Height	22.5	22
Length	4.1	3.1
Width	2 1/4	2

Figure 66. PBR Dimensions

All inlets and outlets consist of threaded fittings placed at the top of the PBR to prevent water leakage. A total of 5 holes were drilled to accommodate research needs:

1. CO_2 Inlet: CO_2 passes from a CO_2 tank through a tube connected to a sparger at the bottom of the PBR. This sparger creates small bubbles for efficient mass transfer.
2. Air Inlet: Air passes from an air compressor through a tube connected to a sparger at the bottom of the PBR. This sparger creates large bubbles for mixing.
3. Gas Sampling: The samples were collected daily from a gas outlet at the top of the PBR. This outlet is connected to a filter to prevent contamination. The samples were then analyzed using gas chromatography. This gas outlet also keeps the gas layer in the PBR at atmospheric pressure.
4. Liquid Inlet and Outlet: Three liquid outlets distributed evenly across the height of the water column to check if any settling occurs.
5. pH Probe: pH probe and an Automatic Temperature Compensation (ATC) probe will stay immersed in the water column throughout the duration of each batch process (~15 days).

Due to sparging method, the PBR was equipped with two different spargers. One will make large bubbles of air for efficient and gentle mixing, and the other will make small bubbles of CO_2 for a high mass transfer rate. Specifically, in this method, a rubber membrane sparger that creates <1 mm diameter CO_2 bubbles, and two single 1 mm orifice spargers that create 5 - 15 mm diameter air bubbles, which contribute 99.9% of the total gas flow used.

So, it is found that a rate of CO_2 addition of 2.5 L/day (~1.74mL/min) and a rate of aeration of 2.5 L/min are sufficient for a 1.7 L PBR. Adjusting for our 2 L PBR, our rate of CO_2 addition will be 2.04mL/min, and our rate of aeration will be 2.94L/min. These flow rates will be measured continuously using an Aalborg GFM17 Mass Flowmeter calibrated CO_2 with a range 0-10 ml/min and an Aalborg GFM17 Mass Flowmeter calibrated with a range 0-2 L/min.

Addition of CO_2 will cause a decrease in pH, since dissolved CO_2 will react with water to form carbonic acid, which dissociates into bicarbonate and protons. Often the addition of CO_2 is used in PBRs to control the pH of the solution. In this project, the researchers experimented with different CO_2 addition rates, so this variable needs to be independent from the control of pH. Thus, pH will be adjusted using adequate additions of 1 M NaOH, if it goes outside of a pH range of 6.5 – 9.5.

The PBR was placed in a 20ºC room and temperature was monitored continuously. If temperature falls outside 22ºC – 28ºC range, then a foam cover is placed around the PBR to keep temperature at 25ºC. This cover will also serve a second function of keeping the PBR isolated from ambient light.

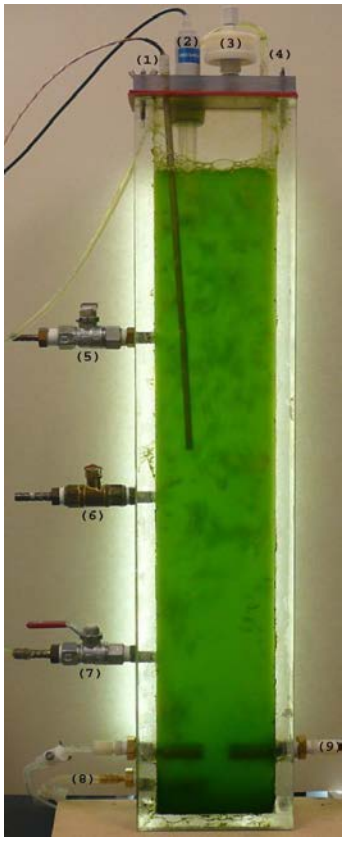

Figure 67. Photobioreactor

Figure 67 shows the bioreactor design. The key is (1) Temperature probe (RTD), (2) pH probe, (3) Air outlet with filter, (4) Medium outlet to continuous flow cuvette, (5) Medium sampling port 1, (6) Medium sampling port 2, (7) Medium inlet from continuous flow cuvette, (8) Air inlet, and (9) CO_2 inlet.

In this project, UV stabilized acrylic (Plexiglas) was used to build the PBR. A height of 50 cm was chosen to achieve good gas-liquid transfer and minimize loss of sparged CO_2. Previous studies have found a 100% transfer of CO_2 for a water column equal to or higher than 50 cm (Eriksen 1998). The depth chosen was 5.1 cm to minimize the light path. The length was chosen to have a volume of 2 L.

Even though the most efficient way of artificially illuminating a PBR is with blue and red LEDs emitting at the maximum absorbance of chlorophyll (around 440 nm), the NMT researchers took a different route. As mentioned previously, the lighting system for this PBR was chosen to mimic sunlight. T5 fluorescent bulbs were chosen because of their better lumen/watt output, as compared to the more common T8 and T12 bulbs.

Based on Eriksen's dual sparging method, the bioreactor is equipped with two different spargers. One makes large bubbles of air for efficient and gentle mixing, and the other makes small bubbles of CO_2 for a high mass transfer rate. CO_2 flows from a CO_2 tank through a mass flow meter to a sparger that produces < 1 mm diameter bubbles at a rate of 1 mL/min. Air flows from an air compressor through a mass flow meter to a sparger that produces > 5 cm diameter bubbles at a rate of 1.5 L/min.

The medium is withdrawn from a glass tube that goes from just above the spargers to the top of the bioreactor. The bottom of the tube is bent upward to prevent bubbles from entering. The medium passes through a continuous flow cuvette inside a spectrophotometer that measures absorbance at 440 nm every 5 minutes. The medium is pumped out of the cuvette and back into the bioreactor through the medium inlet.

Findings

Nitrate was measured daily using the Hach Cadmium Reduction Method. The concentration stayed constant at 0.02 mg/L NO^{3-} as N, showing that nitrate is not the limiting nutrient. C*hlorella* settles and grows on walls when not properly mixed. The pattern in Figure 68 shows settling inside the continuous flow cuvette. The cuvette was shaken to remove accumulation once daily. Despite data collection every 5 minutes, the only reliable points are those collected right after shaking; only these are further analyzed.

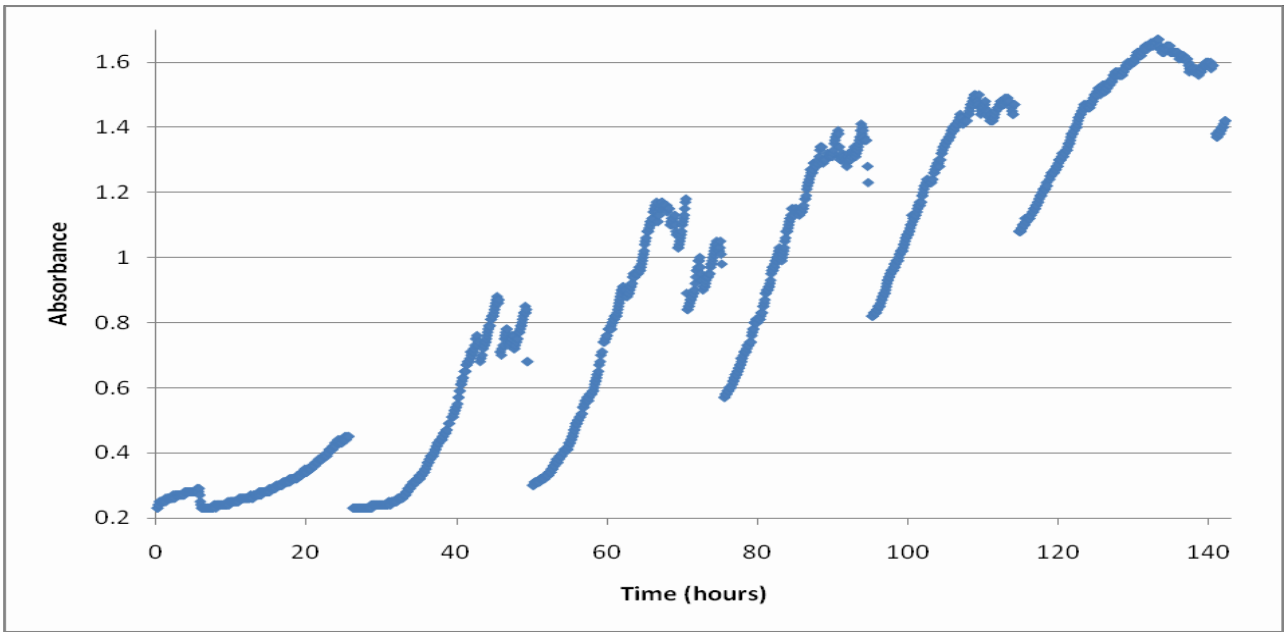

Figure 68. Raw Absorbance Data

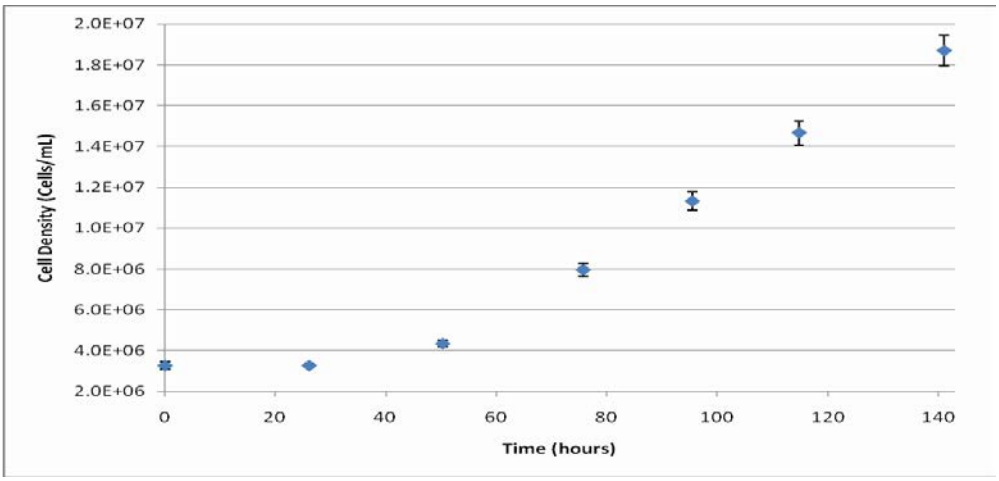

Figure 69. Cell Density versus Time

Cell density is calculated from the cell density-absorbance correlation (R^2 = 0.995). In 1 week, the culture went from 3.3 million cells/mL to 19 million cells/mL

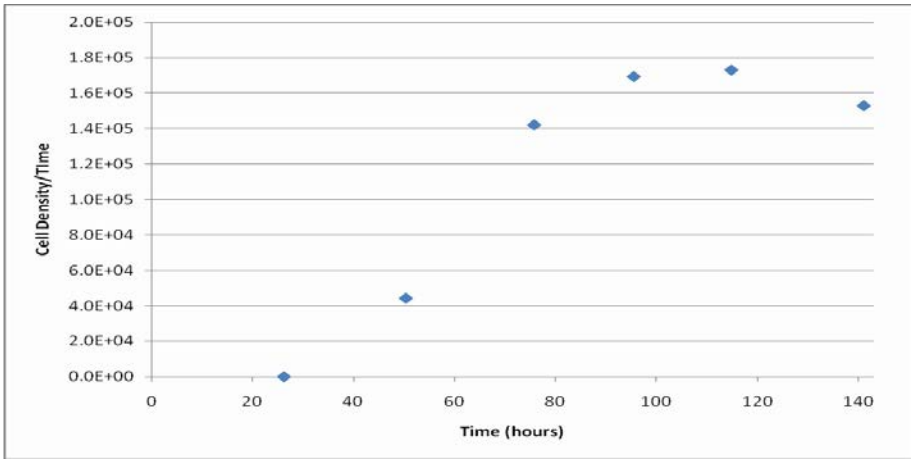

Figure 70. Growth Rate versus Time

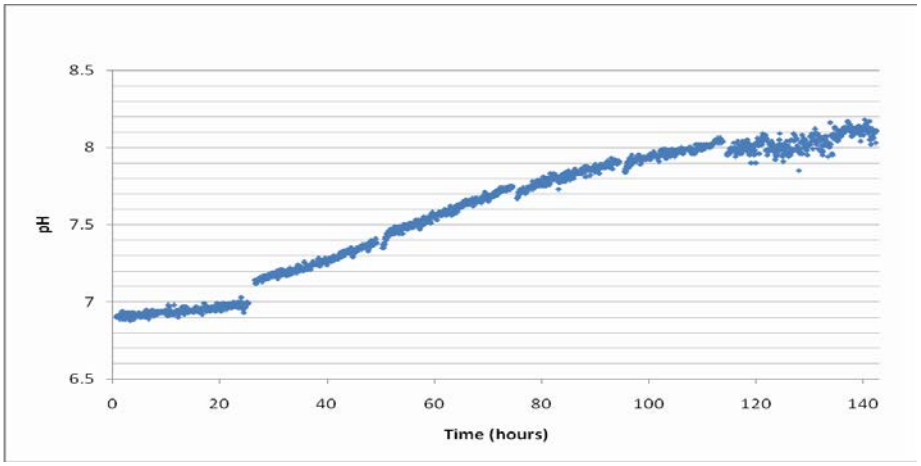

Figure 71. pH versus Time

The peak in growth rate at about 96 hours matches the time when pH reaches 8. For continuous culture, this is the point where the culture should begin to be diluted.

Conclusions

Automated absorbance measurements are a very efficient way of measuring cell-density. However, the flow rate of medium through the cuvette needs to be increased to promote turbulence and prevent settling. The aim of this project is to maximize the growth, CO_2 absorption rate and lipid production of *Chlorella vulgaris* for possible future application in large scale biofuels production. So, future work includes:

1. Maximizing CO_2 fixation rate: running batches with different CO_2 rates and measuring the composition of air above the water column through gas chromatography. The optimum CO_2 rate would be that which maximizes growth rate while minimizing loss of CO_2.
2. Fully automating the bioreactor and switching to continuous process, which will allow us to change the focus from growth to drying and extraction.

Batch Growth of *Chlorella vulgaris* in a 2 L Photobioreactor

Christine Polo, Dr. Frank Y. C. Huang, Idil Ayan
Department of Environmental Engineering
NEW MEXICO TECH
SCIENCE • ENGINEERING • RESEARCH UNIVERSITY

Why *Chlorella*?

This genus is the oldest commercially utilized and one of the most studied microalgae. *Chlorella* species have an oil content of 28 - 32 % dry weight (Chisti 2007). *Chlorella* tolerates high levels of CO_2, sulfur oxides, nitrogen oxides and VOCs (Keffer 2002), allowing it to thrive on the flue gas of coal fired power plants, waste incineration plants or other similar industries. *Chlorella* has the distinctive ability of growing in autotrophic, heterotrophic or mixotrophic conditions, giving this genus great potential for very high growth rates, under properly designed conditions. We grow UTEX 2714, a strain of *Chlorella vulgaris* from a wastewater pond, in Modified Bold 3N freshwater medium.

Experimental Setup

Dimensions

A height of 50 cm was chosen to achieve good gas-liquid transfer and minimize loss of sparged CO_2. Previous studies have found a 100% transfer of CO_2 for a water column equal to or higher than 50 cm (Eriksen 1998). The depth chosen was 5.1 cm to minimize the light path. The length was chosen to have a volume of 2 L.

Carbon Source and Mixing

Based on Eriksen et al.'s dual sparging method, the bioreactor is equipped with two different spargers. One makes large bubbles of air for efficient and gentle mixing, and the other makes small bubbles of CO_2 for a high mass transfer rate.

CO_2 flows from a CO_2 tank through a mass flow meter to a sparger (9) that produces < 1 mm diameter bubbles at a rate of 1 mL/min.

Air flows from an air compressor through a mass flow meter to a sparger (8) that produces > 5 cm diameter bubbles at a rate of 1.5 L/min.

Medium Inlets and Outlets

Medium is withdrawn from a glass tube (4) that goes from just above the spargers to the top of the bioreactor. The bottom of the tube is bent upward to prevent bubbles from entering. The medium passes through a continuous flow cuvette inside a spectrophotometer that measures absorbance at 440 nm every 5 minutes. The medium is pumped out of the cuvette and back into the bioreactor through the medium inlet (7).

Results

Nitrate was measured daily using the Hach Cadmium Reduction Method. The concentration stayed constant at 0.02 mg/L NO^{3-} as N, showing that nitrate is not the limiting nutrient.

Figure 1. Raw Absorbance Data

Chlorella settles and grows on walls when not properly mixed. The pattern in Fig. 1 shows settling inside the continuous flow cuvette. The cuvette was shaken to remove accumulation once daily. Despite data collection every 5 minutes, the only reliable points are those collected right after shaking—only these are further analyzed.

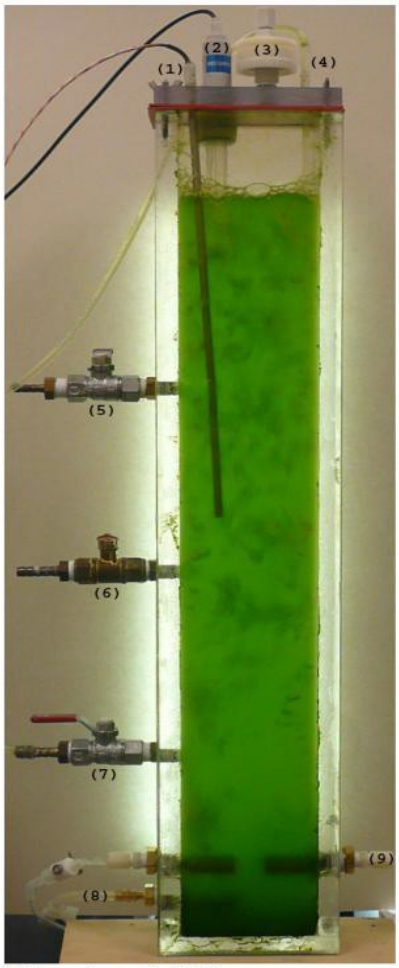

(1) Temperature probe (RTD)
(2) pH probe
(3) Air outlet with filter
(4) Medium outlet to continuous flow cuvette
(5) Medium sampling port 1
(6) Medium sampling port 2
(7) Medium inlet from continuous flow cuvette
(8) Air inlet
(9) CO_2 inlet

Figure 2. Cell Density versus Time

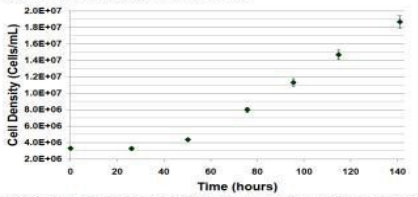

Cell density is calculated from the cell density-absorbance correlation (R^2 = 0.995). In 1 week the culture went from 3.3 million cells/mL to 19 million cells/mL.

Figure 3. Growth Rate versus Time

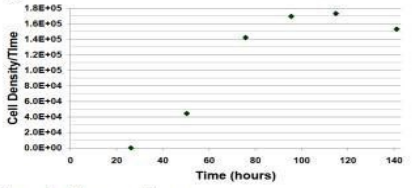

Figure 4. pH versus Time

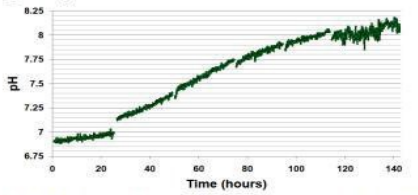

The peak in growth rate at about 96 hours matches the time when pH reaches 8. For continuous culture, this is the point where the culture should begin to be diluted.

Conclusions and Future Work

Automated absorbance measurements are a very efficient way of measuring cell-density. However, the flow rate of medium through the cuvette needs to be increased to promote turbulence and prevent settling.

Future work includes:

1) Maximizing CO_2 fixation rate: running batches with different CO_2 rates and measuring the composition of air above the water column through gas chromatography. The optimum CO_2 rate would be that which maximizes growth rate while minimizing loss of CO_2.
2) Maximizing lipid yield with glycerol.
3) Fully automating the bioreactor and switching to continuous process, which will allow us to change the focus from growth to drying and extraction.

The long-term objective of this research is to maximize the growth, CO_2 absorbtion rate and lipid production of *Chlorella vulgaris* for possible future application in large scale biofuels production.

Acknowledgments

Dr. Frank Huang, Dr. Snežna Rogelj, and Mark Shepard for their crucial advise and abiding guidance.

References

Chisti Y (2007) Biodiesel from microalgae. Biotechnol Adv. 25:294-306.
Eriksen NT, Poulsen BR, Iversen JJL (1998) Dual sparging laboratory-scale photobioreactor for continuous production of microalgae. J Appl Phycol. 10:377-382.
Keffer JE, Kleinheinz GT (2002) Use of *Chlorella vulgaris* for CO_2 mitigation in a photobioreactor. J Indust Microbiol Biotech. 29:275-280.

Task 3.6: NMCEP

NM Center for Energy Policy (NMCEP) is located in Hobbs, New Mexico and is an affiliate of the New Mexico Institute of Mining and Technology (NMIMT).

The previously proposed "Task 3.6: Sustainable Biofuel Crops", was severely impacted by state budget cuts and associated work assignments and conflicts. To continue to be responsive to the project requirements including cost share commitments, NMT replaced the planned work on sustainable biofuel crops with the work at NMCEP. This work has the additional benefit of being more in line with the objectives of the Grid Reliability and Distributed Renewable Energy Research and is more under NMT's control since the work is being performed by NMCEP, an NMT affiliate research center.

NMCEP'S work includes the integration of renewable energy systems and energy policy that is very relevant to the Grid Reliability and Renewable Distributed Energy Project. NMCEP has worked with the Lea County Electric Co-op to install solar electric systems throughout Southwestern New Mexico.

Key work done by NMCEP included the planning and holding of three energy conferences titled "Renewable Energy and Policy". The conferences were held in Hobbs, New Mexico, and four hundred people attended each conference. These conferences focused on policy options that should be implemented at the state and local levels. Key attendees and speakers included Senator Jeff Bingaman, Senator Pete Domenici, Congressman Harry Teague, and Lt. Governor Diane Denish.
Speakers and panels at the conference included:

- Renewable Energy and the Resources: Solar, Wind and Geothermal
- Renewable Energy and Crisis, Cost and Carbon
- Renewable Energy and the Next generation Technologies
- Renewable Energy and the Transmission Grid

Task 3.7: Design and Development of a Supercritical Biodiesel Reactor System (Co-PI: Don Weinkauf)

In this task, a vegetable-oil-to-biodiesel reactor was designed and built for testing and assessment of optimized supercritical reactor conditions. The prototype system was built to be skid mounted for portability, and is capable of producing at least 2000 gallons of biodiesel per year. Work to date has entailed design/assembly of the system, and early results for biodiesel production. The process has been built with the following design specifications:

- Full PLC control system with emergency shut down
- Process temperature range: 300 to 450◦ C
- Process pressure range: 4000 psi
- Feedstocks: any lipid and any alcohol
- All fuel tanks, pumps, heaters, reactor, etc.
- Meet all safety codes (i.e. environmental, fire, exhaust, mechanical, electrical)

The main components of the design, seen in the photograph of Figure 72, include: two feedstock tanks (left), two high pressure pumps, pressure and flow sensors, a pre-heater, guard reactor, fixed bed flow-through reactor, a heat exchanger, back pressure regulator, a gravity separation weir, automated valves, control system and biodiesel & alcohol storage tanks. The entire system was designed with fully automated PLC with touch panel controls.

The reactor system design and construction has been completed as shown in Figure 72. Early testing of the portable system was done using several standard operating conditions: zirconium oxide packed bed reactor, 325◦ C, 3000 psi, with methanol and soybean oil feedstock. Reactor effluent samples were sent to Midwest Laboratories, Inc. for the standard ASTM biodiesel test suite (including ASTM D-6584-07). The biodiesel fuel product passed all elements of the ASTM D-6584-07 (total glycerol = 0.13% mass) testing protocol. As with lab bench scale results, the results from this work indicate that the supercritical process may effectively eliminate glycerol by-product from the standard biodiesel process.

Figure 72. Supercritical Biodiesel Reactor System

Summary

Playas was chosen to test Micro-Grids and other examples of renewable distributed energy resources because researchers were able to isolate their experiments within the town and the entire town if needed. Several proposed distributed energy sources were not implemented as planned including the micro-Grid. However, Micro-Grid design and computer modeling were completed and these results are included in this report.

Four solar generating systems were installed with remote Internet based communication and control capabilities. These systems have been integrated into the local grid (interactive) and are operational. Excess power is or can be exported to the utility grid. Energy efficient LED lighting was installed to further reduce utility power. By combining reduced lighting costs; lowering HVAC loads; and installing smart PV solar generating equipment with energy storage (battery banks) these systems can greatly reduce electrical usage drawn from an older rural electrical Co-Op while providing clean dependable power.

Several additional tasks under this project involved conducting organic materials to energy conversion research, the most successful being the biodiesel reactor. Improvements with Proton Exchange Membranes for fuel cells were demonstrated and advances in Dye Sensitized Solar Cells were also shown. Technical conclusions for each task are described within the corresponding section(s) of this report.

References

Note: *While this report was being circulated for review and comments some of the referenced web sites and pages were modified or discontinued, or the source content was relocated to another page/site. For these instances, the latest known reference source has been included in the following list.*

[1] Susan Kraemer, *"Despite Fears, New Renewables Are Not Bankrupting California,"* May 22, 2013, <http://www.renewableenergyworld.com/rea/news/article/2013/05/despite-fears-new-renewables-are-not-bankrupting-california>.

[2] "U.S. Installs 723 MW of Solar PV in Q1 2013, According to New U.S. Solar Market Insight Report," <http://www.seia.org/news/us-installs-723-mw-solar-pv-q1-2013-according-new-us-solar-market-insight-report>, Tuesday, June 11, 2013.

[3] Renewable Energy Investment Tax Credit (ITC)," < http://selectusa.commerce.gov/investment-incentives/renewable-energy-investment-tax-credit-itc>.

[4] John Farrell, *"Gainesville, Florida, Becomes a World Leader in Solar,"* January 6th, 2012, <http://cleantechnica.com/2012/01/06/gainesville-florida-becomes-a-world-leader-in-solar/>.

[5] Herman K. Trabish, "*Lancaster CA Becomes First US City to Require Solar,*" March 27, 2013, <http://www.greentechmedia.com/articles/read/Lancaster-CA-Becomes-First-US-City-to-Require-Solar>.

[6] "Community Choice Energy," <http://www.localcleanenergy.org/policy-platform/communitychoiceenergy>.

[7] "How It All Started," <https://mcecleanenergy.com/how-we-started>.

[8] Rosana Francescato, "Net Metering: A Net Positive," May 14, 2013, < https://joinmosaic.com/blog/net-metering-net-positive>.

[9] Noel Leon, "Solar Credits – The Engine Behind a Clean Energy Transition for California," August 1, 2013, <http://sierraclub.typepad.com/compass/2013/08/solar-credits-the-engine-behind-a-clean-energy-transition-for-california.html>.

[10] R. Thomas Beach, Patrick G. McGuire, "*Evaluating the Benefits and Costs of Net Energy Metering in California*," Crossborder Energy, The Vote Solar Initiative, January 2013, <http://votesolar.org/wp-content/uploads/2013/01/Crossborder-Energy-CA-Net-Metering-Cost-Benefit-Jan-2013-final.pdf>.

[11] "*Evaluation of Net Metering in Vermont Conducted Pursuant to Act 125 of 2012*," January 15, 2013, <http://publicservicedept.vermont.gov/sites/psd/files/Topics/Renewable_Energy/Net_Metering/Act%20125%20Study%20020130115%20Final.pdf>.

[12] Richard Perez, Ken Zweibel, Thomas E. Hoff, "*Solar Power Generation in the US: Too Expensive, or a Bargain?,*" <http://www.asrc.cestm.albany.edu/perez/2011/solval.pdf>.

[13] Uploaded content removed from slideshare.net
<**http://www.slideshare.net/SEIA/impacts-of-solar-pv-on-texas-electricity-markets**>

Links for new location:
Presentation slides: http://www.seia.org/sites/default/files/2012-Brattle-Group-Report-Potential-Impact-of-Solar-PV-on-Electricity-Markets-Texas-Slides-6.19.12.pdf
Report: http://www.seia.org/sites/default/files/brattlegrouptexasstudy6-19-12-120619081828-phpapp01.pdf

[14] Web page not found <http://www.cpuc.ca.gov/PUC/energy/Solar/nem_cost_benefit_evaluation.htm>.

Links for new location:
http://www.cpuc.ca.gov/PUC/energy/Solar/nem_cost_effectiveness_evaluation.htm
http://www.cpuc.ca.gov/NR/rdonlyres/BD9EAD36-7648-430B-A692-8760FA186861/0/CPUCNEMDraftReport92613.pdf
http://www.cpuc.ca.gov/NR/rdonlyres/C311FE8F-C262-45EE-9CD1-020556C41457/0/NEMReportWithAppendices.pdf
http://www.cpuc.ca.gov/NR/rdonlyres/75573B69-D5C8-45D3-BE22-3074EAB16D87/0/NEMReport.pdf

[15] "*Colorado Community Solar Gardens Act, House Bill 10-1342,*" Representatives Levy, Benefield, Court, Ferrandino, Fischer, Gagliardi, Hullinghorse, Kagan, Merrifield, Peniston, Pommer, Primavera, Solano, Tyler, <http://www.solargardens.org/legislation-news-2/colorado-community-solar-gardens-act/>.

[16] Web page not found <http://californiasharedrenewables.org/>. SB-43 Electricity: Green Tariff Shared Renewables Program, <http://leginfo.legislature.ca.gov/faces/billNavClient.xhtml?bill_id=201320140SB43>.
Link for new location:
http://www.sharedrenewables.org/index.php?option=com_legislation&view=listing&stateCode=CA

[17] Rosana Francescato, "Solar for the 75%," November 13, 2012, <https://joinmosaic.com/blog/solar-75>.

[18] http://www.journals.elsevier.com/international-journal-of-hydrogen-energy

http://www.sciencedirect.com/science?_ob=ArticleListURL&_method=list&_ArticleListID=-730078064&_sort=r&_st=13&view=c&md5=5c3c5957c266408217907495eebc3688&searchtype=a

Effect of preparation method on the performance of the Ni/Al_2O_3 catalysts for aqueous-phase reforming of ethanol: Part II-characterization
Original Research Article
International Journal of Hydrogen Energy, *Volume 37, Issue 24*, *December 2012*, *Pages 18815-18826,* B. Roy, K. Artyushkova, H.N. Pham, L. Li, A.K. Datye, C.A. Leclerc

Effect of preparation methods on the performance of Ni/Al_2O_3 catalysts for aqueous-phase reforming of ethanol: Part I-catalytic activity
Original Research Article
International Journal of Hydrogen Energy, *Volume 37, Issue 10*, *May 2012*, *Pages 8143-8153,* B. Roy, U. Martinez, K. Loganathan, A.K. Datye, C.A. Leclerc

[19] http://www.journals.elsevier.com/journal-of-power-sources/,

http://www.sciencedirect.com/science?_ob=ArticleListURL&_method=list&_ArticleListID=-730069598&_sort=r&_st=13&view=c&md5=15314966be37e9c7c5d71a252fca5dd3&searchtype=a

Aqueous-phase reforming of n-BuOH over Ni/Al_2O_3 and Ni/CeO_2 catalysts
Original Research Article
Journal of Power Sources, *Volume 196, Issue 24*, *15 December 2011*, *Pages 10652-10657,* B. Roy, H. Sullivan, C.A. Leclerc

Effect of variable conditions on steam reforming and aqueous phase reforming of *n*-butanol over Ni/CeO_2 and Ni/Al_2O_3 catalysts
Original Research Article
Journal of Power Sources, *Volume 267*, *1 December 2014*, *Pages 280-287,* B. Roy, H. Sullivan, C.A. Leclerc

[20] National Science Foundation, Search for an REU site page, <http://www.nsf.gov/crssprgm/reu/reu_search.cfm>.

[21] http://www.hindawi.com/journals/ijp/2010/264643/, Hindawi Publishing Corporation, International Journal of Photoenergy, Volume 2010 (2010), Article ID 264643, 7 pages, doi:10.1155/2010/264643
Research Article
N-Aryl Arenedicarboximides as Tunable Panchromatic Dyes for Molecular Solar Cells
Zhi Cao, Premchendar Nandhikonda, Adriana Penuela, Stephanie Nance, and Michael D. Heagy